NASA CONTRACTOR REPORT

NASA CR-1535

THE MEASUREMENT AND ANALYSIS OF PILOT SCANNING AND CONTROL BEHAVIOR DURING SIMULATED INSTRUMENT APPROACHES

by David H. Weir and Richard H. Klein

NATIONAL AERONAUTICS AND SPACE ADMINISTRATION • WASHINGTON, D. C. • JUNE 1970

NASA CR-1535

THE MEASUREMENT AND ANALYSIS

OF PILOT SCANNING AND CONTROL BEHAVIOR

DURING SIMULATED INSTRUMENT APPROACHES

By David H. Weir and Richard H. Klein

Issued by Originator as Technical Report No. 170-4

ABSTRACT

Experimental measurements of pilot scanning and control response in a simulated instrument approach are reported. Seven subjects flew Category II-like ILS approaches in a six degree of freedom fixed-base DC-8 simulator at the NASA Ames Research Center. A conventional instrument panel and controls were used, with simulated vertical gust and glide slope beam bend forcing functions. Pilot eye fixations and scan traffic on the panel were measured using a recently developed eye point-of-regard (EPR) system. The EPR data were reduced for 31 approaches with a cross section of subjects to obtain dwell times, look rates, scan rates, and fractional scanning workload. These data are compared with previous experimental results. Simultaneous recordings were made of displayed signals, pilot response, and vehicle motions to permit their correlation with the eye movement results during the next phase of the overall program.

Flight director (zero reader) and standard localizer glide slope (manual) types of approaches were made. Both fixed and variable instrument range sensitivities were included. The scanning results showed the attitude and glide slope/localizer instruments to be primary in a manual ILS approach, sharing 70 to 80 percent of the pilot's attention. The glide slope/localizer instrument required shorter dwell times with a fixed instrument sensitivity. Differences in dwell time between pilots only occurred on the attitude instrument. With the flight director, glide path deviation errors were reduced and the flight director instrument dominated pilot attention (about 80 percent). There were no apparent circulatory scanning patterns in any of the approaches. These EPR results were generally consistent with prior data where meaningful comparisons could be made.

FOREWORD

This report summarizes experimental research accomplished as one part of an overall program aimed at developing models and methods for the analysis and synthesis of manual control displays. It presents the results of the first phase of a two phase effort to measure and correlate pilot eye movements and control actions during instrument approach. The research was conducted for the Man-Machine Integration Branch of the NASA Ames Research Center under Contract NAS2-3746. The NASA project monitors were M. K. Sadoff and W. E. Chase. The STI Technical Director was D. T. McRuer. The project engineer for this part of the program was D. H. Weir.

CONTENTS

FIGURES

TABLES

SYMBOLS

a_y	Lateral acceleration
$\bar{f}_s$	Scan rate, all instruments
$\bar{f}_{s_i}$	Look rate at ith instrument
FD_p	Flight director pitch
FD_r	Flight director roll
h	Altitude
$\dot{h}$	Rate of climb
LOS	Line of sight
M	Number of instruments
N	Number of fixations
N_d	Number of dwells
N_δ^u	Numerator of $u \longrightarrow \delta$ transfer function
p	Roll rate
q	One way link value
r	Heading rate
R	Range to nominal touchdown
s	Laplace transform variable
T_d	Dwell time
$\bar{T}_d$	Mean dwell time
T_i	Time fixating ith instrument
T_R	Total run time
$\bar{T}_s$	Look interval
$u,\ U$	Airspeed
w_g	Vertical gust
y	Lateral displacement

α	Angle of attack
β	Sideslip angle
γ	Flight path angle
δ	Deflection angle
$\triangle$	Transfer function denominator
ϵ_{GS}	Glide slope deviation
ϵ_{LOC}	Localizer deviation
η_i	Dwell fraction, ith instrument
θ	Pitch angle
μA	Micro amperes
ν_i	Look fraction, ith instrument
σ	Standard deviation
φ	Roll angle
ψ	Heading angle
ω_{s_i}	Scanning workload, ith instrument
ω	Frequency

Special Subscripts

a	Aileron
AP	Autopilot
c	Command
e	Elevator
e	Error
FD	Flight director
g	Atmospheric gust
GS	Glide slope
H	Horizontal

i	Index (instrument)
i	Input
j	Index (instrument)
k	Index (dwell)
lat	Lateral
long	Longitudinal
LOC	Localizer
o	Trim condition or value
o	Output
p	Phugoid
r	Rudder
T	Throttle
T	Tracer
v	Vertical

Displayed Signal and Instrument Abbreviations

ADF	Automatic direction finder
ALT	Altimeter
AS	Airspeed
ATT	Roll and pitch attitude
DG	Directional gyro
EMD	Eye movement device
EOG	Electro-oculograms
EPR	Eye point of regard
FD	Flight director
GCA	Ground control approach
GH	Gyro horizon

GSD	Glide slope deviation
HDG	Heading (indicator)
HMD	Head movement device
HSI	Horizontal situation indicator
IAS	Indicated airspeed
ILS	Instrument landing system
IVSI	Instantaneous vertical speed indicator
LOC	Localizer deviation
MACH	Machmeter
PALT	Pressure altimeter
RMI	Radiomagnetic indicator
RPM	Engine speed
RVR	Runway visual range
T & B	Turn and bank
VS	Vertical speed
XPT	Cross pointer

SECTION I

INTRODUCTION

A. OBJECTIVES

Further development and validation of the theory of manual control displays (Ref. 1) required simultaneous eye movement and pilot response data in flight control tasks under realistic instrument conditions. The primary objective of this research program was to obtain such data for instrument approach tasks. A second objective was to reduce the eye point-of-regard data to the scanning statistics needed to continue the development of methods for analysis and synthesis of manual control displays. These objectives have been accomplished, and data are now in hand for several airline pilots in more than a hundred simulated instrument approaches in a subsonic jet transport. Detailed scanning statistics have been computed for a cross section of thirty-one 2 minute runs. These results are part of the data base for the next objective—correlation of eye point-of-regard with control response and displayed motion variables.

B. BACKGROUND

The first definitive experimental research in this area was accomplished by Milton, Jones, and Fitts in a herculean 8-year experiment. They used an eye camera to measure the instrument scanning patterns of pilots in a variety of actual IFR maneuvers (Refs. 2, 3, 4, 5, and 6), but no records were made of the concomitant instrument readings or pilot responses. Very stable statistical traffic patterns appeared in their results for various pilots and maneuvers. A reexamination of this work with an attempt at supplying the missing signal properties by pilot vehicle analysis (Ref. 7) was indicative but inherently inconclusive.

Other workers who have measured instrument scanning behavior have been concerned mostly with the statistical models of the scanning process, rather than with the establishment of connections with the causal factors of the displayed signals themselves (e.g., Refs. 8, 9, and 10). Again, the displayed signals were either not recorded or not correlated against the scanning behavior.

1

A theory for manual control displays is presented in Ref. 1. It combines servo analysis techniques, multiloop pilot response models, and a scanning and sampling perceptual theory (updated in Ref. 11) to obtain a procedure useful in prediction and display design. The procedure is applied in Ref. 1 to a piloted jet-transport Instrument Landing System (ILS) landing approach as an analytical example. No experimental data were available to validate the predicted pilot response and scanning traffic.

The first effort to measure and correlate the visual sampling process and pilot control is reported in Ref. 12. It was aimed primarily at validating a queing theory for display scanning. Although detailed, the Ref. 12 results are not complete enough to validate the overall theory and methods of Refs. 1 and 11. Specific shortcomings from our viewpoint include lack of a contemporary panel layout, no forcing functions (useful in measuring pilot response), and inadequate definition of the controlled element dynamics.

In these past studies the data-taking process has used eye movement cameras, electro-oculographics, or corneal reflection techniques. These tend to be expensive, difficult to operate, and detrimental to the experimental environment. A recently developed eye point of regard (EPR) system provides simple, inexpensive direct readout of the coordinates of eye fixations on the instrument panel. This, coupled with proven experimental techniques for measuring pilot dynamic response in multiloop tasks (Refs. 13 and 14), and the availability of a high fidelity simulation facility at NASA Ames Research Center, gives the tools to perform the needed behavioral measurement program.

C. PREVIEW OF THE REPORT

This study used a NASA Ames Research Center, fixed-base six degree of freedom simulator, configured as a DC-8. Current commercial airline pilot subjects flew landing approach tasks. Pertinent displayed variables, eye fixations, pilot response, and vehicle motions were measured.

Section II describes the experiments. This includes a detailed description of the equipment, controlled element (simulator) properties, system

forcing functions and signal recording. The qualifications of pilot subjects, experimental procedures, tasks, and instructions are detailed.

Section III presents the eye scanning data and statistics for 31 selected runs. Both manual ILS and flight director results are given. Dwell times, scan rates, display workloads and link values between instruments are derived. Tests of significance are used to differentiate the data and provide a basis for lumping like results. Previous eye fixation data are presented where applicable, to place the present results in context and to highlight differences. Finally, additional features of the EPR data such as blinks, transitions, and looks within instruments are described.

The final section summarizes the results and conclusions.

SECTION II

DESCRIPTION OF THE EXPERIMENTS

The experiments involved pilot control in a conventional Category II-like* instrument approach in a six degree of freedom fixed-base simulation of a DC-8 aircraft. The panel layout was typical of a subsonic jet transport, with some configurations employing a flight director (FD). The subjects were airline pilots and copilots. The task was to fly an ILS (Instrument Landing System) approach from the outer marker (30,000 ft from threshold) to the middle marker in the presence of vertical gusts, θ_c, and glide slope beam bends, ϵ_{GS_c}. Aircraft motions, displayed signals, pilot response, and eye point of regard were tape recorded. The system block diagram is shown in Fig. 1. Details of the experimental setup and procedures are given in this section and its appendices. The experiments were performed at the NASA Ames Research Center.

A. EXPERIMENTAL SETUP

The experimental configurations are described in Table I. Configuration A was a pitch attitude tracking task designed to provide single-loop response data on the present subjects for correlation with past data and models. Configurations B, C, and D involved a "raw presentation" of localizer and glide slope deviation, pitch and roll attitude, and peripheral instruments, but no flight director display. These tasks varied in their detail in order to explore effects of scanning and statistical stationarity. Configurations E and F employed all the displays of C and D, respectively, plus a lateral and longitudinal flight director display superimposed on the artificial horizon. The visual breakout runs were peripheral to the main experimental program. The "fixed range" configurations had the instrument range varying sensitivities

---

*The approach was like Category IIB, because it involved at least 1,200 ft RVR and 100 ft decision altitude minimums. It differed from usual Category II procedures because the pilots were asked to fly it on basic ILS needles (with no flight director) in some cases.
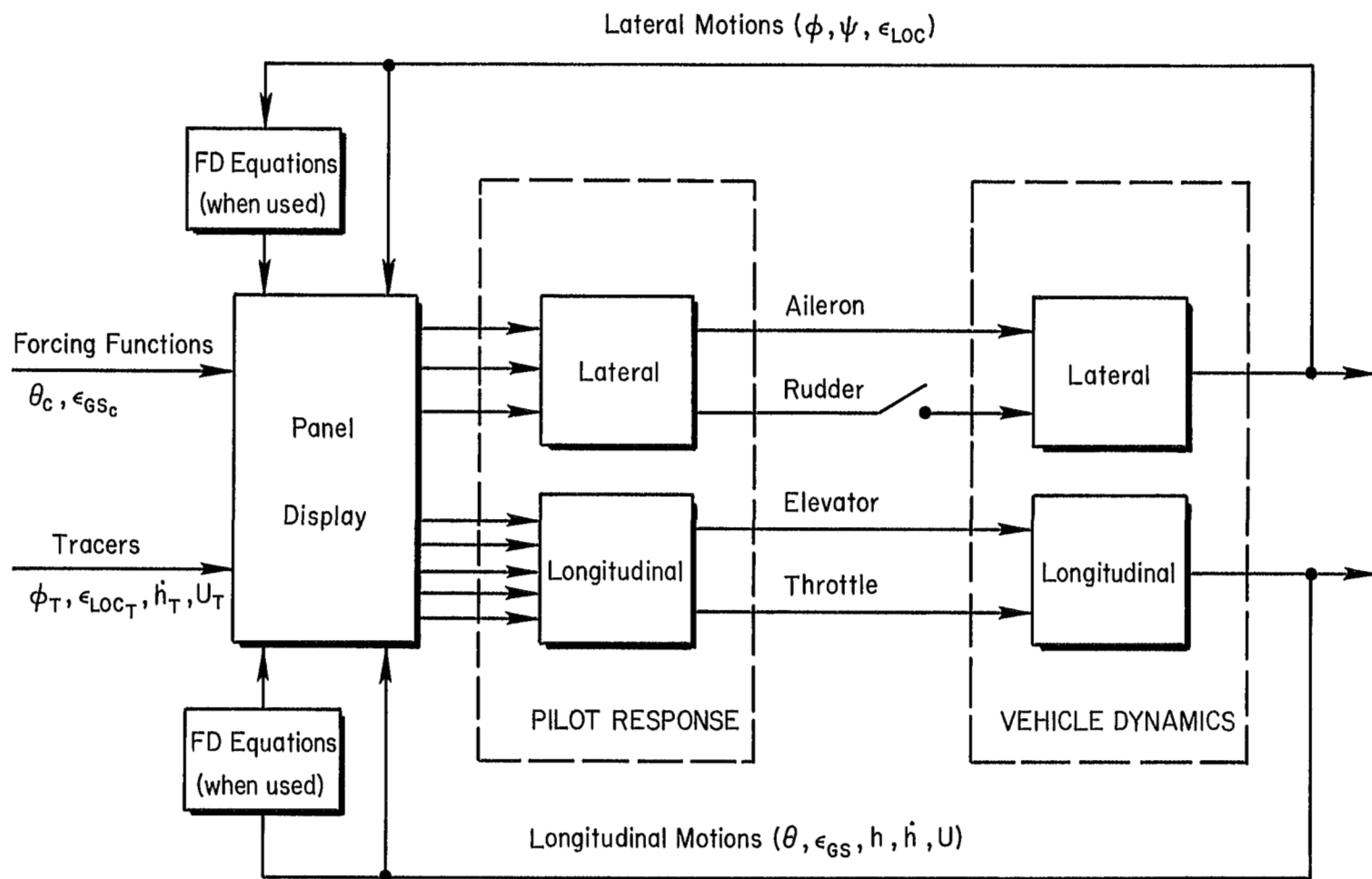
Figure 1. Block Diagram of Experimental Task

TABLE I

EXPERIMENTAL CONFIGURATIONS

CONFIGURATION	DESCRIPTION	PURPOSE	INSTRUCTIONS TO SUBJECTS
A (Pitch attitude regulation only)	Single axis tracking task with pitch attitude display and forcing function. Other instruments masked. Other axes controlled by autopilot. No flight director.	Tie in with single loop tracking data.	Simulates a portion of the approach task. Control pitch attitude only, and try to keep pitch error equal to zero. There is some turbulence. The lateral autopilot is ON.
B (Split axis manual ILS, fixed range)	Three degree of freedom longitudinal task. Forcing functions and tracers on. Lateral axes under autopilot control, but meters visible. No flight director.	Provide longitudinal scanning task, and basis for validating multiloop pilot response model.	Simulates a split-axis manual approach under Category II conditions. Control only the longitudinal motions. An autopilot is controlling the lateral motions. There is some turbulence. Try to keep the glide slope needle centered at all times.
C (Manual ILS, fixed range)	All axis approach task with forcing functions and tracers on. The glide slope deviation computer range was fixed at 30,000 ft from threshold. The altimeter and rate of climb meters appeared normal (varying range). No flight director.	Provides stationary all axis task. Reference case for comparison with split axis, range varying, and flight director cases.	Simulates a Category II manual ILS approach. There is some turbulence. Try to keep the glide slope and localizer needles centered at all times.
D (Manual ILS, varying range)	All axis approach task with forcing functions and tracers on. The range varied throughout the run. Glide slope deviation per unit altitude error increases with decreasing range. No flight director.	Provides nonstationary longitudinal task. Typical of "old fashioned" cross pointer ILS display.	
E (Flight Director, fixed range)	All axis approach task with forcing functions and tracers on. Flight director on, and driven by forcing function. Same as Configuration C plus flight director.	Provides equalized, integrated display and stationary all axis task. Reference flight director case. Typical of modern practice.	Simulates a Category II FD approach. There is some turbulence. Use the Director to follow the approach path, keeping the glide slope and localizer needles centered. Pitch commands must be obeyed immediately to avoid a standoff. The glide slope and localizer needles must be monitored.
F (Flight Director, varying range)	All axis approach task with forcing functions and tracers. Flight director on. Glide slope component of FD forcing function attenuated with range by flight director computer. Same as E, except range varying.	Provides equalized, integrated display but nonstationary forcing function.	
Visual Breakout	All axis approach task with Configurations D or F, except that the CPS system was used to provide an external visual field display at 200 ft above ground. Pilot looked up when told by copilot/experimenter. Breakout occurred some time after the 100 sec run.	Exploratory investigation of the feasibility of measuring both visual field and panel EPR. Used with only a few runs at the end of the experimental program.	Same as D or F, except that copilot calls out altitude and says "runway in sight" when visual acquisition occurs.

9

fixed at the values existing near the outer marker, 30,000 ft range from threshold. Specific differences between the configurations arise in controlled element dynamics, displayed signals, and forcing function properties; and these are detailed subsequently.

1. **Apparatus**

The experimental apparatus was located at the NASA Ames Research Center. It is described in Appendix A, and consisted of:

- analog computers
- recording equipment (FM tape and strip chart)
- taped forcing functions
- instruments and their drive mechanisms
- cockpit, panel, and control column
- eye point of regard (EPR) measuring system
- interconnections

The computers and recording equipment were in a building separate from the cockpit containing the subject, experimenter, and EPR system as shown in Fig. 2. The allocation of functions was conventional, with the vehicle dynamics, control equations, and scaling done on the analog computers; recording of EPR, vehicle motions, displayed signals, pilot response, etc., was done on an FM tape and strip chart recorder.

2. **Controlled Element**

Properties of the various controlled elements and the panel layout are detailed in Appendix B. The simulated vehicle was nominally a subsonic jet transport in the landing approach configuration. The dynamics were defined by a linearized set of perturbation equations in six degrees of freedom. The simulator was stabilized with full flaps and gear down at 135 kts on the approach path at the outer marker at the start of the run. The speed was nominally that of the United Airlines DC-8 for turbulence conditions as recommended by the Flight Manual (Ref. 15). No changes in flaps, trim, or power setting were required during the run — although the pilot was free to make throttle corrections. The vehicle transfer functions and sample transient responses are given in Appendix B.

7

COMPUTER ROOM

Brush Record 8 ch

Brush Record 8 ch

FM Tape Record 14 ch

Brush Record 8 ch

Input Tape

TR-48 Analog Computer

AD-256 Analog Computer

EPR Set-Up
⊗
Experimenter

Pilot ⊗ Cockpit

Instrument Bay

SIMULATOR BUILDING
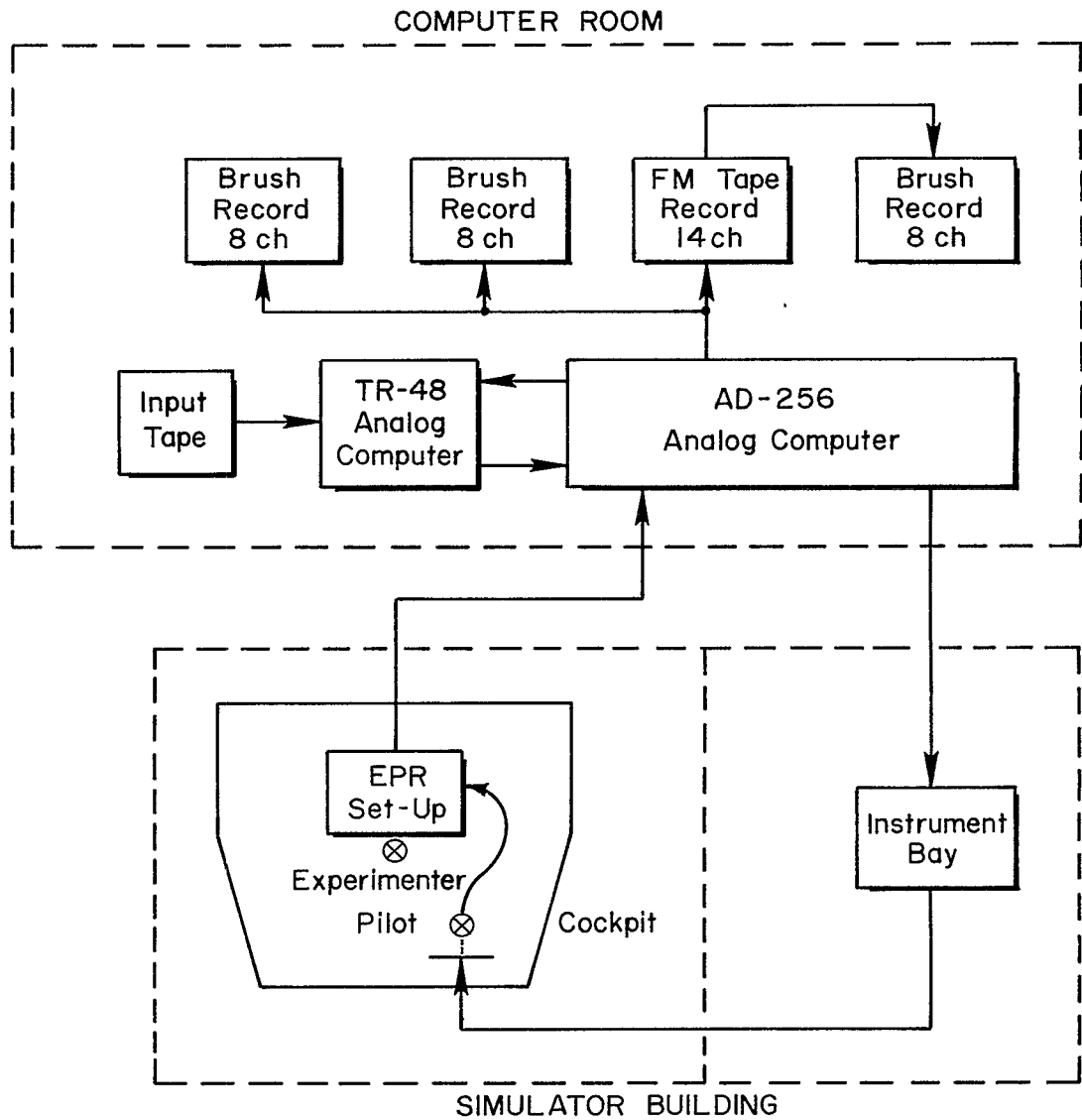
Figure 2. Topological Layout of Equipment

The panel layout for the manual ILS configurations is shown in Fig. 3. The instrument needles have been deleted for clarity. The flight director bar appeared on instrument 2 for Configurations E and F.

The flight director provided pitch and roll commands. The equations are given in Appendix B. The longitudinal director mixed pitch attitude and altitude errors. The latter were computed from the angular glide slope deviation by multiplying by the range to the glide slope transmitter. This caused the forcing function amplitude (component due to the glide slope command) to decrease during Configuration F runs. The lateral director mixed roll angle, heading angle, and (angular) localizer deviation errors.

A low gain "autopilot" was used in Configuration B to simulate human pilot control of the lateral axes. It is described in Appendix B.

The panel instrument dynamics are part of the controlled element and their properties are shown in Appendix B. The attitude ball, glide slope bar, localizer bar, and pitch and roll director display frequency responses all looked like well damped second-order systems with break frequencies in the region 1 to 1.5 Hz. The peripheral instruments were more responsive.

Properties of the elevator, aileron, and rudder manipulator were measured, and these are shown in Appendix B. The column and wheel operated a hydraulic feel system. The DC-8 pilots termed it a reasonable facsimile of that aircraft, the Boeing 707 pilots felt it was somewhat light and sensitive, and the Convair 990 pilot thought it too sluggish and insensitive.

3. Forcing Functions and Tracers

Two independent longitudinal forcing functions, a pitch attitude command, θ_c, and a glide slope deviation command, ϵ_{GS_c}, were used in the experiments. This permits multiloop describing functions to be computed from the data. Tracers, consisting of one or two low amplitude sine waves, were added to some displayed signals. The forcing functions and tracers are detailed in Appendix C and summarized below.
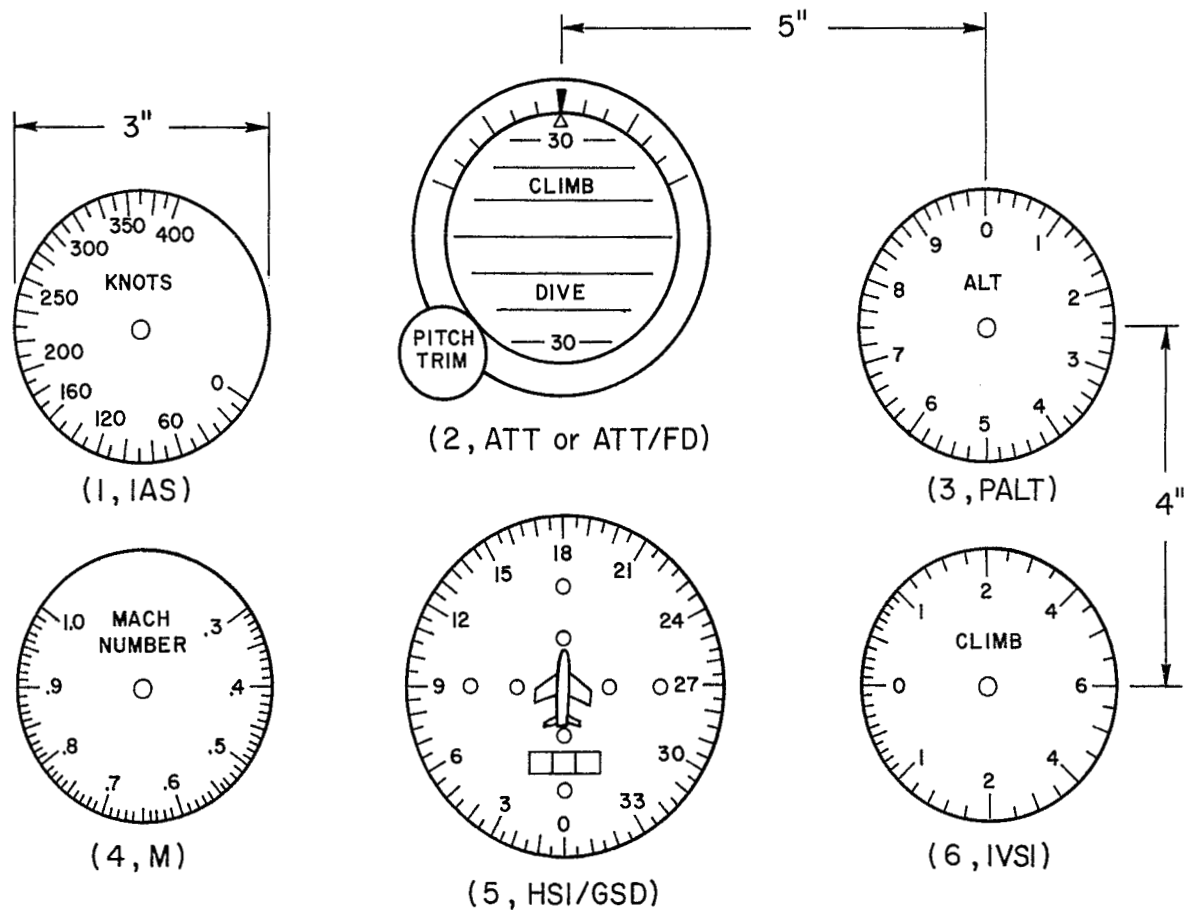
Figure 3. Layout of Basic Flight Instruments

The pitch attitude command simulated a vertical gust input. It was a stationary random-appearing signal composed of a sum of sine waves. It had a bandwidth of 0.8 rad/sec and an rms amplitude of 1.2 deg. Lower amplitude higher frequency components comprised a "shelf" to facilitate response measurements in the region of the θ-loop pilot crossover frequency (see Fig. C-3 in Appendix C). The pitch command was roughly equivalent to a 5 ft/sec rms vertical gust acting on the closed-loop pilot/vehicle system. The subject pilots felt in general that it represented fairly large (but not unrealistic) turbulence for landing approach. Pilot 3 had only encountered that turbulence level once (during landing) in thunderstorm conditions, and another pilot said he would not try to land in those conditions. Subjects were instructed that they had no choice but to make the approach.

The glide slope command forcing function simulated low frequency beam bends. It was a random-appearing sum of sine waves with an effective bandwidth of about 0.3 rad/sec and a mid-frequency low amplitude shelf. It had an rms amplitude of 0.04 deg path angle or about 0.2 dots of needle deflection. This input magnitude was around the upper limit of acceptability for Category II beam bends, and occasionally exceeded it. The limit is 30 μA decreasing to 20 μA at the middle marker (Ref. 16), which corresponds to about 0.3 dots. The glide slope command always entered the simulation as an angular deviation. This gave a statistically stationary forcing function on instrument 5 (glide slope deviation) for all configurations.* The glide slope command component of the flight director pitch command was nonstationary in Configuration F, decreasing with range; because of the altitude computation in the flight director computer.

The two command inputs were independent, containing different component sine waves which were "interleaved," as shown in Appendix C. The presence of two independent inputs occasionally troubled some subjects because they

_____

*Note that the displayed glide slope deviation per unit altitude displacement was nonstationary in the range varying configurations (D and F), requiring the pilot to reduce his altitude loop gain as the approach progressed.

could be pitching up while the glide slope deviation indicated they were
descending. This and other glide slope deviations were interpreted as
large vertical shears even though they were due to beam bends. Subjects
commented that the airspeed was unusually stable, and that they would
expect it to vary more in that level of turbulence. The displayed rate
of climb excursions were sometimes quite large (for approach conditions,
particularly) due to pilot efforts to perform the task. The pitch and
glide slope commands were fed into the flight director computer for
Configurations E and F, and some of the subjects said that the resulting
pitch bar excursions (closed-loop with the inputs) were larger than they
were used to (on different directors).

Tracer frequencies were added to the following displayed motions:

- Localizer deviation
- Roll angle
- Rate of climb
- Forward velocity

The details are given in Table C-I, Appendix C. They consisted of
sinusoids with amplitudes just above threshold on the non-driven meter.
They were designed to detect pilot response to these meters through
examination of elevator and aileron spectra for peaks at the tracer
frequencies. Their use was exploratory, although the potential feasi-
bility had been demonstrated in prior laboratory studies using two
displays.

4. Signals Recorded

The displayed signals, pilot response, vehicle motions, and eye
movements were recorded during the runs. The specific quantities
recorded on 14 channel FM-tape included:

- Vertical coordinate of eye point of regard, EPR_V
- Horizontal coordinate of eye point of regard, EPR_H
- Pitch attitude command, θ_c
- Glide slope command, ϵ_{GS_c}
- Pitch attitude error, θ_e

- Glide slope deviation error, ϵ_{GS_e}
- Elevator deflection, δ_e
- Roll angle, φ
- Localizer deviation, ϵ_{LOC}
- Aileron deflection, δ_a
- Rate of climb, $\dot{h}$
- Heading angle, ψ
- Voice commentary and identification
- 40 Hz digitizing tone

During flight director runs (Configurations E and F) the pitch and roll director commands were recorded in lieu of rate of climb and heading angle.

Two 8 channel strip chart recorders were used to record all but the voice channel, plus:

- Flight director pitch command, FD_p
- Airspeed, U, or flight director roll command, FD_r
- Mean-square localizer deviation, $\overline{\epsilon_{LOC}^2}$
- Mean-square glide slope deviation, $\overline{\epsilon_{GS}^2}$

The latter two were duplexed on one channel.

B. PILOT SUBJECTS

Seven pilot subjects participated in the program, and data for four of them are considered in this report. Their flight experience and panel arrangements of aircraft they currently fly are summarized in Appendix D. Pilots 1, 2, and 4 had prior experience on this particular simulator in other research programs, but under slightly different instrument arrangements and test conditions. Pilot 4 was used in the shakedown runs associated with setting up and validating the simulation. Pilot 3 was unfamiliar with this simulator but had participated in previous STI experiments at other facilities. The subjects were all current professional airline pilots or copilots. The simulation was sufficiently similar to their current experience that the pilots were able to achieve a stable level of proficiency within a few runs.

13

All the pilots were volunteers who had an interest in the program and its eventual outcome. They were paid a modest hourly rate. Their selection was based on the following factors:

- Interest, motivation, and availability
- Experience and current flight assignment
- Acceptance of the simulation
- Quality of EPR data (minimum saccade artifacts, eyelid lag, drift, etc.)
- No need for corrective glasses, since it interferes with the eye movement device.

These qualities were also considered in selecting the data for detailed analysis. Pilot 4 normally wore glasses, but he did not require them for instrument flight (panel scanning).

The pilots reflect a cross section of age and background. Pilot 1 is a senior instructor captain with multiengine piston and jet bomber experience. Pilot 2, a younger copilot, transitioned to commercial flying via the general aviation/light aircraft route. Pilot 3, although a copilot, has extensive military single engine fighter/bomber experience, and Pilot 4 is a multiengine test pilot of long standing.

C. EXPERIMENTAL PROCEDURE

The experimental procedure involves the instructions given to the subjects, familiarization, and the steps used during experimental sessions. These are summarized below.

1. Instructions to Pilot Subjects

Prior to any simulator flying, each of the pilot subjects was given an overall briefing on the program and its research goals. The following points were covered in this briefing:

- Simulated airplane is a DC-8
- The task involves a Category II-like approach using conventional instruments with no visual runway acquisition, flare, or landing. There will be no surprises or unexpected emergencies.

14

- A set of sensors mounted on eyeglass frames will be used to monitor eye scanning.

- Pitch attitude and glide slope deviation inputs are used to make the task difficult. It will look like severe turbulence and it may seem a little artificial, but try and fly it as you would an actual approach.

- This study is considering "limiting cases" which are the ones which govern designs. Assume that you have to make <u>this</u> approach and that you can't abort. The only alternative is to bail out or crash land.

This was followed by an informal discussion of the simulation layout and general procedures.

After becoming settled in the left seat in the simulator the pilots were given general instructions regarding the initial conditions and cockpit procedures. These instructions were:

> "The task is to fly the approach from outside the outer marker to inside the middle marker. You will begin stabilized on the 3 deg glide slope. Beam acquisition is not required. The 'bug speed' is 135 kts. Both gear and flaps are down and all check-lists are completed. The initial altitude is 2,000 ft and the field elevation is 312 ft. The problem will end prior to runway visual range and there is no need to flare or look for the runway. The experimenter will announce the end of the run. Try to keep the glide slope and localizer needles centered at all times.
>
> Due to the simulation setup and limitations we would like you to try to follow these additional conditions:
>
> - Retrim pitch attitude ball at start of run.
> - Don't use the trim button or trim wheels.
> - Full flap all the way down
> - There should be no need for throttle movements (it's initially trimmed).
> - After run, take hands off wheel and throttle.
> - Try not to clamp jaw, squint, or move ears.
> - Even if very difficult — try to stay with it.
> - Don't say anything during the run.
> - After the run, describe any control problems or difficulties.
>
> Are there any questions?"

These general instructions were not given to the pilot more than once or twice, but the appropriate instructions in the right hand column of Table I were given to the pilot prior to each individual run. The need to try to keep the glide slope and localizer needles centered at all times was reemphasized continuously.

A few runs were made on the last two days of the experiments which involved visual breakout and required the pilot to acquire the runway, flare, and land. These were purely exploratory and followed the main experimental program (so as not to influence the latter). Revised instructions and procedures were used for these runs, including the experimenter/copilot calling "runway in sight." These are described more fully in subsection 3, below.

2. Run Sequence

Each pilot was given several initial familiarization runs of both manual ILS and flight director tasks without input forcing functions. This enabled the pilots to evaluate the aircraft's flying characteristics, become familiar with new instrumentation, and experience the cockpit procedures. Familiarization runs were only performed during the pilot's first training session (1 or 2 hours) and were not tape recorded.

Practice runs (involving 1 or 2 sessions) followed the familiarization and enabled the pilots to experience the input forcing functions as applied to the three basic configurations (B, C, and E). Frozen range tasks were used in practice because: they could be of any run length; they allowed stationary pilot behavior; and they were to comprise the bulk of the final data runs. During the practice runs the EPR system was explained and the equipment fitted to the subject. All practice runs were tape recorded.

All formal record runs (after the familiarization and practice sessions) included 2 or 3 "warm-up" runs with the basic configurations, usually 1 of each without the EPR system. The final data runs were made with the EPR system. A data session usually involved 5 or 6 100 sec runs in succession, divided at random between manual ILS and flight director configurations. Fixed range and varying range

16

configurations were not mixed in the same session, but were run on separate days.

3. Procedure

A session began with warm up runs, followed by installation of the EPR system. Two experimenters were required to make the runs. While one was in the simulator cab trimming the EPR system and instructing the pilot on the task, the other rewound the input forcing function tape, set the mechanization for the next task, and updated the run log.

When the pilot was ready the FM tape recorder was started and an EPR calibration made. This consists of looking at each instrument in sequence. This calibration record was made before and after each run so that even a nonlinear eye angle transducer adjustment could be later reduced off-line to the actual instrument regarded. Immediately after calibration the forcing function tape was started and the simulation was placed in operation. The pilot began performing the task as soon as he saw the forcing functions appear. The digitizing tone, signifying the start of the 100 sec run was turned on about 10 sec after the start of the run. After approximately 2 min of running the experimenter would call "run completed," at which time the simulator would be reset and another EPR calibration made. The digitizing tone was turned off 10 or 15 sec before the end of the run.

All communication channels were common, and any conversation taking place during the run was recorded on the FM data tapes. Pilot comments were also recorded on a hand held tape recorder for a standard series of questions and as much pilot/experimeter interchange as possible.

Rest periods of 15-20 min for every 5 runs (about 30 min of data taking) were required. Normal data taking sessions were 2 to 2.5 hr duration, including EPR setup, with only one session per day per pilot.

For the visual breakout runs a "copilot" performed any additional cockpit procedures desired by the pilot. This included such things as 100 ft altitude increments when below 500 ft, speed below bug, excessive rates of descent, etc., depending on individual pilot preference. The

17

forcing functions were gradually turned to zero inside the middle marker. The EPR system was reset to provide an indication of when the pilot looked up at the "real world" display.

D. SHAKEDOWN RUNS

A short preliminary series of experiments was accomplished near the outset of the project to shakedown and validate the simulation. This involved (to the extent possible) all of the apparatus, inputs, configurations, procedures, etc., to be used in the formal data runs. Pilot 4 was the main subject, although several other engineer/pilots flew the simulation for evaluation purposes.

The specific objectives of the shakedown runs were to check out and validate:

- The forcing function amplitudes and bandwidths
- The EPR system operation, data quality, and EPR data reduction procedures
- Pilot response measures, data quality, and data reduction procedures
- The overall simulation for fidelity, realism, and pilot acceptability
- Session schedules, timing, check lists, and detailed sequence of procedures

Several changes were made as a result, although the overall validity was confirmed.

Important changes were made in the pitch attitude and glide slope forcing functions. The original effective input bandwidths were 1.0 and 0.5 rad/sec, respectively. The high frequency shelf was only 14 dB down from the amplitude of the low frequency sine wave components. These effects combined to produce a lot of high frequency content in all the longitudinal displays. The pilot had some difficulty trying to fly it and he felt that it was unrealistic and "jumped up and down" too much. As a result the bandwidths and shelf amplitude were reduced to the levels shown in Appendix C. The amplitude was rescaled upward to preserve about the same rms level. The revised inputs were subsequently judged to be acceptable, although of fairly large amplitude for an approach task.

The altimeter, rate of climb meter, and pitch attitude ball were not biased (to simulate descent) for the fixed-range configurations during the shakedown. This detracted from the realism of the simulation and tended to distract the pilot. The necessary changes were made to make the panel appear as if range were decreasing along the nominal 3 deg glide slope.

Pilot operation of peripheral controls occurred during the shakedown runs. This was judged to be bad as it tended to increase his workload (probably unnecessarily) and to bias the pilot/vehicle dynamic response in an undesirable way. Several remedial steps were taken. The rudder pedals were electrically disconnected from the simulation, so the pilot could still "coordinate" aileron motions without introducing additional remnant in the lateral axis (which had no forcing function in the first place!). The pilot was requested not to use the electric trim buttons (on the wheel) during the run, but to use elevator instead. The pilots were told that throttle corrections weren't required (it was initially trimmed), but that they could use throttle if the airspeed got too far off. This reduced throttle activity quite a bit, resulting typically in only one or two minor corrections per run.

SECTION III

EYE POINT OF REGARD DATA

Detailed eye scanning data and statistics comprise a primary result of this part of the program. The other major result was simultaneous recordings of control response and displayed variables, suitable for correlation with these eye movement data. Eye point of regard (EPR) data for 31 runs involving 3 subjects and 5 configurations have been analyzed in detail. The results include dwell properties, scanning workload, and link values. They show little difference between similar configurations for the same pilot, major differences between dissimilar configurations (with and without the flight director), and some significant differences between pilots in similar tasks. The results, data reduction details, and comparisons with past work are given in this section.

A. DEFINITIONS AND REDUCTION PROCEDURE

A standard set of calculations and reduction procedures were defined in advance so that the data would be consistent. The raw vertical and horizontal eye traffic was picked off manually* and reduced to punch cards. The scanning traffic and statistics were obtained with a Fortran IV program on a time sharing computer.

Some definitions of the properties of the raw and reduced EPR data are needed. For a given run of T_R sec duration:

M is the number of instruments

N_i is the number of fixations on instrument i

N_M is the total number of fixations on all instruments

N is the total number of fixations on instruments, elsewhere, blinks, etc.

It follows that

$$N_M = \sum_{i=1}^{M} N_i$$

---

*Manual reduction was most expeditious for the amount of data analyzed in this study. The raw analog EPR data are intended to be digitized and entered directly into the computer with no manual steps, but there was no provision for program development as part of this project.

The duration of a look at a given instrument is called the dwell time, T_d, and

$T_{d_{i_k}}$ is the duration of the kth dwell on instrument i

$$T_i = \sum_{k=1}^{N_i} T_{d_{i_k}} \quad \text{is the total time fixating i}$$

$$T_R = \sum_{i=1}^{M} T_i + T_{other}$$

where T_{other} includes blinks and looks elsewhere than at the defined instruments. For data reduction convenience we assign a number to blinks and other regions of the panel so that all time during the run is subscripted and allocated.

Average properties of the data are important. The mean dwell time on instrument i is

$$\overline{T}_{d_i} = \frac{1}{N_i} \sum_{k=1}^{N_i} T_{d_{i_k}} = \frac{T_i}{N_i}$$

The "scan rate" over all instruments on the panel is the average number of fixations per second, given by

$$\overline{f}_s = \frac{N}{T_R}$$

The scan rate on a given instrument is called the "look rate," given by

$$\overline{f}_{s_i} = \frac{N_i}{T_R}$$

The fraction of fixations on the ith instrument, ν_i, is called the "look fraction,"

$$\nu_i = \frac{N_i}{N}$$

The "dwell fraction" is the fraction of time spent on instrument i, given by

$$\eta_i = \frac{T_i}{T_R}$$

This is also called the "fractional scanning workload." The "look interval" is the inverse of the scanning workload, i.e.,

$$\overline{T}_{s_i} = \frac{1}{\overline{f}_{s_i}}$$

The look interval is a measure of the recycle time, and it can also be computed from the individual scan intervals (the time between successive looks at an instrument).

The six instruments and other regions of the panel were numbered for analysis as shown in Fig. 4. Looks at region 8 were usually blinks, and they resulted in the total workload on the instruments being less than unity. There were essentially no looks at regions 7, 9, and 10 in the data analyzed.
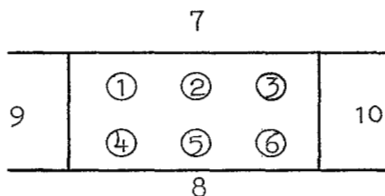
Figure 4. EPR Regions

A typical segment of data is shown in Fig. 5. The major part of the dwell is well defined. The transitions between dwells take a small amount of time and may contain artifacts such as an overshoot, cross talk and fake looks (e.g., going from 5 to 1, passing over 2 but not dwelling on it). The transitions are defined as having a duration no greater than 0.15 sec. Typical vertical transition times (over all pilots) between instruments are in the range .06 to .09 sec. The horizontal transitions are slightly faster, .05 to .08 sec. Additional details are given in subsection F. The difference probably reflects eyelid lag on the vertical

22
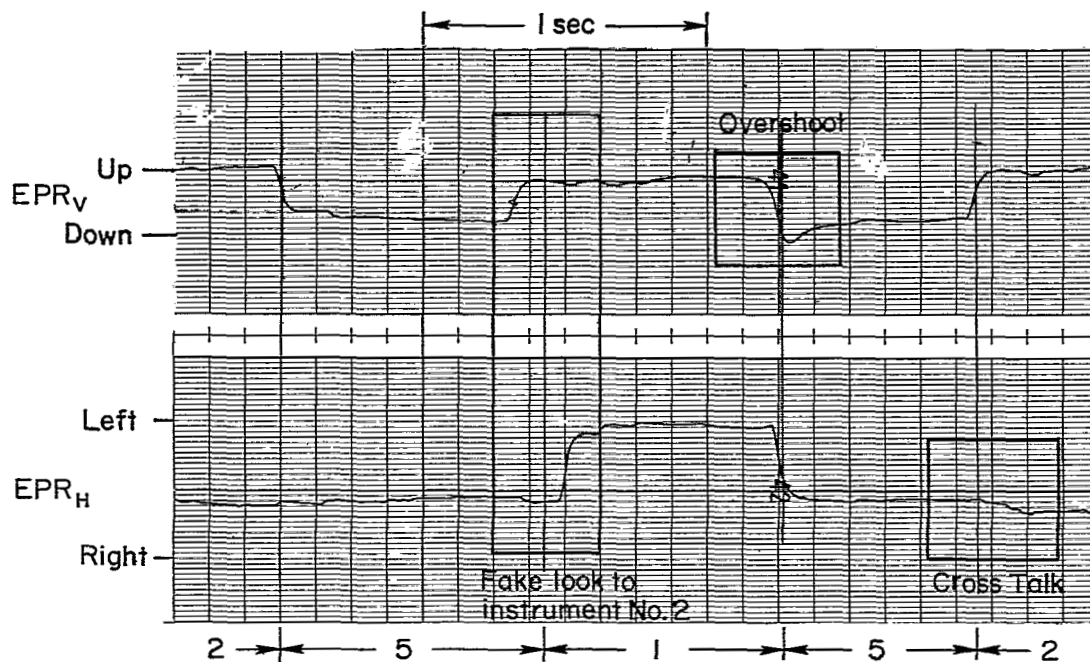
Figure 5. Illustrative Data Sample

channel, which varies between subjects. If the transition times are
longer than .15 sec they become an actual look, blink, etc. The transi-
tion times are allocated to the adjacent dwells in roughly equal propor-
tions as shown in Fig. 5. The alternative procedure, deleting the
transition times from the run, involves substantial reduction diffi-
culties that are avoided by the method used. Detailed artifacts of
the data such as scanning within a given instrument and blinks are
discussed in subsection F, below.

The nominal run length is at least 100 sec. Analysis starts with
the first complete dwell after the digitizing tone. The data are then
reduced for at least 100 sec, finishing with the end of a complete dwell.

A Fortran IV program was written to statistically reduce the EPR data.
The output consisted of dwell time statistics and histograms for each instru-
ment, summations for all instruments, and one way link transitions between
instruments. This program was run on a "Tymshare" remote terminal. The
following quantities were output for each instrument:

23

- Total dwell time, T_i
- Number of fixations, N_i
- Mean dwell time, $\overline{T}_{d_i}$
- Dwell time standard deviation, σ_{T_i}
- Dwell fraction, η_i
- Look fraction, ν_i
- Look rate, $\overline{f}_{s_i}$
- Dwell time histogram at .25 sec intervals

The data for all instruments included:

- Total dwell time, $\sum T_i$
- Total number of fixations, N_M
- Scan rate, $\overline{f}_s$
- One way transition links

The program required 220 statements, and it took approximately 5 min to process and type out the results of one run. The program allowed selected runs to be pooled together and processed as one long run. This gave the configuration averages for each pilot.

B. SCANNING STATISTICS

Over 100 EPR data runs were made, involving a total of seven pilot subjects and six configurations (A through F). A cross section of 31 of the best runs were selected from these for detailed analysis. The remaining runs are available on magnetic tape. The select runs comprise an "experimental design," shown in Table II. Each cell is denoted by a shorthand notation, e.g., C1 is Configuration C with Pilot 1. The configurations are described in Section II. The subject pilot backgrounds are given in Appendix D. Configuration A is not included, because it was a single axis task with no scanning. Pilot 1 was the principal subject and replications for each configuration are shown. Runs for Pilots 2 and 3 help define interpilot and interconfiguration differences.

Some of the range-varying runs involved a "visual breakout" and transition to an outside visual field display. This transition occurred

TABLE II

RUNS ANALYZED IN DETAIL

CONFIGURATION	SUBJECT		
	2	1	3
B (Split-axis manual ILS, fixed range)	B2 690219-17	B1 690217-18 690219-5	
C (Manual ILS, fixed range)	C2 690219-16 690219-19 690219-21 690219-23 690219-25	C1 690217-15 690219-4 690219-10 690219-11 690219-13	
D (Manual ILS, varying range)		D1 690217-16 690226-5 690226-9 690227-3* 690227-6*	D3 690228-5* 690228-8*
E (FD, fixed range)	E2 690219-18 690219-22 690219-24	E1 690213-20 690217-19 690219-8 690219-12	
F (FD, varying range)		F1 690226-7 690226-8 · 690227-5*	F3 690228-7*

*Visual breakout occurred later.

at least 10 to 15 sec after the 100 sec run interval, on verbal instructions from a "copilot" experimenter. It did not affect the pre-breakout data.

The detailed scanning statistics for each of the 31 runs comprise the data base, and they are given in Table E-I of Appendix E. Results are shown for each instrument and for all-instrument averages. Averaging these data over a given pilot/configuration "cell" yields Table III, which is discussed in detail subsequently.

TABLE III

AVERAGE SCANNING STATISTICS

CONF.	SUBJ.	NO. RUNS AVG.	INSTRUMENT 1, IAS						INSTRUMENT 2, ATT OR ATT/FD					
			N_1	$\bar{T}_{d_1}$	σ_{T_1}	$\bar{X}_{s_1}$	η_1	ν_1	N_2	$\bar{T}_{d_2}$	σ_{T_2}	$\bar{X}_{s_2}$	η_2	ν_2
B	1	2	18	.57	.18	.09	.051	.068	89	.67	.29	.446	.296	.337
B	2	1	2	.64	.05	.02	.013	.015	61	.82	.36	.607	.498	.462
C	1	5	25	.69	.28	.05	.034	.042	238	.74	.33	.474	.353	.397
C	2	5	1	.63	0	.002	.001	.002	254	.95	.33	.511	.483	.453
D	1	5	43	.69	.35	.085	.059	.066	282	.81	.38	.560	.452	.431
D	3	2	3	.88	.40	.015	.013	.013	85	1.00	.45	.423	.425	.357
E	1	4	44	.55	.15	.110	.06	.113	171	1.73	1.72	.428	.739	.438
E	2	3	13	.54	.11	.043	.023	.070	84	3.03	3.41	.276	.836	.454
F	1	3	53	.56	.15	.177	.099	.163	147	1.50	1.36	.492	.737	.453
F	3	1	6	.59	.10	.059	.035	.079	37	2.19	1.80	.366	.80	.487

CONF.	SUBJ.	NO. RUNS AVG.	INSTRUMENT 3, PALT						INSTRUMENT 5, HSI/GSD					
			N_3	$\bar{T}_{d_3}$	σ_{T_3}	$\bar{X}_{s_3}$	η_3	ν_3	N_5	$\bar{T}_{d_5}$	σ_{T_5}	$\bar{X}_{s_5}$	η_5	ν_5
B	1	2	23	.38	.12	.115	.044	.087	111	1.02	.80	.557	.567	.421
B	2	1	2	.57	.04	.02	.011	.015	57	.78	.25	.567	.443	.432
C	1	5	40	.42	.16	.08	.034	.067	255	1.09	.72	.508	.551	.425
C	2	5	5	.41	.15	.01	.004	.009	242	.98	.40	.486	.476	.431
D	1	5	27	.45	.22	.054	.024	.041	265	.84	.43	.527	.444	.405
D	3	2	9	.44	.15	.045	.020	.038	96	.93	.51	.479	.443	.403
E	1	4	51	.40	.10	.128	.051	.131	76	.57	.20	.190	.109	.195
E	2	3	18	.50	.11	.059	.03	.097	41	.51	.12	.135	.069	.222
F	1	3	34	.35	.07	.113	.039	.105	59	.46	.13	.197	.090	.181
F	3	1	4	.34	.05	.04	.013	.053	27	.54	.25	.267	.145	.355

CONF.	SUBJ.	NO. RUNS AVG.	INSTRUMENT 6, IVSI						ALL INSTRUMENTS			
			N_6	$\bar{T}_{d_6}$	σ_{T_6}	$\bar{X}_{s_6}$	η_6	ν_6		N_M	$\sum T_1$	$\bar{X}_s$
B	1	2	10	.40	.14	.05	.020	.038		264	200	1.32
B	2	1	1	.55	0	.01	.005	.008		132	101	1.31
C	1	5	16	.38	.07	.032	.012	.027		600	502	1.19
C	2	5	2	.47	.23	.004	.002	.004		561	497	1.13
D	1	5	5	.40	.18	.010	.004	.008		654	503	1.30
D	3	2	43	.45	.14	.214	.095	.181		238	200	1.19
E	1	4	16	.44	.11	.04	.018	.041		390	400	.976
E	2	3	14	.49	.10	.046	.023	.076		185	305	.607
F	1	3	9	.35	.12	.033	.012	.031		325	300	1.08
F	3	1	1	.49	0	.01	.005	.013		76	101	.752

Dwell time histograms for each of the cell averages in Table III are given in Figs. E-1 to E-5 of Appendix E. These aid in interpreting the tests of significance described below. Some of the histograms can be lumped, and this is accomplished as their homogeneity is established.

The look rates, $\overline{f}_{s_i}$, and dwell times, $\overline{T}_{d_i}$, in Table III were examined to determine similarities and differences among the pilots and configurations. The results of these statistical tests and other observations are discussed in succeeding sections.

1. **Stationarity Within a Run**

A key question in computing average scanning statistics over a 100 sec run is whether there is any significant change in the pilot's scanning behavior with time. One potential source of nonstationarity arises in the glide slope deviation bar and pitch flight director whose gains change in the range-varying configurations. Several of the range-varying runs were processed in three successive intervals and their statistics compared, in order to determine if the scanning statistics were nonstationary. Table IV shows the mean dwell time and dwell fraction for each of the five instruments for three typical runs. These results show no important range-varying effects as discussed below, and the EPR can be considered statistically stationary within a run.

In general, the mean dwell times do not change significantly (at the 95 percent confidence level) for successive thirds of runs. The dwell time on instrument 2 in the last one-third of Run 26-09 is significantly smaller than during the first two-thirds because the first 2 parts each have one very long dwell (i.e., 2.5 sec). If these long dwells are deleted there is no longer a significant difference. A comparison of Runs 26-05 and 26-09 shows no significant differences for instruments 2 and 5. Other instruments were not analyzed in detail, because the number of looks were too few for meaningful comparisons.

The tests for significance were not performed on the dwell fractions, but these data do not show any consistent trends between runs and their variability is probably not significant.

TABLE IV

SCANNING STATISTICS FOR RUN SEGMENTS

INSTRUMENT	TIME INTERVAL (SEC)	RUN 26-05, D1		RUN 26-09, D1		RUN 26-07, F1	
		$\overline{T}_d$	η	$\overline{T}_d$	η	$\overline{T}_d$	η
1, IAS	0-33	.67	.080	.61	.056	.47	.116
	33-67	.56	.050	.66	.079	.65	.110
	67-100	.54	.082	.50	.044	.54	.102
2, ATT/FD	0-33	.78	.468	1.02	.557	1.38	.716
	33-67	.84	.529	.84	.477	1.64	.735
	67-100	.71	.500	.66	.440	1.25	.709
3, PALT	0-33	.53	.031	.47	.014	.40	.048
	33-67	.24	.007	.44	.026	.36	.040
	67-100	.50	.046	.39	.034	.33	.063
5, HSI/GSD	0-33	.75	.379	.68	.332	.46	.099
	33-67	.69	.395	.83	.395	.44	.086
	67-100	.68	.354	.85	.486	.43	.109
6, IVSI	0-33	.32	.010	.32	.010	.20	.006
	33-67	.61	.018	.26	.023	.40	.011
	67-100	0	0	.55	.016	.37	.012

2. Peripheral Instrument Look Rates

The peripheral instruments are the airspeed (No. 1), altimeter (No. 3), and rate of climb (No. 6). Their average look rates are given in Table III. These rates are based on a small number of looks (all are less than 10 percent) and they do not really warrant elaborate tests of significance. They are generally scattered, but some trends do emerge:

- Similar configurations with the same pilot are about the same

- There are some large between-pilot differences with the same configuration

Other look rate results are mixed. For example, in some cases the rates are larger with the manual ILS configurations than with the flight director, while others are the reverse.

3. Primary Instrument Look Rates

The average look rates on the primary instruments (ATT/FD and HSI/GSD) are given in Table III. On the attitude instrument (No. 2) the look rates are essentially the same over all pilots and configurations, except that the E2* look rate is significantly[†] smaller. On the HSI/GSD instrument (No. 5) the flight director runs (Configurations E and F) have a significantly lower look rate than the manual ILS runs. There is no difference between pilots within similar configurations, except that E2 is again smaller.

The all instrument scan rates, $\overline{f}_s$, are compared using Table III. The B, C, and D runs are homogeneous among themselves as are the E and F runs. The variance in the means among the B, C, and D runs is significantly less than that for the E and F runs. The mean of the B, C, and D scan rates is significantly greater than the mean of the E and F scan rates.

4. Peripheral Instrument Dwell Times

The average dwell times, T_{d_i}, on the peripheral instruments are shown in Table III. The airspeed indicator mean dwell times, $\overline{T}_{d_1}$, show no significant differences over all pilots and conditions. Neither do the altimeter or rate of climb (IVSI) indicator. Furthermore, the IVSI and

---

*E2 stands for Configuration E with Pilot 2.

[†]All significance tests were accomplished at the 95 percent confidence level unless otherwise stated.

29

altimeter mean dwell times are not different, but they are less than the mean airspeed indicator dwell times at a very high level of significance.

These results are illustrated by the peripheral instrument histograms of Fig. 6. Some of the dwell time variances are significantly different between runs, due to unusually long dwells which occurred occasionally for some pilots.

ALL PILOTS , ALL CONFIGURATIONS

Percent of Fixations

Altimeter and Rate of Climb Indicator

$$\overline{T}_{d_{3,6}} = .42$$

$$\sigma_{T_{3,6}} = .26$$

Airspeed Indicator

$$\overline{T}_{d_1} = .64$$
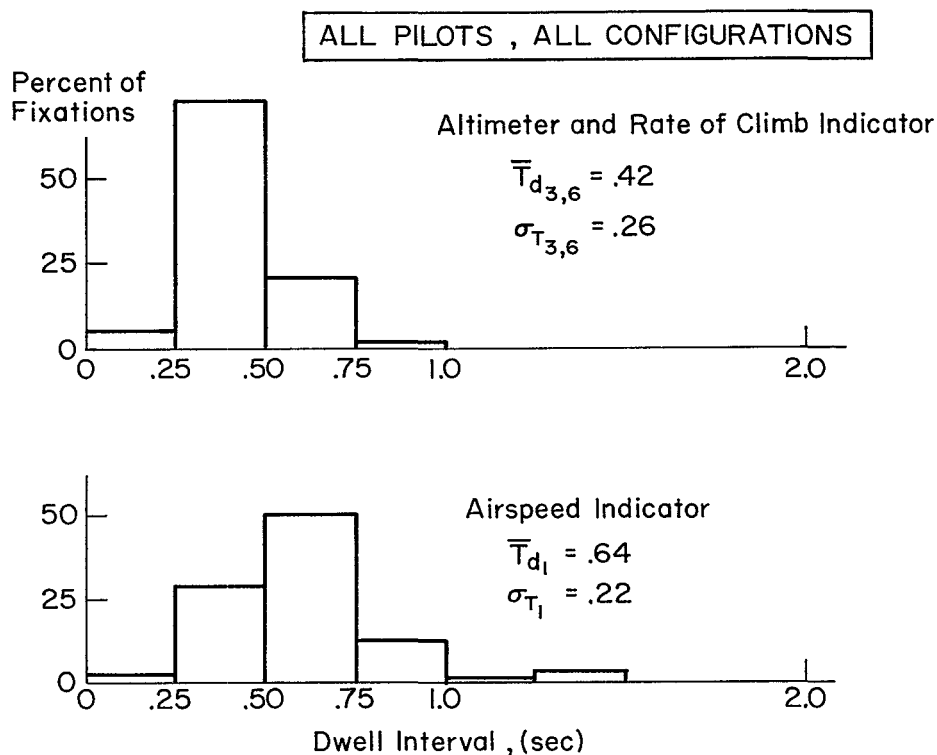
$$\sigma_{T_1} = .22$$

Dwell Interval , (sec)

Figure 6. Peripheral Instrument Dwell Times

5. Primary Instrument Dwell Times

The average dwell times on the primary instruments (2 and 5) are shown in Table III. Four cases are of interest: each of the two instruments with manual ILS and flight director configurations. The comparisons are discussed below.

Table V compares the attitude instrument (No. 2) dwell times over pilots for the manual ILS configurations. Configuration B is often different from C and D. A given pilot is about the same over minor configuration changes (e.g., C versus D), and these intrapilot data

TABLE V

MEAN DWELL TIME COMPARISON; INSTRUMENT 2,
MANUAL ILS CONFIGURATION

EFFECT OF CONFIGURATION	EFFECT OF PILOT
$B1 \doteq C1$	$C1 < C2$
$C1 \doteq D1$	$B1 < B2$
$B1 < D1$	$D1 < D3$
$B2 < C2$	

can be lumped. The pilots are significantly different in the same task. The dwell time variances over these pilots and configurations are not significantly different, except that D3 is significantly larger than the rest.

The comparisons for the attitude instrument (No. 2) with the flight director configuration are given in Table VI. The dwell time variance

TABLE VI

MEAN DWELL TIME COMPARISON; INSTRUMENT 2,
FLIGHT DIRECTOR CONFIGURATION

EFFECT OF CONFIGURATION	EFFECT OF PILOT
$E1 \doteq F1$	$E2 < E1$
	$F1 \doteq F3$

for E2 is larger than the others, and the F1 variance is significantly smaller. Table VI shows that E1, F1, and F3 are the same and E2 is different. Thus, the Pilot 1 flight director data can be lumped, and there are some interpilot differences.

31

Comparing the instrument 2 dwell times between the manual ILS and flight director configurations shows the manual ILS to be less than the latter at a very high level of significance. The flight director dwell time variances are much greater than those for the ILS configuration, also. The results are illustrated by the average histograms of Fig. 7.

Percent of
Fixations

CONFIGURATIONS C AND D, MANUAL ILS

$\overline{T}_{d_2} = .775$
$\sigma_{T_2} = .36$

CONFIGURATIONS E AND F, FLIGHT DIRECTOR

$\overline{T}_{d_2} = 1.62$
$\sigma_{T_2} = 1.66$

Dwell Interval,(sec)

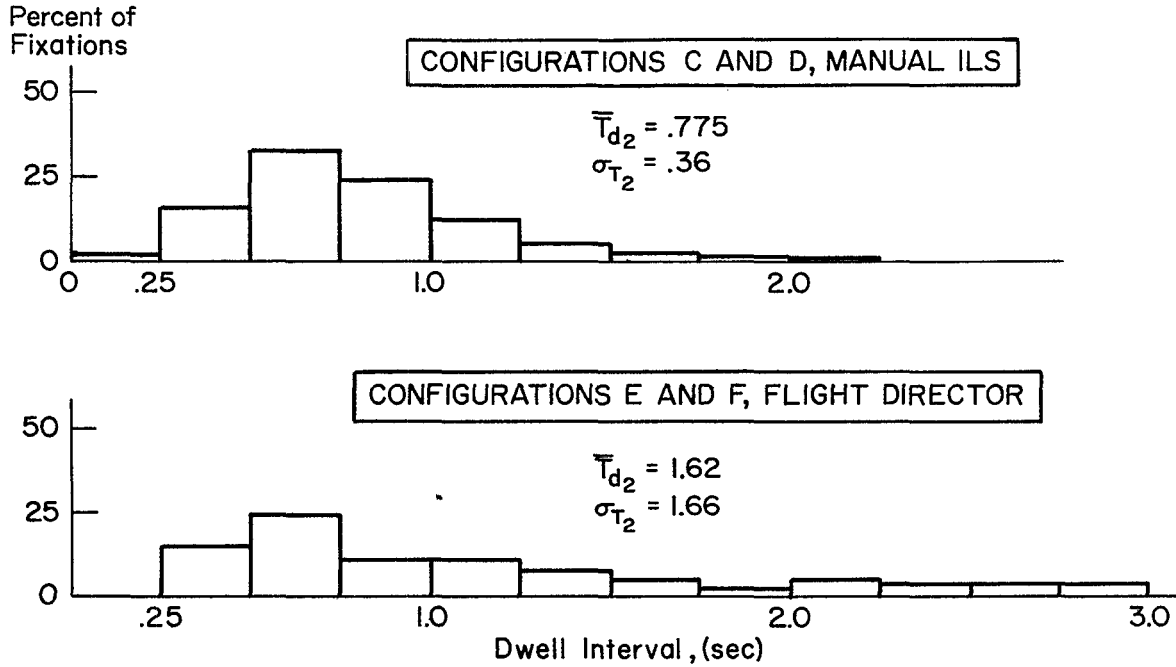Figure 7. Attitude Instrument Dwell Times for Pilot 1

The comparisons for the HSI/GSD instrument (No. 5) with the manual ILS configuration are given in Table VII. The B configurations are mixed.

TABLE VII

MEAN DWELL TIME COMPARISON; INSTRUMENT 5,
MANUAL ILS CONFIGURATION

EFFECT OF CONFIGURATION	EFFECT OF PILOT
B1 $\doteq$ C1	B1 > B2
C1 > D1	C1 $\doteq$ C2
B2 < C2	D1 < D3

Configurations C1, C2, and D3 are alike while D1 is significantly less. The dwell time variances for B, C, and D are homogeneous except B1 and C1 are greater than the others while the B2 variance is significantly less.

The comparisons for the HSI/GSD instrument with the flight director configuration are given in Table VIII. Here, the range-varying case has

TABLE VIII

MEAN DWELL TIME COMPARISON; INSTRUMENT 5,
FLIGHT DIRECTOR CONFIGURATION

EFFECT OF CONFIGURATION	EFFECT OF PILOT
E1 > F1	E1 ≐ E2
	F1 ≐ F3

shorter dwell times, but there are no interpilot differences. The dwell time variances for these runs are scattered, i.e.,

$$\sigma_{E1}^2 > \sigma_{E2}^2$$
$$\sigma_{F1}^2 < \sigma_{F3}^2$$
$$\sigma_{E1}^2 > \sigma_{F1}^2$$

The Pilot 1 difference is in the same direction as the mean.

The mean dwell times on the HSI/GSD instrument (No. 5) for the flight director runs are less than the manual ILS runs at a high level of significance. The dwell time variances in the flight director runs are much less, also. This is consistent with the attitude instrument (No. 2) result, of course, since instruments 2 and 5 are primary and they share most of the scanning workload.

Changes in configuration involving fixed range versus varying range on the glide slope deviation have a significant effect on the HSI/GSD instrument dwell time as shown by the Pilot 1 data in Tables VII and VIII. This may correlate with the larger glide slope deviations (per unit altitude

33

error) which occur as range decreases. None of the other-instrument dwell times showed a fixed versus varying range effect. Closer examination of the Pilot 1 dwell times on the HSI/GSD instrument indicates the following rank order (all differences are significant at the 95 percent level).

$$C1 > D1 > E1 > F1$$

This result is illustrated by the average dwell time histograms in Fig. 8.

6. Scanning Workload

The dwell fraction, η_i, also called the fractional scanning workload, is the fraction of time during a run that the pilot is looking at that instrument. Average values for each instrument with each subject/ configuration are given in Table III. Tests of significance were not made but certain trends are obvious:

- The dwell fraction on peripheral instruments varies from run to run but there are no clear differences between pilots or configurations.

- The dwell fraction on peripheral instruments is much less than that on the primary instruments (by definition!)

- The dwell fractions on the attitude and HSI/GSD instruments are about equal with the manual ILS configurations.

- The dwell fraction on the attitude instrument is much larger with the flight director configurations than with the manual ILS ones.

- The dwell fraction on the HIS/GSD instrument goes way down when the flight director is in use, and it becomes effectively a peripheral instrument.

These differences in scanning workload are due mainly to differences in dwell time, and to some extent changes in scan rate as shown in Table III. For example, the unusually low E2 scan rate combines with the unusually long mean dwell time on the attitude instrument to give the highest observed mean scanning workload.
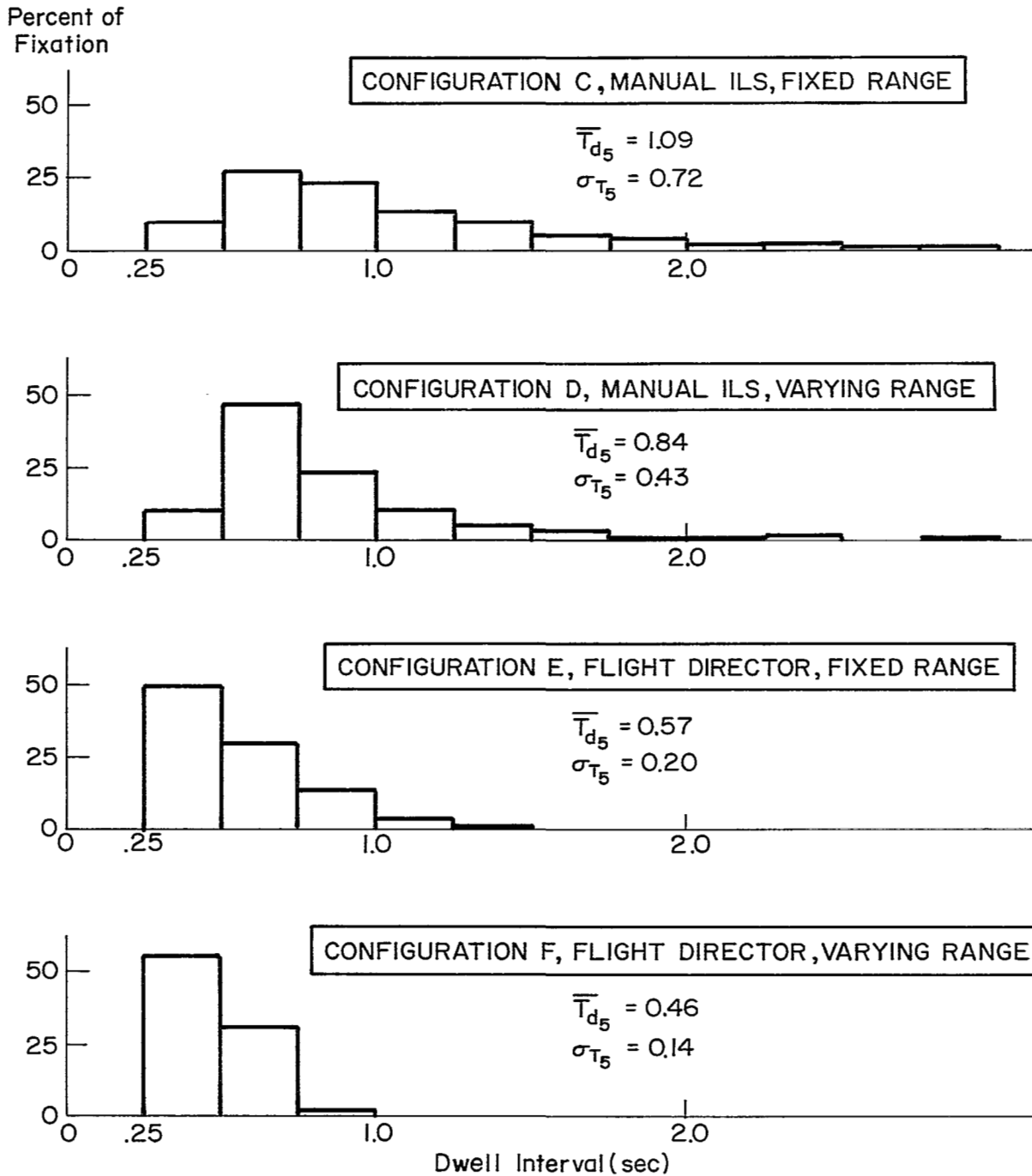
34

Figure 8. HSI/GSD Instrument Dwell Times for Pilot 1

C. ONE WAY LINK VALUES

The "one way" link value, q_{ij}, is the fraction of all real fixation transitions that go from instrument i to j. The fraction of fixation transitions in the opposite direction is q_{ji}. The sum $q_{ij} + q_{ji}$ is the "two way" link value and represents the fixation transitions between points i and j. Fitts, Jones, and Milton (Ref. 2) hypothesized that the link values between instruments are indicative of the goodness of panel arrangements. If the pilot is stationary over a run, one way link values are also indicative of dominant scan patterns.

The observed eye point of regard data have been reduced to show one way link values, and to determine the one and two way differences. Appendix E contains the link transition matrices for each of the pilot/configuration cells in Table II. Each matrix represents a lumping of replications. These results show that the major differences in transitions occur in going from the manual ILS task to the flight director task. There are also some differences between pilots in the manual ILS task.

Typical link vectors for Pilot 1 in the manual ILS and flight director tasks are compared in Fig. 9. The width of the link vector represents its magnitude, and the diameters of the shaded instrument centroids represent the dwell fraction. The sum of the dwell fractions is less than one due to blinks. The data show no dominant circulation of scanning, and the one way link values are approximately equal. The flight director task has a more evenly distributed percentage of scans to secondary instruments, although a high percent of time was spent on the attitude/flight director indicator. There were very few (i.e., < 1 percent) link transitions across instruments indicating the primary instruments were centrally located.

D. PERFORMANCE MEASURES

Mean square values of important response signals were computed. Particular attention was paid to the longitudinal stimuli, pitch attitude and glide slope deviation error, and elevator response. These are discussed below.
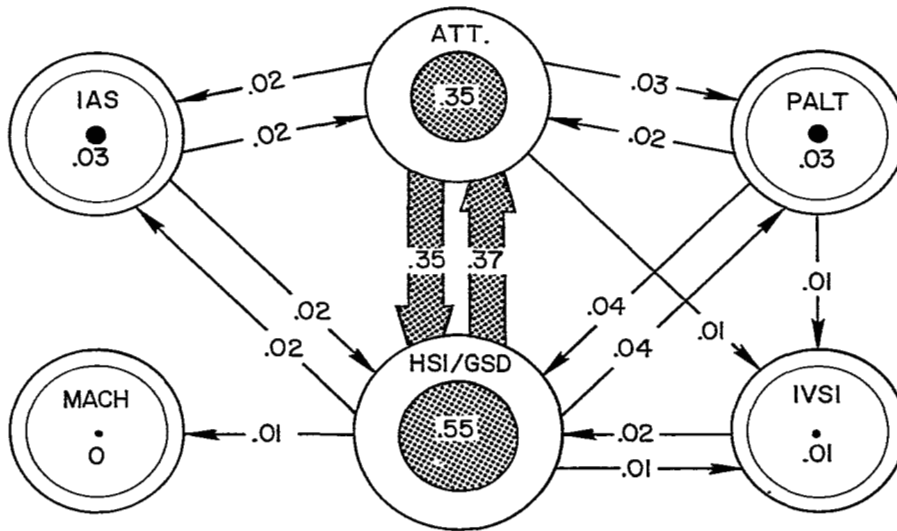
Manual ILS CONFIGURATION, CI
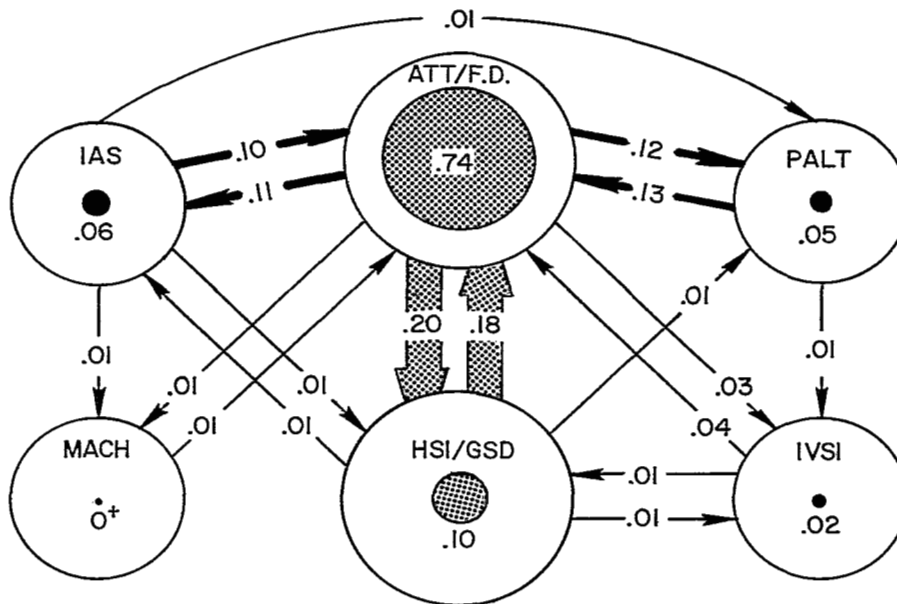
Flight Director Configuration, EI

Figure 9. Typical Transition Link Vectors
and Dwell Fractions

37

The root mean square glide slope errors for Configurations B, C, and D are given in Fig. 10. Run 27-3 is anomalous, because the pitch attitude and glide slope forcing functions were inadvertently (almost 50 percent) too large. Assuming a glide slope error signal bandwidth of about 0.3 rad/sec gives 10 degrees of freedom in a 100 sec run, and permits tests of significance using the F-distribution. Paired comparisons showed no significant differences* over pilots and configurations (B, C, and D). Their overall average is significantly greater than the glide slope deviation forcing function as shown in Fig. 10.

The rms glide slope errors for the flight director configurations are plotted in Fig. 11. The bandwidth is assumed to be 0.3 rad/sec. Run 27-5 is significantly larger than the others, but this may be associated with the pilot's use of unusually large throttle corrections during this run. Paired comparisons on the remaining points show no significant differences, with the possible exception of F3 which is borderline at the 95 percent level.

The nondifferent E and F mean square values were lumped and compared with the lumped B, C, and D results. The flight director runs had significantly lower glide slope deviation error than do the manual ILS runs. This correlates with the scanning statistics on instrument 2 which show that the look rates are higher and the dwell times are longer (larger dwell fraction) with the flight director configurations.

The rms pitch attitude errors are plotted in Figs. 12 and 13. Assuming a signal bandwidth of about 1.5 rad/sec gives 50 degrees of freedom per run and permits tests of significance.

The C1 data in Fig. 12 show a significant increase in error during a session (e.g., 19-4, 10, 11), but no apparent day to day differences; i.e., it starts at a lower level on a different day and progresses. Other configurations and subjects don't show this within-session trend. The C1,

_____

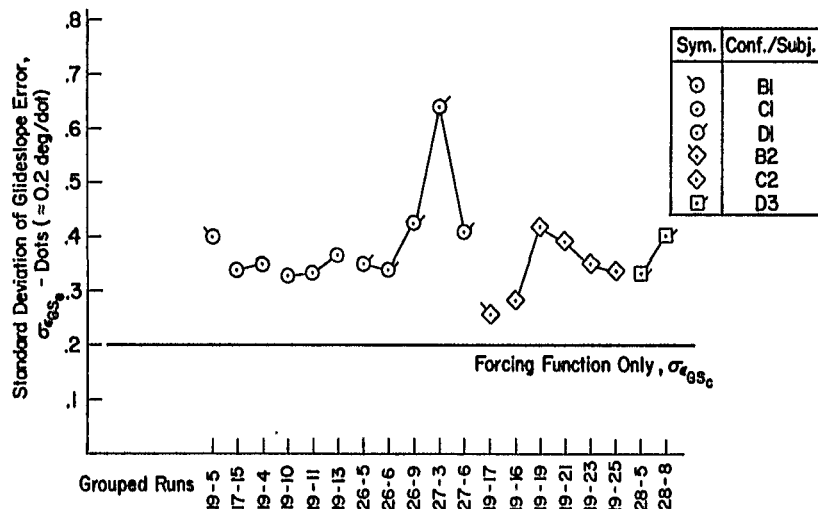*The 95 percent confidence level is used in all significance tests unless otherwise noted.

Figure 10. Glide Slope Performance with Manual ILS Configurations
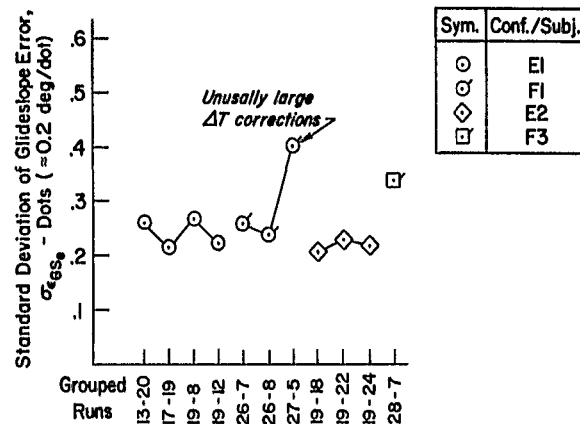

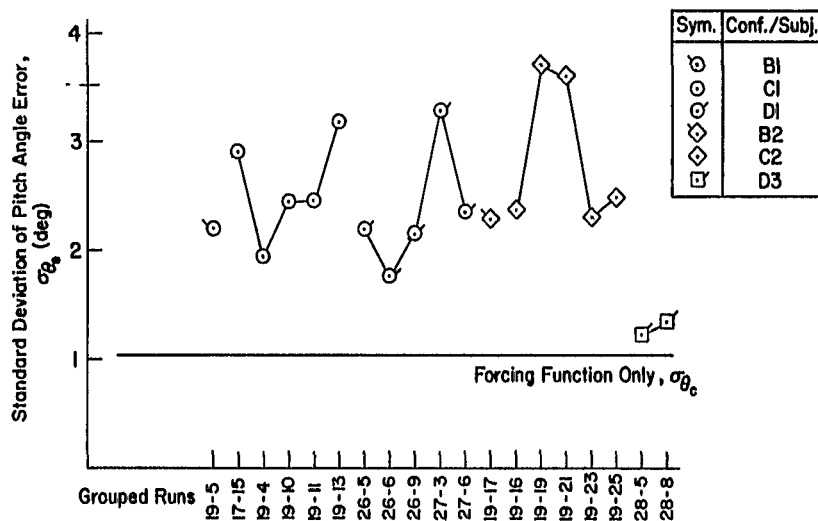Figure 11. Glide Slope Performance with Flight Director Configurations

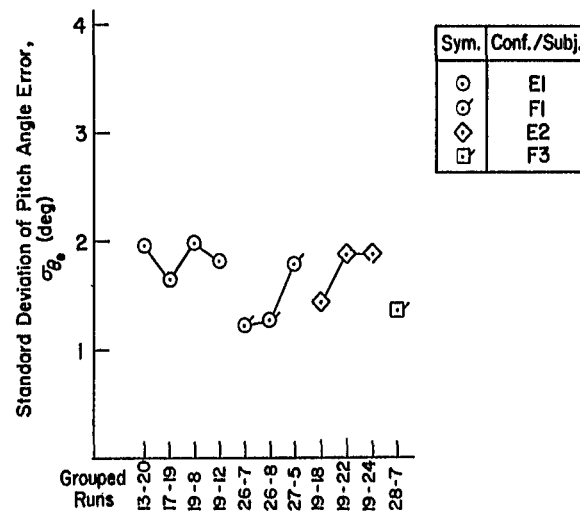Figure 12. Pitch Attitude Performance with Manual ILS Configurations

Figure 13. Pitch Attitude Performance with Flight Director Configurations

D1, and C2 data show run to run scatter which tends to mask differences between subjects and configurations. The D3 pitch attitude errors are significantly smaller than the others, reflecting a difference in Pilot 3.

Paired comparisons of the flight director pitch attitude errors in Fig. 13 show one or two significant differences but no trends. The E and F data are generally the same.

The manual ILS and flight director pitch attitude results can be compared using Pilot 1 data. C1 and D1 are significantly larger than E1 and F1. This is the same difference that occurred with glide slope deviation errors.

Mean square measures of elevator response, $\overline{\delta_e^2}$, were computed. Detailed comparisons were not made, but the flight director runs generally had larger values than the manual ILS runs. The run to run variation in $\overline{\delta_e^2}$ correlates better with $\overline{\theta_e^2}$ variations than with $\overline{\epsilon_{GS_e}^2}$. This is not unexpected, since $\theta \longrightarrow \delta_e$ is the dominant inner loop.

Mean square elevator and aileron were cross plotted for the various runs. There was no particular correlation between the two, indicating that crosstalk between the axes of control was small, as expected.

E. COMPARISONS WITH OTHER EYE SCANNING DATA

The largest and most thorough data on pilot eye movements were collected by Fitts, Milton, Jones, McIntosh, and Cole in a continuing program from 1949 to 1952. The Fitts data were obtained from eye camera films of 40 subjects in a C-45 aircraft. Of the eight individual reports, four were concerned with routine IFR flying, and four with the landing approach phase. These four studies are listed as Refs. 2 to 5, respectively.

Similar, but more recent, measurements have been made by Senders in Ref. 12, utilizing electro-oculograms (EOG) of three subjects in a fixed base simulator. The panel arrangement was identical to the standard instrument arrangement used by Fitts in Refs. 2 and 3 and shown in Fig. 14.
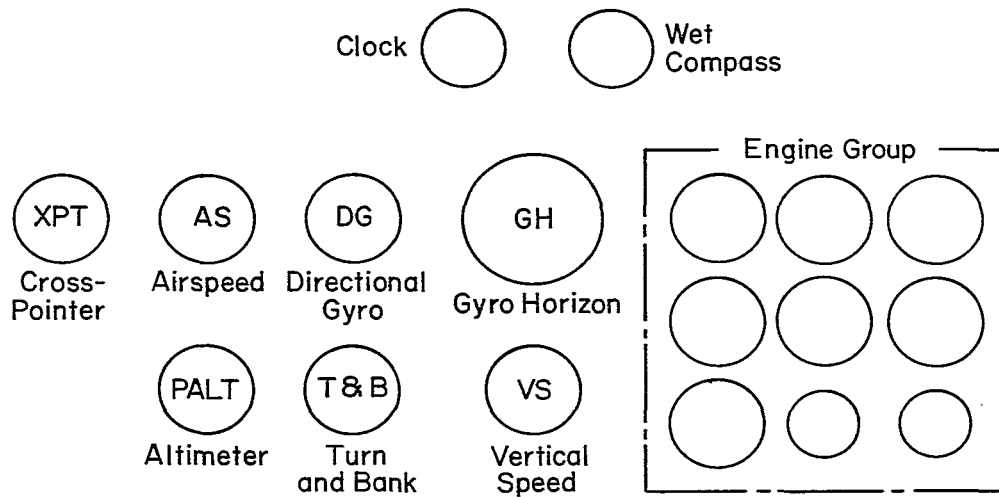
Figure 14. Standard Instrument Arrangement Used
by Fitts (Refs. 2 and 3) and Senders (Ref. 12)

An experimental panel used by Fitts in Refs. 4 and 5 is shown in
Fig. 15 and more nearly resembles the panel arrangement used in this
program. Neither Fig. 14 or 15 is similar to the DC-8 panel used in
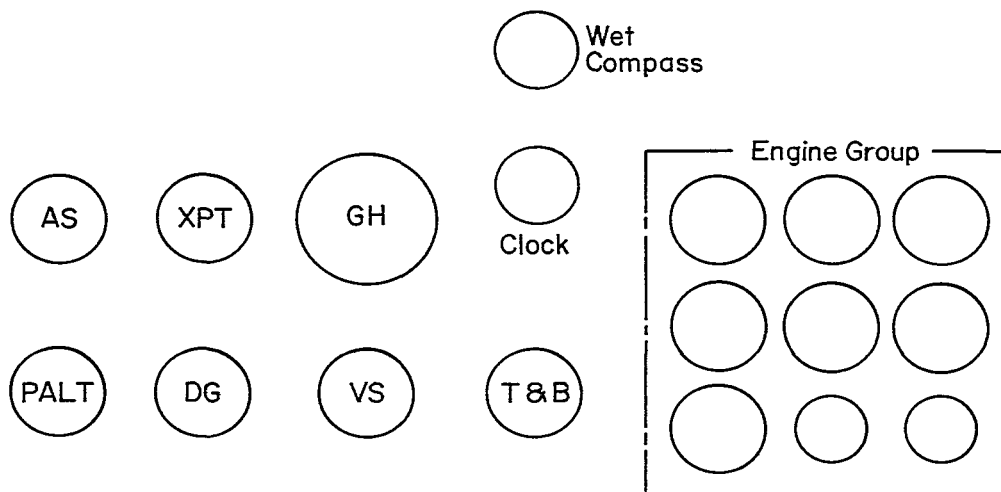this program.

Figure 15. Experimental Instrument Arrangement
Used by Fitts (Refs. 4 and 5)

The last report of the Fitts series (Ref. 6) was concerned with flight director* approaches. Measurements were made of 10 pilots who each flew one approach from the rear seat of a T-33 aircraft. The flight director indicator was a separate instrument as can be seen from Fig. 16. With this exception the panel was very similar to the experimental instrument arrangement of Refs. 4 and 5.
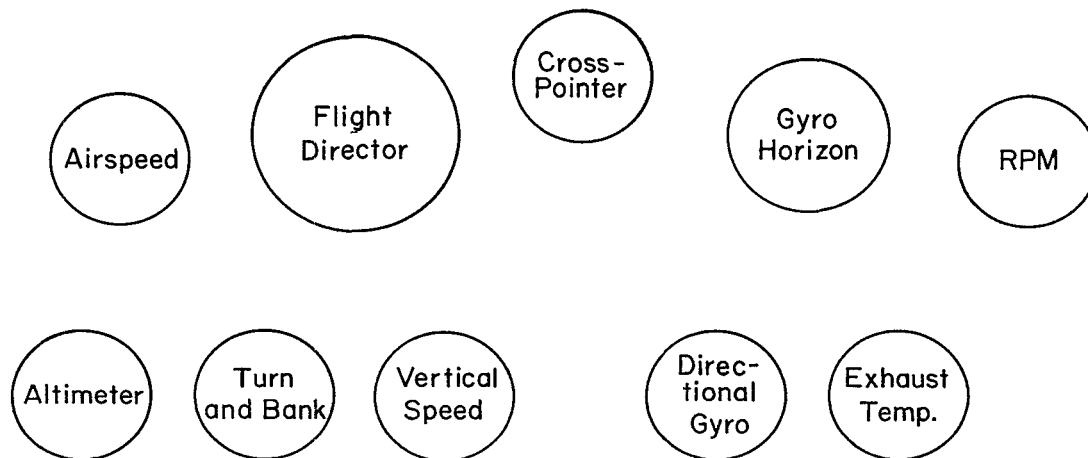
Figure 16. Panel Arrangement Used by Fitts (Ref. 6) for Flight Director Approaches

Table IX compares dwell fractions from Fitts (Refs. 2 and 4) and Senders with those from the DC-8 simulation. Since these past data do not include flight director approaches, only Configurations C and D are used. The individual dwell fractions of the directional gyro display and the cross-pointer display for the past data were summed to compare with the dwell fractions for the integrated HSI/GSD display in the STI data. The sum of the dwell fractions (workload) on instruments in these tables is less than unity; due to blinks (and looks at 4) in the STI data, and because other (noncomparable) instruments were present in the other data. The comparison of available mean dwell times is presented in Table X.

---

*Zero reader.

TABLE IX

COMPARISON OF DWELL FRACTIONS WITH PAST DATA

INSTRUMENT	DWELL FRACTION			
	STI*	SENDERS[†] (REF. 12)	FITTS[‡] (REF. 2)	FITTS[‡] (REF. 4)
ATTITUDE	.438	.282	.15	.11
HSI/GSD	.472	.445	.655	.650
PALT	.018	.070	.02	.02
AS	.020	.073	.10	.07
IVSI	.035	.128	.05	.05

*Average of 3 pilots (Configurations C and D)
[†]Average of 2 pilots (Phase III)
[‡]Average of 40 pilots (instrument low-approaches)

TABLE X

COMPARISON OF MEAN DWELL TIMES WITH PAST DATA

INSTRUMENT	MEAN DWELL TIME (SEC)	
	STI*	FITTS (REF. 4)
ATTITUDE	.85	.37
HSI/GSD	.96	XPT .76 DG .54
PALT	.43	.38
AS	.70	.49
IVSI	.43	.39

*Weighted average of 3 pilots (Configurations C and D)

The two way link values for the weighted average of the three pilots in Configurations C and D is shown in Table XI along with the experimental panel results of Fitts (Ref. 4). Since the number of instruments differed a direct comparison is not meaningful, however, the primary link in the Fitts data is XPT-DG which is the currently integrated HSI/GSD display. Combining the second largest link, XPT-GH, with the XPT-DG would approximate the current HSI/GSD-ATT link value.

TABLE XI

COMPARISON OF AVERAGED TWO WAY LINK VALUES

STI		FITTS (REF. 4)	
LINK	VALUE	LINK	VALUE
HSI/GSD-AS	.03	XPT-AS	.10
HSI/GSD-ATT	.77	XPT-GH	.22
HSI/GSD-PALT	.04	XPT-PALT	.02
HSI/GSD-IVSI	.04	XPT-VS	.04
ATT-AS	.04	XPT-DG	.31
ATT-PALT	.04	GH-AS	.02
ATT-IVSI	.02	GH-ALT	<.02
AS-IVSI	0	GH-VS	.02
AS-ALT	0	AS-PALT	.02
		AS-DG	.02
		GH-DG	.06
		VS-DG	.05
		PALT-DG	.02

Tables IX, X, and XI serve to compare rather than evaluate the data. There are many differing factors in the three sets of data which would influence the results. For example, the gyro horizon was just replacing the "needle-ball-airspeed" technique during the period of Fitts' studies. The current technique supported by nearly all pilots rests primarily on attitude control and therefore has a higher fractional workload and associated dwell time. The peripheral instruments (i.e., PALT, IVSI) are comparable and do show similar workloads and dwell times.

44

The scanning rates should be heavily influenced by the vehicle dynamic properties, stability and responsiveness. For the same dwell time the scanning workload will be directly proportional to the scan rate (i.e., $\omega_{s_i} = \overline{T_{d_i}}\,\overline{f_{s_i}}$). Additional factors noted by Fitts as having a significant effect on the dwell time and fraction were interpilot differences, day versus night operation, and manual ILS versus ground controlled approaches (GCA).

The GCA data is compared in Refs. 3 and 5 for the standard and experimental panel arrangements, respectively. Table XII summarizes the Ref. 3 results. This shows that the glide slope-localizer pointers were not looked at during the entire approach. The engine instruments and turn and bank indicator were not included in the Table XII data.

TABLE XII

RESULTS FOR NIGHT GCA APPROACHES IN C-45 (FITTS, REF. 3)

INSTRUMENT	DWELL TIME (SEC)	DWELL FRACTION	TWO-WAY FRACTIONAL LINK VALUES	
AS	.57	.17	AS-DG	.29
DG	.90	.50	AS-GH	.06
GH	.56	.19	AS-ALT	.04
PALT	.39	.03	AS-VS	.02
VS	.47	.05	DG-GH	.31
XPT	0	0	DG-ALT	.04
			DG-VS	.05
			GH-ALT	.01
			GH-VS	.05
			ALT-VS	.01

The flight director data of Ref. 6 is shown in Table XIII with those obtained from the DC-8 simulation (Configurations E and F combined). The dwell fractions (fractional scanning workload) can be added and as such compare very closely with the current attitude/flight director result.

45

TABLE XIII

COMPARISON OF FLIGHT DIRECTOR EYE TRAFFIC WITH PAST DATA

INSTRUMENT	DWELL FRACTION		MEAN DWELL TIME (SEC)		SCAN RATE (LOOKS/SEC)	
	STI	FITTS (REF. 6)	STI	FITTS (REF. 6)	STI	FITTS (REF. 6)
[FLIGHT DIRECTOR] ATTITUDE	.77	.64 .13	1.94	1.29 .48	.40	.50 .27
[LOCALIZER/ GLIDE SLOPE] HEADING	.095	0 .01	.52	.25 .50	.18	.022 .02
AIRSPEED	.055	.09	.55	.52	.11	.168
VERTICAL SPEED	.02	.02	.44	.45	.04	.049
ALTIMETER	.04	.01	.40	.42	.10	.037
MISC.	.02	.10	—	—	.06	.46

Mean dwell times, a parameter likely to be independent of vehicle charac-
teristics, exhibits the same trends between instruments and possibly exhibits
an additive property for integrated displays. The total scan rate in the
Ref. 6 study was 92/min or 1.53/sec. This compares to the .89/sec in the
DC-8 study. The scan rates show the flight director receives the most
frequent looks. The large number of miscellaneous scans in the Ref. 6 data
was due mainly to unresolved looks. It also included looks at the rpm, exhaust
temperature, and turn and bank indicators, blinks and looks at switches. The
relevant data comparison is consistent.

The link values recorded in Ref. 6 support the finding that the one-way
links between pairs of instruments are approximately equal, and that the
flight director is the center of attention. Table XIV presents the link
values between pairs of instruments, disregarding the values less than
2 percent. The STI data are for Configurations E and F combined.

TABLE XIV

COMPARISON OF AVERAGED TWO-WAY LINK VALUES WITH PAST DATA
WITH FLIGHT DIRECTOR DISPLAYS

| INSTRUMENT LINKS	STI	FITTS (REF. 6)
FD-ATT	Integrated	.38
FD-AS	.24	.24
FD-PALT	.21	.04
FD-VS	.07	.05
FD-RPM	0	.06
ATT-RPM	0	.03
FD-T&B	0	.03
FD-HSI/GSD	.41	<.02

F. DETAILED FEATURES OF THE EPR DATA

1. Artifacts and Details

Several fundamental eye movement artifacts were observed in addition
to the desired dwell properties. These include details related to transitions
between instruments, looks within an instrument, and blinks. Figure 17 shows
typical horizontal and vertical EPR recordings at slow and high paper speeds
in which these three features are apparent.

Transition times were taken as the 10-90 percent rise time in a look
from one instrument to another. This typically was between .05 and .1 sec
±.01 sec for all subjects. The transitions were slightly (i.e., approximately
.01 sec) slower in the vertical direction than in the horizontal. This is
most likely due to the eyelid response from which the vertical motion is
detected.

On many runs the EPR system was calibrated such that it was able to
detect 1 deg to 2 deg changes in eye movement. On instrument 2 for example,
it was possible to distinguish looks between the pitch bar and the bank angle
sky pointer. On the HSI/GSD display, instrument 5, the glide slope bar could
be distinguished from the heading bug.
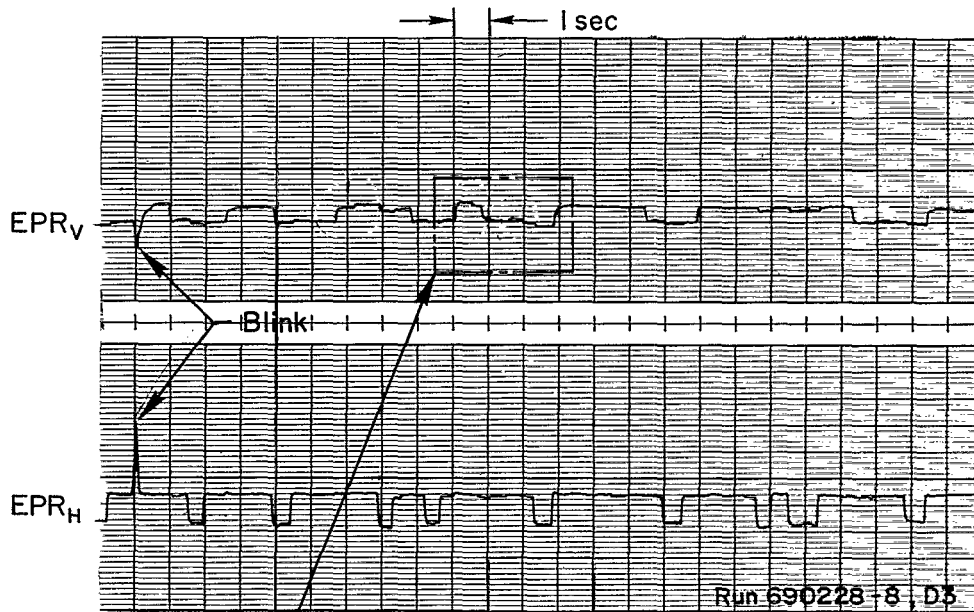
a) Slow Paper Speed
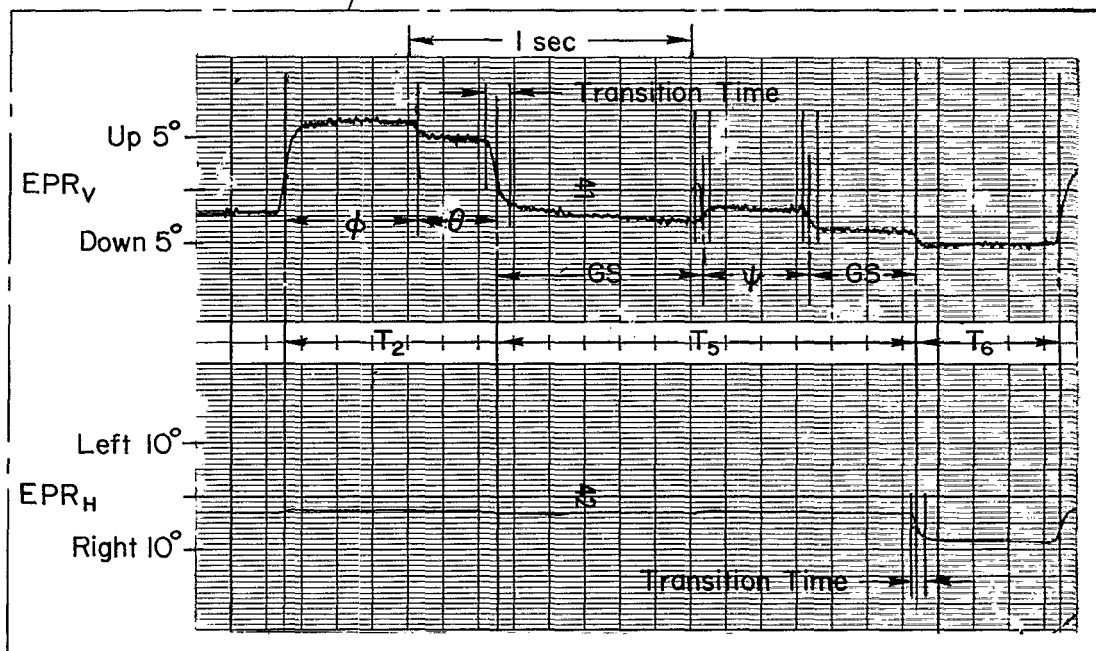
b) Fast Paper Speed, Expanded Scale

Figure 17. Detailed Features of EPR Data

48

Blinks are easily distinguishable artifacts. The interruption time may not be equal to the blink time, because the vertical motion sensor uses the eyelid. The mean blink time was .27 sec and typical within-run standard deviations varied from .07 sec to .25 sec for different subjects. It has been found in some subjects that the eyelid lag can completely mask the true vertical motion. There will be some horizontal voltage change for a purely vertical eye movement, because the infrared sensors cannot be located exactly on the iris periphery. This artifact is called crosstalk and can be used to check the eyelid tracking ability.

One additional artifact resembling a blink but of significantly shorter duration was attributed to eyeball saccades. The saccades were less than or equal to .1 sec and were not removed from the dwell time data. The saccade time was equally distributed to adjacent dwells.

2. Dwell Time Quantization

Some of the manual ILS data for Pilot 1 were quantized into .05 sec intervals to determine if there was any tendency for the dwell times to be multimodally distributed (bunched at discrete durations). The results are shown in Fig. 18 for the attitude indicator and the horizontal situation indicator.

These distributions are similar to the ones obtained for the coarser intervals and do not exhibit any particular multimodality. These and other distributions were generally limited to a minimum value of about .25 sec with a positive skewness. The individual runs did not appear to differ significantly from the pooled results.
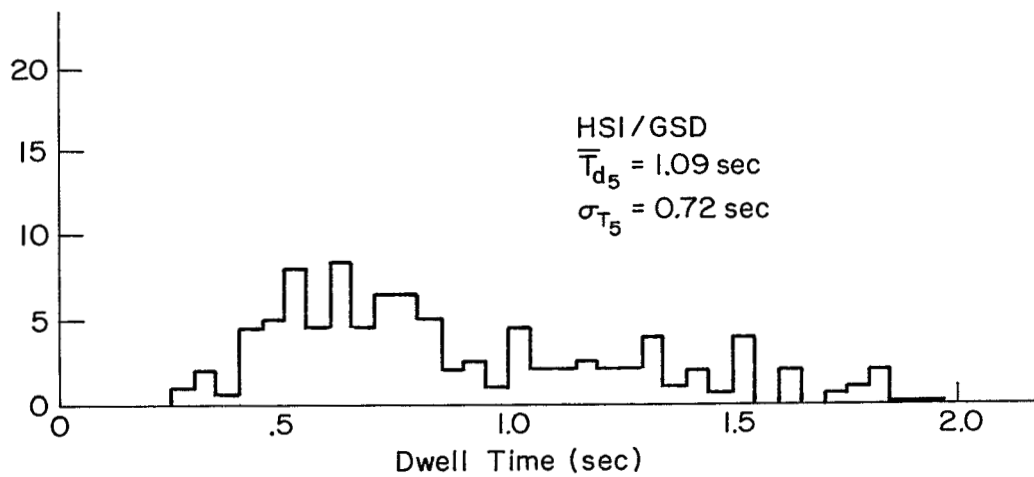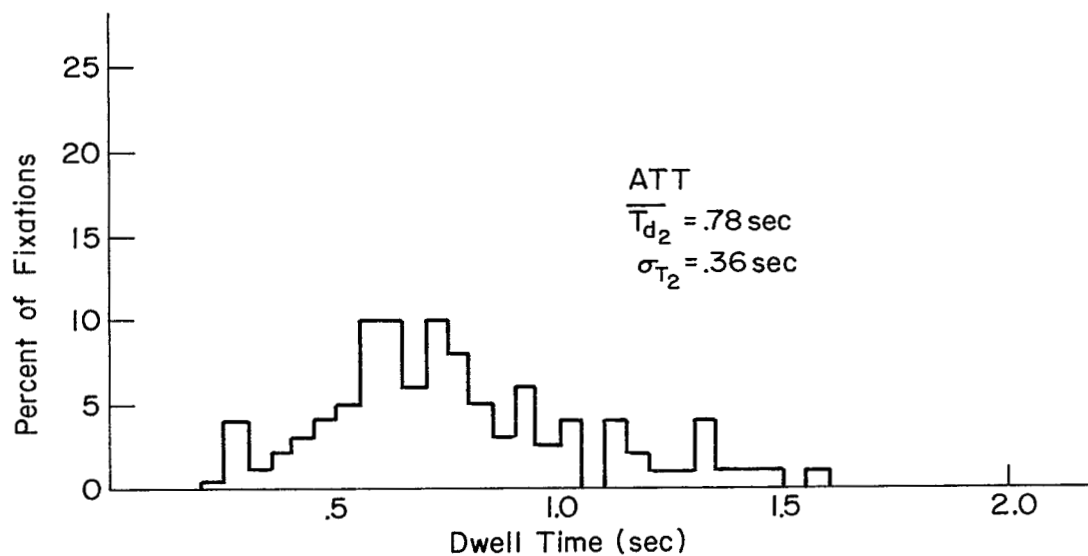
Figure 18. Finely Quantized Dwell Time Histograms

SECTION IV

SUMMARY AND CONCLUSIONS

The major conclusions of the phase of the program described in this report relate to the utility of the eye point of regard system and to the eye scanning traffic results. These reduced data are in a form suitable for correlation with the simultaneously recorded pilot and system response.

A. EYE POINT OF REGARD SYSTEM

The EPR system worked satisfactorily throughout these experiments. Six of the seven subjects were able to wear it without discomfort for periods of half an hour. The seventh had a dental problem and could not hold the head movement device. The pilots felt they could wear it for in-flight measurements. Once fitted, it could be reinstalled and nulled in about 5 min. Observed performance attributes included:

- Drift-free operation for 2 min
- Always resolved looks between instruments (3 deg to 5 deg), and frequently resolved looks within a single instrument (1 deg to 2 deg).
- Produced vertical and horizontal coordinates suitable for direct entry into a digital processor.

The unit experienced only one failure in 3 months of almost daily operation, during which time well over one hundred 2 min runs were made.

B. MEASURED SCANNING TRAFFIC

The scanning traffic includes individual instrument dwell properties and scanning among the instruments.

1. Stationarity

The scanning data during the range-varying runs were examined for statistical stationarity. No systematic differences were found in successive 33 sec intervals.

2. Look and Scan Rates

Look rates involve the scanning frequency on a given instrument while scan rates involve the entire panel. The results show:

- The attitude or attitude/flight director instrument (No. 2) look rates are generally the same over all pilots and configurations.

- The HSI/GSD instrument (No. 5) look rates are significantly lower for flight director than manual ILS runs.

- The peripheral instrument look rates are scattered and show no strong trends.

- The all-instrument scan rates are significantly greater for the manual ILS runs than for the flight director runs.

These results correlate with the dwell time and workload results summarized below.

3. Peripheral Instrument Dwell Times

The dwell time is the average length of one instrument fixation. The peripheral instrument results show:

- Mean dwell times on the altimeter instruments (No. 3) and IVSI (No. 6) are homogeneous over all pilots and configurations, and are not significantly different from one another. The mean is .42 sec.

- The mean dwell times on the airspeed instrument (No. 1) are homogeneous over all pilots and configurations, and their average ($\overline{T}_{d_1} = .64$ sec) is significantly greater than the other peripheral instruments (3 and 6).

There is no evidence of quantization in the individual dwell times.

4. Primary Instrument Dwell Times

The dwell time results on the attitude gyro (No. 2) and the HSI/GSD (No. 5) for the various pilots and configurations show:

52

- Mean dwell times on the attitude and HSI/GSD
  instruments for Configuration B are often
  different from C and D, indicating that the
  additional lateral axes of control have an
  effect with some pilots. Recall that bank
  angle is on 2 and localizer deviation and
  heading are on 5.

- Differences between fixed and varying range
  had no effect on the attitude instrument dwell
  times for either the manual ILS or flight
  director configurations. Intrapilot data
  on similar configurations can be lumped.

- Fixed versus varying range had a significant
  effect on the HSI/GSD instrument dwell times
  for both manual ILS and flight director con-
  figurations. In each case the varying range
  version had a shorter mean dwell time.

- The mean dwell times on attitude instrument
  with the manual ILS configurations are less
  than with the flight director at a very high
  level of significance. The dwell time variances
  are also much less.

- The dwell times on the HSI/GSD instrument show
  the opposite trend. The manual ILS means are
  greater than the flight director means at a high
  level of significance, as are the dwell time
  variances.

- These results are consistent, because attitude and
  localizer/glide slope are primary and share 80-90 per-
  cent of the scanning workload.

- Interpilot differences in mean dwell time on the
  primary instruments often occurred. These were
  most pronounced on the attitude instrument with
  the manual ILS configuration, and did not occur
  at all on HSI/GSD instrument with the flight director.

5. Fractional Scanning Workload

The dwell fractions (percent of time fixating) on the attitude
instrument are much larger with the flight director than with the manual
ILS configurations. In the flight director configurations, the HSI/GSD
instrument workload goes way down and it becomes essentially a peripheral
instrument.

6. Transition Links

There is a big difference between the manual ILS and flight director configurations, related to the big difference in scanning workload. The manual ILS results have dominant links from attitude to HSI/GSD and back. The flight director links appear more "scattered," because these central links are relatively smaller. The one-way link vectors are about equal in opposite directions (e.g., 2 to 5 $\doteq$ 5 to 2) so that two-way links can be used. This is closely related to the observation that the scan patterns show no strong evidence of "circulation."

C. PERFORMANCE MEASURES

Mean-square values of system errors and control actions for the various runs show the following:

- Glide slope deviation errors are about the same over the split-axis and manual ILS configurations (B, C, and D).

- The glide slope deviation errors are about the same over the flight director configurations (E and F).

- The glide slope errors with the flight director are less than with the manual ILS configurations.

- The glide slope deviation errors are larger than the glide slope command in all cases.

- The pitch attitude errors are less with the flight director than with the manual ILS configurations.

- The mean square elevator activity is greater with the flight director.

D. COMPARISONS WITH OTHER DATA

The current eye scanning data (dwell times and fractional scanning workload) are generally consistent with the results of prior research (e.g., Fitts, et al; and Senders) where meaningful comparisons can be made.

Most of the Fitts and Senders data were taken with the then standard panel, which differs from the current T-layout. Nevertheless, their results can be compared with current nonflight director data. The STI data show a larger dwell fraction on the gyro horizon than past data. The dwell fraction for the HSI/GSD instrument in the STI data is less than the lumped dwell fraction for directional gyro and crosspointer in either the Fitts or Senders results. There are only minor differences in other dwell fractions. The dwell times are similar among respective peripheral instruments and between the then primary and the current primary displays. Differences in dwell fraction can be attributed to differences in panel arrangement, and to the evolution of a pilot technique using attitude control.

Fitts also studied an experimental panel with crosspointer and gyro horizon instruments in the center, adjacent to a flight director instrument. His dwell fraction data agree well with the present (flight director configuration) data for most instruments. The exception is that the STI data show a larger dwell fraction on HSI/GSD than does the sum of his crosspointer and DG data. The respective dwell times are comparable.

The comparison of link values between past and present data is not too meaningful, because the major link in the Fitts data (FD-ATT), for example, is now eliminated with a combined instrument.

REFERENCES

1. McRuer, Duane, Henry R. Jex, Warren F. Clement, and Dunstan Graham, *Development of a Systems Analysis Theory of Manual Control Displays*, Systems Technology, Inc., Tech. Rept. 163-1, Oct. 1967.

2. Milton, J. L., R. E. Jones, and P. M. Fitts, *Eye Fixations of Aircraft Pilots: Frequency, Duration, and Sequence of Fixations When Flying the USAF Instrument Low Approach Systems (ILAS)*, USAF Tech. Rept. No. 5839, Oct. 1949.

3. Fitts, P. M., R. E. Jones, and J. L. Milton, *Eye Fixations of Aircraft Pilots: Frequency, Duration, and Sequence of Fixations When Flying Air Force Ground Controlled Approach System (GCA)*, AF Tech. Rept. No. 5967, Feb. 1950.

4. Milton, J. L., B. B. McIntosh, and E. L. Cole, *Eye Fixations of Aircraft Pilots: Fixations During Day and Night ILAS Approaches Using an Experimental Instrument Panel Arrangement*, USAF Tech. Rept. 6570, Oct. 1951.

5. Milton, J. L., B. B. McIntosh, and E. L. Cole, *Eye Fixations on Aircraft Pilots: Fixations During Day and Night GCA Approaches Using an Experimental Instrument Panel Arrangement*, USAF Tech. Rept. 6709, Feb. 1952.

6. Milton, J. L., and F. J. Wolfe, *Eye Fixations of Aircraft Pilots: Fixations During Zero Reader Approaches in a Jet Aircraft*, WADC Tech. Rept. 52-17, Feb. 1952.

7. Clement, Warren F., Dunstan Graham, and John J. Best, *A Reexamination of Eye Movement Data*, Systems Technology, Inc., Tech. Memo. 163-A, 30 Nov. 1966 (revised 28 Feb. 1967).

8. Gainer, C. A., R. D. Monroe, J. E. Brown, et al, *All Weather Landing Simulation for Category III Airborne Configuration: Volume I. Summary of Studies on Flight Directors and Split Axis Control*, Bunker-Ramo Corp., July 1967.

9. Watts, A. F. A., and H. C. Wiltshire, *Investigation of Eye Movements of an Aircraft Pilot under Blind Approach Conditions*, College Note No. 26, the College of Aeronautics, Cranfield, May 1955.

10. Lennox, D., *Airline Pilots' Eye Movements During Take-off and Landing in Visual Meterological Conditions*, Aeronautical Research Lab. Human Engineering Note 15, Australian Defense Scientific Service, Aug. 1963.

11. Allen, R. W., W. F. Clement, and H. R. Jex, *Research on Display Scanning, Sampling, and Reconstruction Using Separate Main and Secondary Tracking Tasks*, Systems Technology, Inc., Tech. Rept. No. 170-2 (forthcoming).

12. Senders, John W., Jaime R. Carbonell, and Jane L. Ward, *Human Visual Sampling Processes: A Simulation Validation Study*, NASA CR-1258, Jan. 1969.

13. Stapleford, R. L., D. T. McRuer, and R. E. Magdaleno, "Pilot Describing Function Measurements in a Multiloop Task," *Second Annual NASA-University Conference on Manual Control*, NASA SP-128, 1966, pp. 181-204.

14. Stapleford, Robert L., Samuel J. Craig, and Jean A. Tennant, *Measurement of Pilot Describing Functions in Single-Controller Multiloop Tasks*, NASA CR-1238, Jan. 1969.

15. *DC-8 Flight Manual*, United Air Lines, 1 Sept. 1964.

16. *Application of Flight Inspection Tolerances When Using the Telemetering Theodolite*, Dept. of Transportation, Federal Aviation Admin., Order No. 8200.11A, 1968.

17. McRuer, Duane, Irving Ashkenas, and Dunstan Graham, *Aircraft Dynamics and Automatic Control*, Systems Technology, Inc., Tech. Rept. 129-1, Aug. 1968.

18. Stapleford, Robert L., Donald E. Johnston, Gary L. Teper, and David H. Weir, *Development of Satisfactory Lateral-Directional Handling Qualities in the Landing Approach*, NASA CR-239, July 1965.

19. Wright, Bruce R., and Margaret L. Brower, *Aerodynamic Damping and Oscillatory Stability in Pitch for a Model of a Typical Subsonic Jet-Transport Airplane*, NASA TN D-3159, Jan. 1966.

20. Weir, David H., *Compilation and Analysis of Flight Control System Command Inputs*, AFFDL-TR-65-119, Jan. 1966.
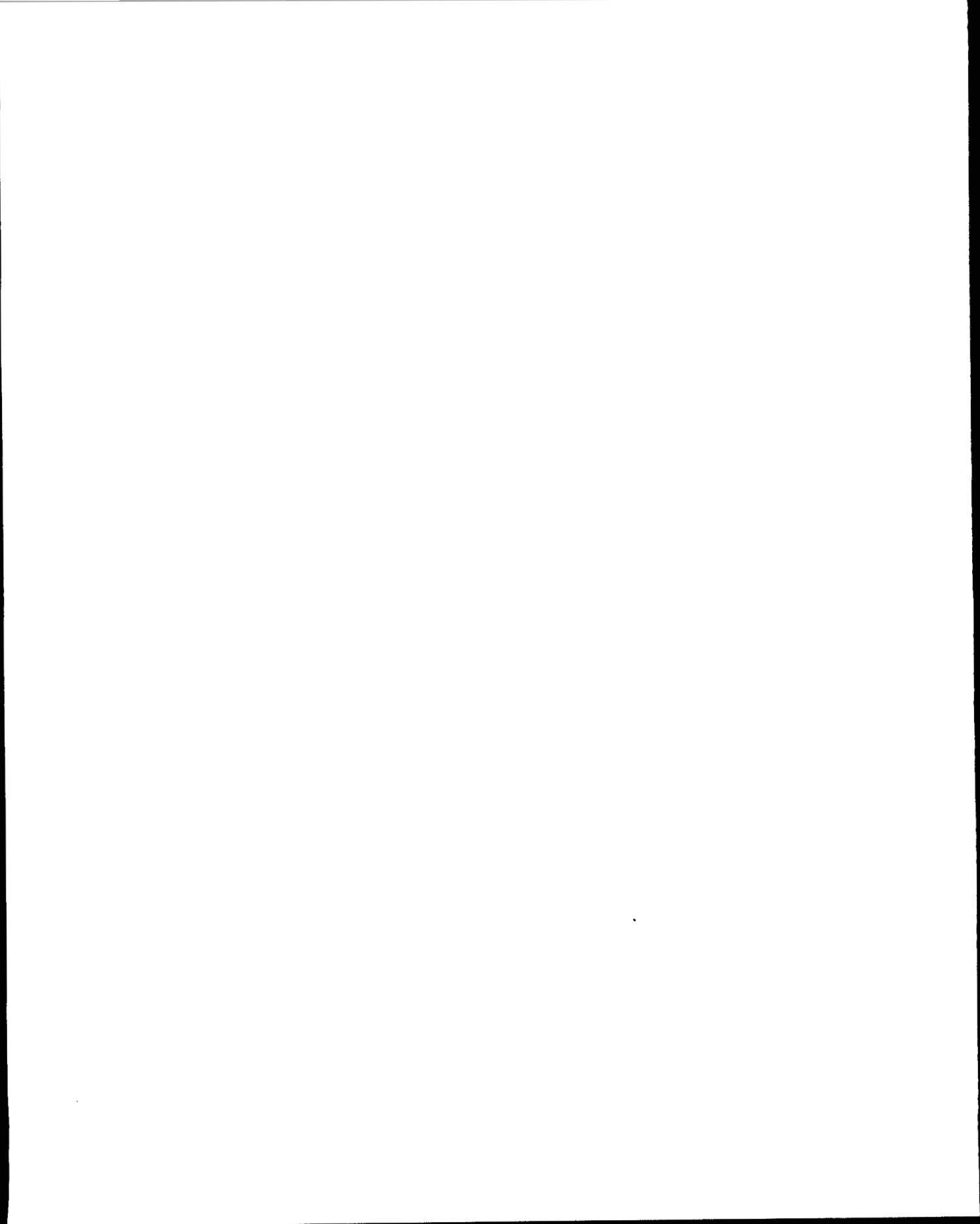
APPENDIX A

EQUIPMENT DESCRIPTION

OVERALL LAYOUT

The experiments were performed using the DC-8 Landing Simulator of the Man-Machine Integration Branch at NASA Ames Research Center. This facility is divided between two buildings; one housing the analog computing equipment, recorders and master control, and the other housing the fixed-base cockpit, visual display and instrument bays. The mechanizations, interconnects, etc., were set up by NASA at the outset and were simply utilized for these experiments.

The computer room is a fairly compact area focused around the AD-256 analog computer. All trunking to and from other equipment passes through selectable tie points on its console. Trunk lines, including communication, connect the simulator building, approximately 100 ft away, with the computer room. The instrument bay receives the analog signals inside the simulator building and drives the instruments in the cockpit another 100 ft away. The pilot completes the loop by actuating the controls which send signals back to the computer room.

COMPONENTS

The flow diagram and specific functions performed by the individual components are shown in Fig. A-1. A brief description of each component is given below.

Input Tape

The forcing functions and tracers presented to the pilot were contained on A. R. Vetter Model A, FM tape recorder. It had seven FM-100 record channels and 1 DC record channel. It used 1/4 inch tape and was operated at 7.5 inches per second. The FM channels are 100 Hz bandwidth with center frequency 2.2 KC $\pm$ 80 percent modulation (non IRIG). Noise with grounded input is about 42 dB down at bandcenter.
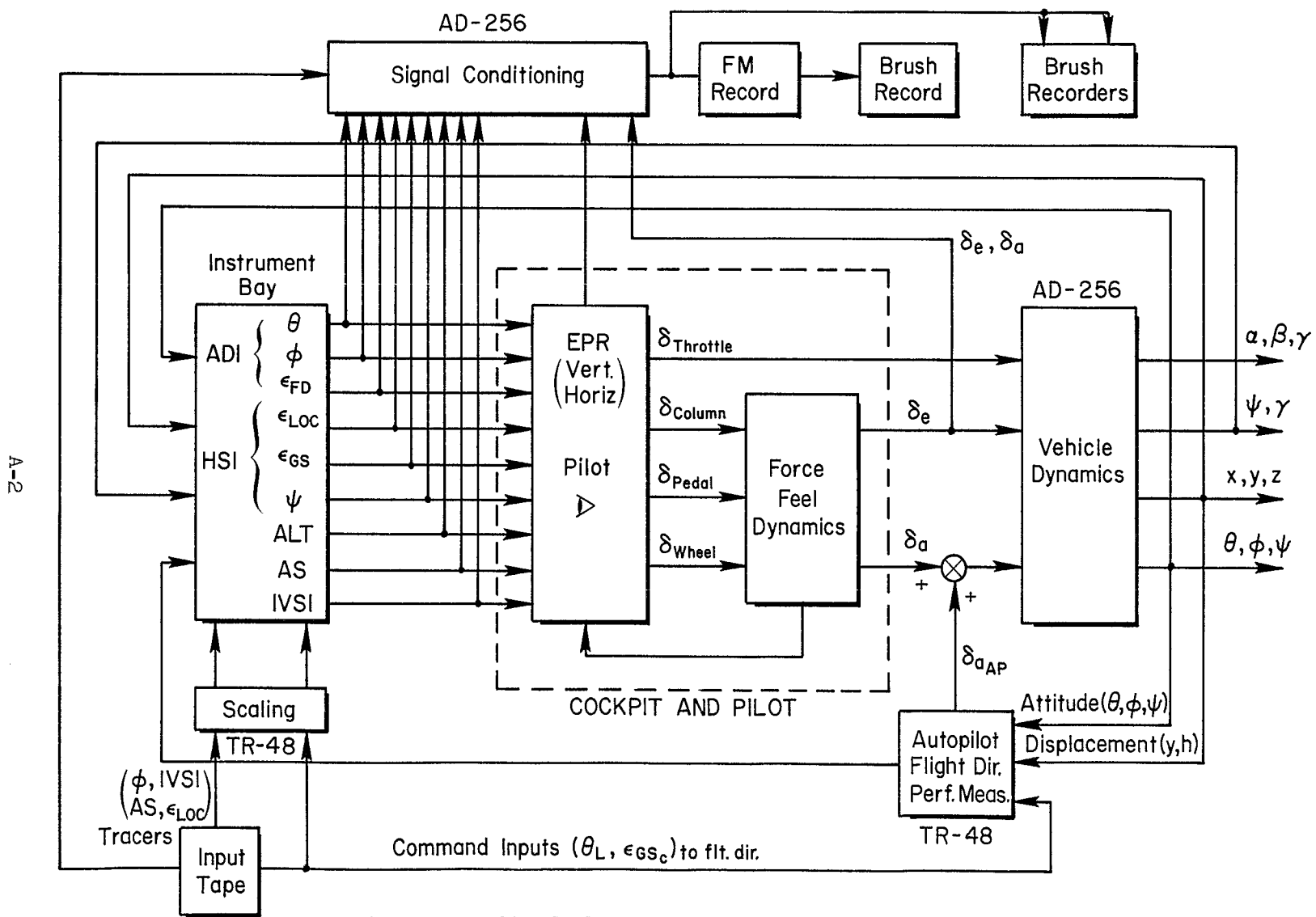
Figure A-1. Signal Flow Diagram and Equipment Functions

TR-48 Analog Computer

An Electronics Associates, Inc. (EAI) TR-48 portable analog computer served to scale the input signals, compute the flight director and auto-pilot dynamics, and record several on-line rms signals. The mechanization utilized 48 amplifiers, 4 quarter square multipliers, 3 double pole relays, 45 pots and 10 switches (7 external). Forty trunk lines provided communication to the AD-256 computer.

AD-256 Analog Computer

The Applied Dynamics analog computer contained the major mechanization. This included the 6 degree of freedom vehicle dynamics, direction cosines for body to inertial axis transformations, Euler angles, glide slope and localizer computations, performance measures and considerable digital logic for switching, data recording, etc. The computing elements included 250 bipolar amplifiers, 20 quarter square multipliers, 7 function generators, 3 external resolver racks, and over 150 pots. 160 trunk lines connected the computer with the simulator building.

Instrument Bay

Computed signals from the AD-256 were conditioned by an EAI analog computer in the instrument bay in order to properly drive the cockpit instrumentation. Over 50 amplifiers and pots were required. The scale factors for the instrument drives were not derived.

Cockpit

A separate room contained the fixed-base cab, hydraulic force feel system, and EPR setup. The background engine sound system was not available and the visual display was not used.* The environment was somewhat noisy due to the hydraulic force feel system. The pilot station

---

*The visual display system was used in a few unscheduled "visual breakout" runs as noted in Section II.

was similar in layout and dimension to that of a large jet transport
aircraft although actual subsonic jet hardware was not used. The instru-
ment panel configuration, meter properties and force feel system properties
are discussed in Appendix B. A remote OPERATE, HOLD, RESET switch allowed
the pilot to independently operate the analog computer when appropriate.

Eye Point of Regard (EPR) System

The EPR apparatus and the experimenter were located directly behind
the pilot. The purpose of the EPR system is to provide a simple measure
of the intersection of the visual line-of-sight and a selected normal
picture plane in an instrument scanning situation. The apparatus measures
the angle of the eye in the head by corneal-scleral reflectance, and the
motion of the head with respect to the reference point electromechanically.
These two quantities are summed appropriately to obtain the net point-of-
regard for the eye/head combination.

The output of the EPR system was displayed on a CRT. By drawing the
panel layout to scale on a CRT mask, the instruments being fixated could
be seen as the EPR dot moved over the field.

Figure A-2 shows the EPR setup and components. Their installation on
a subject is shown in Fig. A-3. The fundamental components are the eye
movement device (EMD), the head movement device (HMD), and the EPR computer.

The head movement device is an electromechanical sensor connected by a
telescoping linkage to an anchor point on the instrument panel. The nominal
angular range of the HMD is $\pm 40^{\circ}$ horizontally and $\pm 20^{\circ}$ vertically, with
resolution of about $\pm 1^{\circ}$ in either axis.

The eye movement device used was a Space Sciences, Inc., Model SGHV-2
designed to measure the horizontal and vertical movement of the eye with
respect to the head by a corneal-scleral boundary contrast technique. Its
operation depends on

> "...detecting the changes in reflected light between the
> white sclera and the left and right sides of the iris when
> making horizontal measurements, and between the eye itself
> and its upper lid for vertical measurements. The pulsed
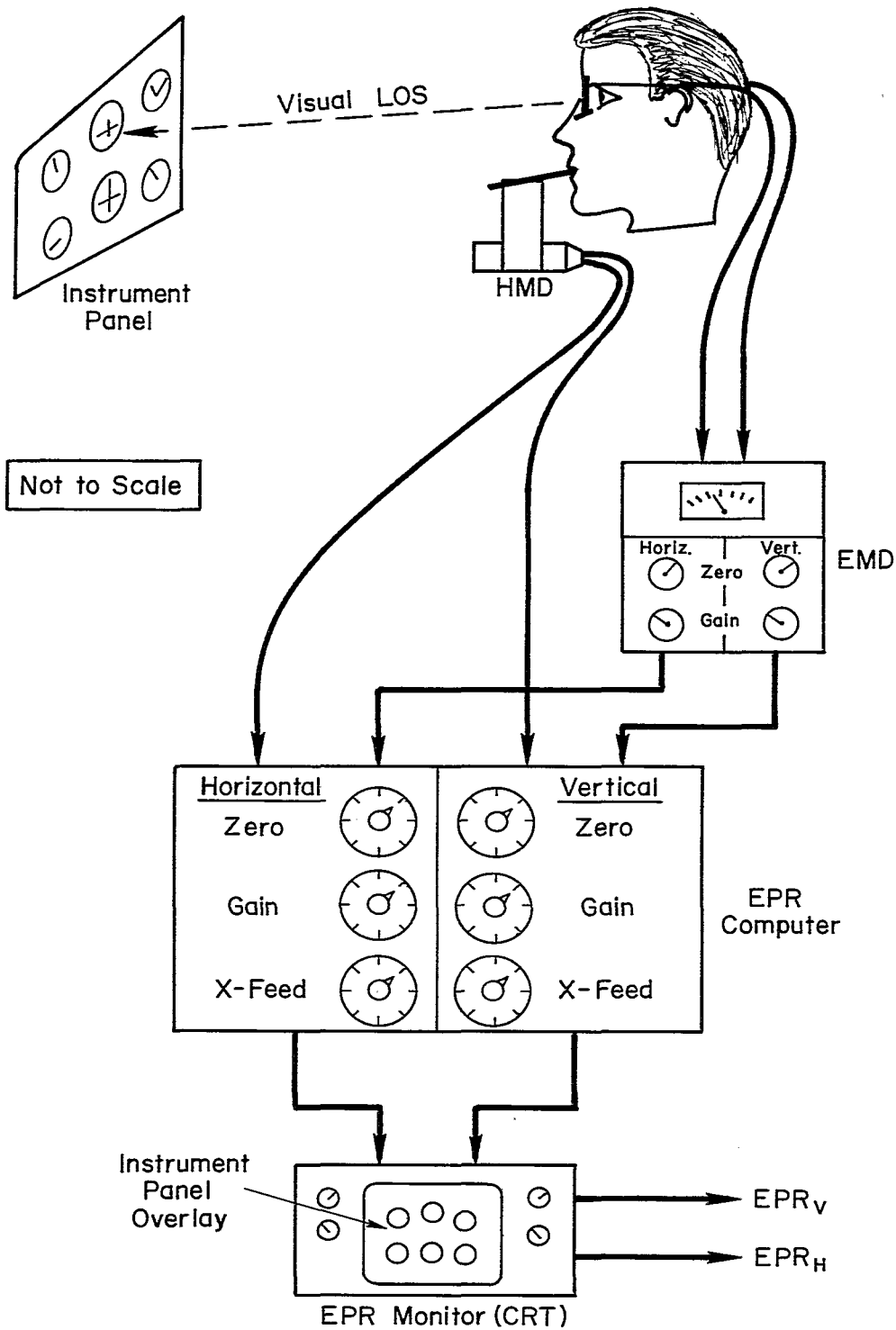> IR light source illuminates the eye with invisible light.
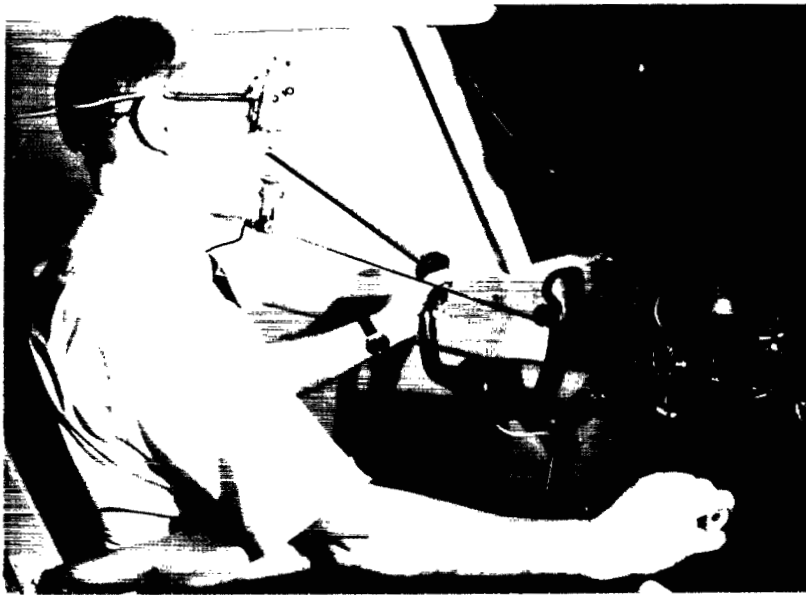
Figure A-2. EPR System Components

Figure A-3. Use of EPR System

The transducers are placed close to the eye, each facing
the eye, one from the left side and the other from the
right side. The photodiodes are fast response devices
sensitive in the near-infrared region. In both cases an
amplifier-demodulator acts on the current produced by the
diodes to yield a single ended, low impedance, output
voltage proportional to the angular displacement of the
eye." (Quote from the SGHV-2 operation manual)

The vertical and horizontal eye movement voltages are filtered, $\tau = .016$ sec,
to reduce AC pickup. The usable angular range of the EMD is $\pm 20^{\circ}$ horizontally
and $\pm 10^{\circ}$ vertically with accuracies of 1° and 2°, respectively. The EMD is
self-contained with rechargeable batteries.

The eye point of regard computer is a special purpose miniaturized analog
computer which combines the horizontal and vertical eye and head angles to
yield the coordinates of the eye line-of-sight intercept with the display.
It is a solid state device, powered by 115 VAC line. Potentiometers control
HMD zero offset, gain, and crosstalk with the EMD. The EPR computer output
provides linearized eye angles of 0 to ± 10V horizontally and vertically,
linearized head angles of 0 to ± 15V horizontally and vertically, and total
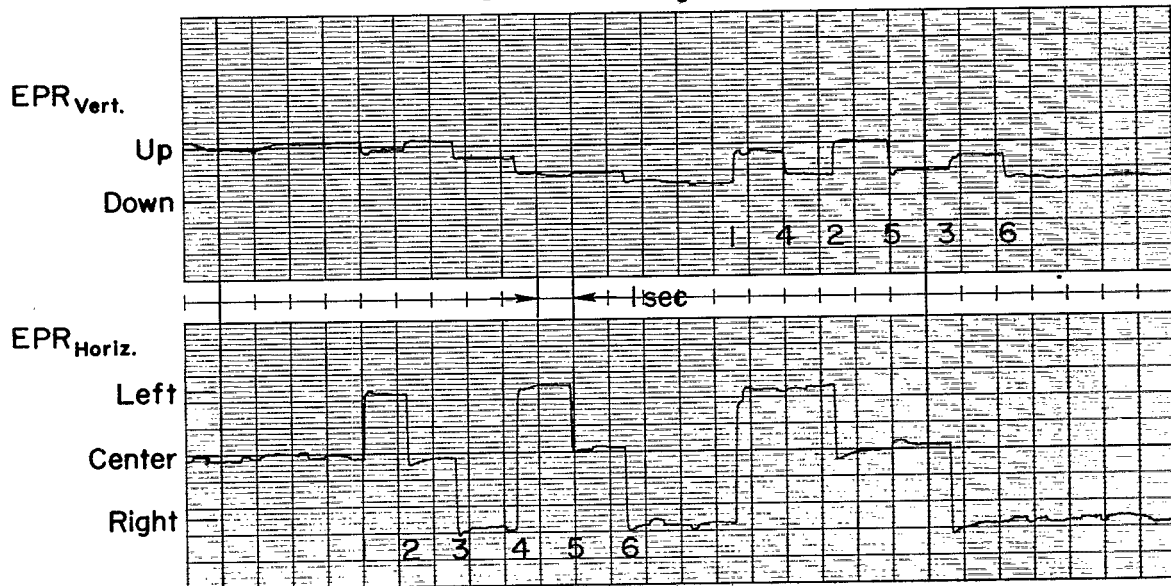EPR angle of 0 to ± 10V. Offsets and drift were less than 5 mV.

A sample of the output for the 6 meter calibration is shown on Fig. A-4.
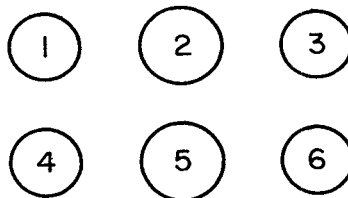
Recorders

Pertinent data recording was done by an Ampex Model CP-100 FM magnetic
tape recorder. Thirteen FM channels were set up with center frequency
3.375 kc and recording was done at 3.75 ips (narrow band). The heads were
IRIG configuration. The remaining channel was set up for direct voice
record since no edge track was available. Input voltages of ± 1.414V
provided ± 40 percent modulation.

In parallel with the FM recorder were two 8 channel linear Brush strip
chart recorders. Another 8 channel Brush was used for monitoring the FM
output to ensure good quality recording.

Scale   0.2 deg/division

EPR Vert.

Up

Down

| 1 4 2 5 3 6

← 1 sec

EPR Horiz.

Left

Center

Right

2 3 4 5 6

Instruments

①   ②   ③

④   ⑤   ⑥

Horizontal Scan   1-2-3-4-5-6
Vertical Scan   1-4-2-5-3-6

Figure A-4.   Sample EPR Calibration

CONTROLLED ELEMENT PROPERTIES

VEHICLE DESCRIPTION

The linearized model of the DC-8 in the landing approach configuration was derived from data used in the NASA simulation. It specifies nonlinear lift and drag characteristics, but at small angles of attack this effect is minimum and straight-line slopes are representative. Other nonlinear data are added due to ground effect, but they have no influence on the basic data for altitudes above 80 ft. Linearized perturbation equations are adequate for this analysis, and the longitudinal body-fixed stability axis and lateral body axis equations of Ref. 17 are appropriate. These are given below.

Longitudinal Body-Fixed Stability-Axis Perturbation Equations

$$
\begin{bmatrix}
s - X_u & -X_w & g\cos\gamma_o \\
-Z_u & s - Z_w & -V_{T_O}s + g\sin\gamma_o \\
-M_u & -(M_{\dot{w}}s + M_w) & s^2 - M_q s
\end{bmatrix}
\begin{bmatrix} u \\ w \\ \theta \end{bmatrix}
=
\begin{bmatrix}
X_{\delta_e} & X_{\delta_T} & -X_w \\
Z_{\delta_e} & Z_{\delta_T} & -Z_w \\
M_{\delta_e} & M_{\delta_T} & -M_w
\end{bmatrix}
\begin{bmatrix} \delta_e \\ \delta_T \\ w_g \end{bmatrix}
\tag{B-1}
$$

$$
\dot{h} = -w\cos\gamma_o + u\sin\gamma_o + (V_{T_O}\cos\gamma_o)\theta = V_{T_O}\sin\gamma
$$

Lateral Body-Axis Perturbation Equations

$$
\begin{bmatrix}
s - Y_v & -\left[(\sin\alpha_o)s + \dfrac{g}{V_{T_O}}\cos(\alpha_o + \gamma_o)\right] & (\cos\alpha_o)s - \dfrac{g}{V_{T_O}}\sin(\alpha_o + \gamma_o) \\
-L_\beta & s(s - L_p) & -\left[\dfrac{I_{xz}}{I_x}s^2 + L_r s\right] \\
-N_\beta & -\left[\dfrac{I_{xz}}{I_z}s^2 + N_p s\right] & s(s - N_r)
\end{bmatrix}
\begin{bmatrix} \beta \\ \dfrac{p}{s} \\ \dfrac{r}{s} \end{bmatrix}
=
\begin{bmatrix}
Y^*_{\delta_a} & Y^*_{\delta_r} \\
L_{\delta_a} & L_{\delta_r} \\
N_{\delta_a} & N_{\delta_r}
\end{bmatrix}
\begin{bmatrix} \delta_a \\ \delta_r \end{bmatrix}
$$

$$
\dot{\varphi} = p + r\tan(\alpha_o + \gamma_o) \quad ; \quad \dot{\psi} = \frac{1}{\cos(\alpha_o + \gamma_o)}r
\tag{B-2}
$$

One landing approach flight condition was used with an approach speed of 135 kts, gross weight of 180,000 lbs, flaps 50°, and gear down. The yaw damper was assumed on. No other augmentation, such as autothrottle, was used. For the frozen range configurations (B, C, and E), the aircraft was trimmed straight and level ($\alpha_O = .62^O$, $\delta_{e_O} = -.72^O$, $T_O = 23,700$ lbs) at a range of 30,000 ft and 1,650 ft altitude above ground level. The rate of climb and pitch attitude meters were appropriately biased, and the altimeter was driven by an integrator to make the display represent descent along the 3° glide slope. For the range varying configurations (D and F) the aircraft was retrimmed for descent on a 3° glide slope and no meter biases were needed. All prelanding check lists were assumed complied with.

The dimensional stability derivatives for this flight condition are given in Table B-I which also includes a comparison with a typical jet transport (Boeing 707-320) used in a previous study, Ref. 18. The Ref. 18 data in Table B-I have C_{m_q} corrected to -18.0 in accordance with NASA TN D-3159, Ref. 19.

The longitudinal transfer functions are given in Table B-II and the lateral transfer functions are presented in Table B-III.

Transient responses were computed from the given transfer functions for

- 10° δ_e pulse held for 1 sec
- 5° δ_a step
- 5° δ_r step

Figures B-1, B-2, and B-3 present the respective vehicle response to these inputs. The solid lines are the analog responses. The dotted lines in Figs. B-2 and B-3 are theoretical results from the linear transfer functions.

FLIGHT DIRECTOR PROPERTIES

The flight director already mechanized on the NASA simulator was used. The equations for the longitudinal and lateral directors are given below. Linear units are feet, angular units are radians. The units of the flight

AMES DC-8 SIMULATOR PARAMETERS FOR LANDING APPROACH CONFIGURATION

GEOMETRY & INERTIA	DC-8*	707-320†	LONGITUDINAL STABILITY AXES	DC-8*	707-320†	LATERAL BODY AXES	DC-8*	707-320†
h (ft)	0	0	X_u (1/sec)	−0.0372	−0.0356	Y_v (1/sec)	−0.0887	−0.112
M (−)	.204	.20	X_w (1/sec)	0.136	0.103	$Y_{\delta_a}^*$ (1/sec)	0	0
V_{T_0} (ft/sec)	228.	223.	X_{δ_e}(ft/sec²/rad)	0	−−	$Y_{\delta_r}^*$ (1/sec)	0.031	0
γ_0 (deg)	0	−2.86	X_{δ_T}(ft/sec²/%)	0.106	(1.0 ref)	L_β (1/sec²)	−1.40	−1.33
q (lb/ft²)	61.8	59.2	Z_u (1/sec)	−0.283	−0.289	L_p (1/sec)	−1.04	−0.99
S (ft²)	2758.	2890.	Z_w (1/sec)	−0.750	−0.585	L_r (1/sec)	0.474	0.825
b (ft)	142.4	142.4	$Z_{\dot{w}}$ (−)	0	−−	L_{δ_a} (1/sec²)	1.13	1.03
c (ft)	22.16	22.7	Z_{δ_e}(ft/sec²/rad)	−9.25	−7.65	L_{δ_r} (1/sec²)	0.159	0.074
W (lb)	180,000.	181,000.	Z_{δ_T}(ft/sec²/%)	−0.00097	−0.0306 X_{δ_T}	N_β (1/sec²)	0.368	0.381
m (slugs)	5,580.	5,590.	M_u (1/sec-ft)	0	−0.000139	N_p (1/sec)	−0.029	−0.112
I_x (slug-ft²)	3.2×10	3.3×10⁶	M_w (1/sec-ft)	−0.00461	−0.0026	N_r (1/sec)	−0.257	−0.187
I_y (slug-ft²)	3.8×10⁶	5.×10⁶	$M_{\dot{w}}$ (1/ft)	−0.00085	0	N_{δ_a} (1/sec²)	0	0.0264
I_z (slug-ft²)	6.6×10⁶	8.3×10⁶	M_q (1/sec)	−0.594	−0.87	N_{δ_r} (1/sec²)	−0.368	−0.381
I_{xz} (slug-ft²)	0	0	M_{δ_e}(1/sec²)	−0.923	−0.619			
X_{CG} (% c)	25.2	?	M_{δ_T}(1/sec²/%)	0	0.00685 X_{δ_T}			
δ_{F_0} (deg)	50	?	M_α (1/sec²)	−1.05	−0.581			
α_0 (deg)	0.62	?	$M_{\dot{\alpha}}$ (1/sec)	−0.1936	0			

I_x, I_y, I_y, and I_{xz} are given for Body Axes.

*Simulated.

†Ref. 18 for comparison.

TABLE B-II

LONGITUDINAL STABILITY AXIS TRANSFER FUNCTIONS FOR
THE DC-8 IN THE LANDING APPROACH CONFIGURATION

$$\Delta \;=\; [0.0865\,;\,0.166][0.627\,;\,1.23]\,\text{*}$$

$$N_{\delta_e}^{\theta} \;=\; -0.915(0.101)(0.646)$$

$$N_{\delta_e}^{u} \;=\; -1.258(-4.12)(4.03)$$

$$N_{\delta_e}^{w} \;=\; -9.25(23.3)[0.090\,;\,0.198]$$

$$N_{\delta_e}^{\dot{h}} \;=\; 9.25(-3.63)(0.0352)(4.42)$$

$$N_{\delta_T}^{\theta} \;=\; 0.82 \times 10^{-6}(5.4)(31.1)$$

$$N_{\delta_T}^{u} \;=\; 0.106(-0.0009)[0.636\,;\,1.22]$$

$$N_{\delta_T}^{w} \;=\; -0.00097(31.1)(0)(0.59)$$

$$N_{\delta_T}^{\dot{h}} \;=\; -0.00097(0.38)(1.02)(31.1)$$

$$N_{\delta_e \delta_T}^{\theta\; w} \;=\; 0.0009(31.1)$$

$$N_{\delta_e \delta_T}^{\theta\; u} \;=\; -0.097(0.709)$$

$$N_{\delta_e \delta_T}^{w\; u} \;=\; -0.98(-0.0013)(23.3)$$

$$N_{\delta_e \delta_T}^{\theta\; \dot{h}} \;=\; -0.0009(31.1)$$

$$N_{\delta_e \delta_T}^{w\; \dot{h}} \;=\; -0.203(31.1)$$

$$N_{\delta_e \delta_T}^{u\; \dot{h}} \;=\; -0.98(-3.63)(4.41)$$

$$N_{w_g}^{\dot{h}} \;=\; -0.75(0.871)[0.113\,;\,0.254]$$

$$N_{w_g}^{\theta} \;=\; 0.004(-0.0087)(0.0378)$$

$$N_{w_g}^{u} \;=\; -0.136(0)[0.407\,;\,0.975]$$

$$N_{w_g \delta_e}^{\dot{h}\; \theta} \;=\; 0.649(0.092)$$

$$\frac{\theta}{\delta_e} \;=\; \frac{N_{\delta_e}^{\theta}}{\Delta}\;,\;\text{etc.;}\;\; N_{\delta_e \delta_T}^{\theta\; u}\,,\;\text{etc., are coupling numerators (see Ref. 17).}$$

------

*Polynomial factors: Throughout this appendix $A[s^2 + 2\zeta\omega s + \omega^2]$ is
written $A[\zeta\,;\,\omega]$; and $A(s+a)$ is written $A(a)$.

TABLE B-III

LATERAL BODY AXIS TRANSFER FUNCTIONS FOR
THE DC-8 IN THE LANDING APPROACH CONFIGURATION

$$\Delta = (0.0467)(1.18)[0.107\,;\,0.728]$$

$$N^r_{\delta_a} = -0.032(-1.35)(1.33)$$

$$N^\phi_{\delta_a} = 1.13[0.277\,;\,0.625]$$

$$N^\beta_{\delta_a} = 0.01(0.213)(19.42)$$

$$N^r_{\delta_r} = -0.367(1.19)[-0.097\,;\,0.397]$$

$$N^\phi_{\delta_r} = 0.159(-2.37)(1.34)$$

$$N^\beta_{\delta_r} = 0.031(-0.043)(1.16)(12.16)$$

$$N^{p\ \beta}_{\delta_a\delta_r} = 0.035(-0.00002)(12.2)$$

$$N^{r\ \beta}_{\delta_a\delta_r} = 0.0026(22.18)$$

$$N^{p/s\ r}_{\delta_a\,\delta_r} = -0.415(0.058)$$

$$\frac{\phi}{\delta_a} = \frac{N^\phi_{\delta_a}}{\Delta}\,,\ \frac{r}{\delta_r} = \frac{N^r_{\delta_r}}{\Delta}\,,\ \text{etc.;}\ N^{p\ \beta}_{\delta_a\delta_r}\,,\ \text{etc., are coupling numerators.}$$
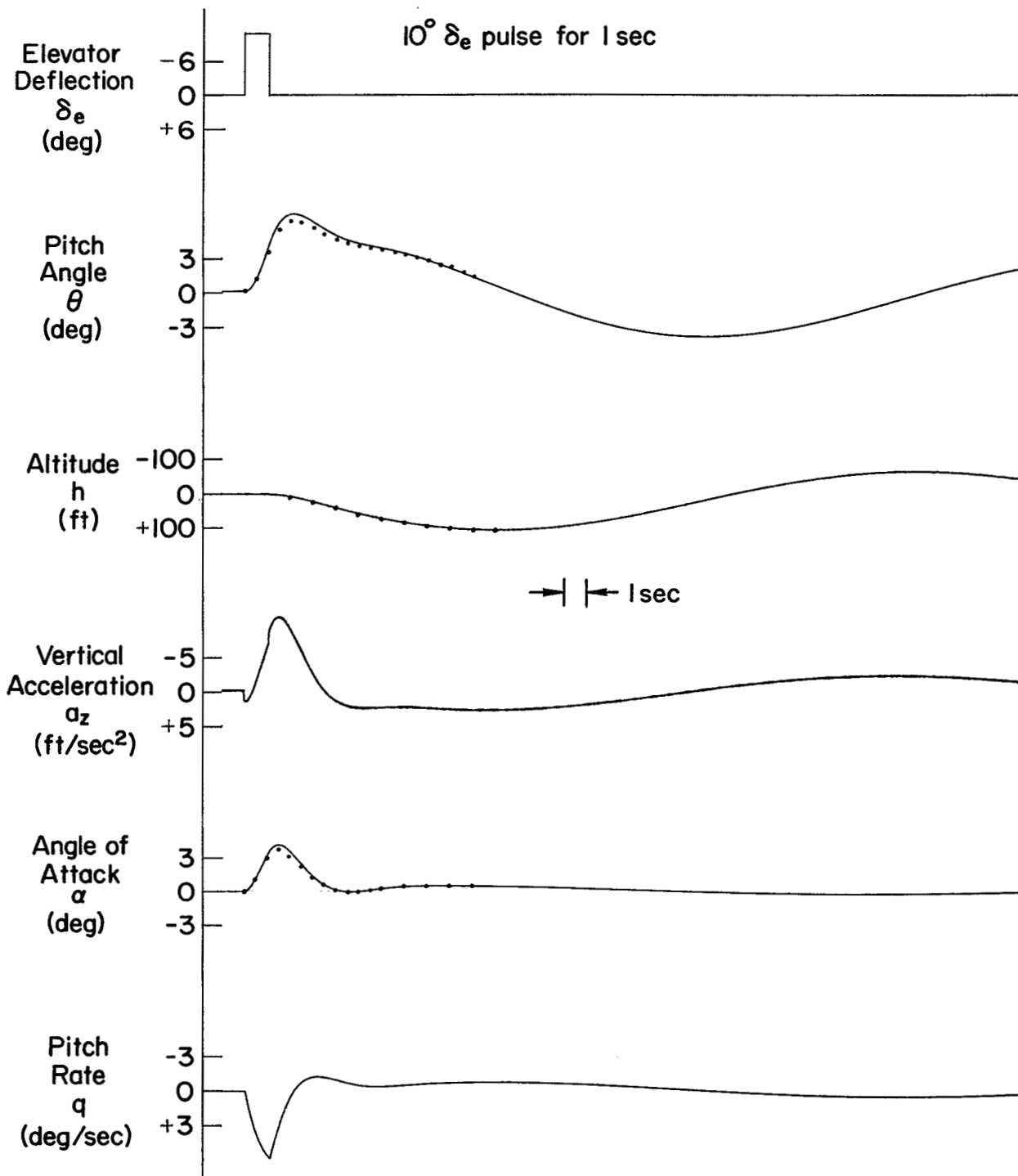
Figure B-1. Open-Loop Transient Response to 1 sec Elevator Pulse of 10°
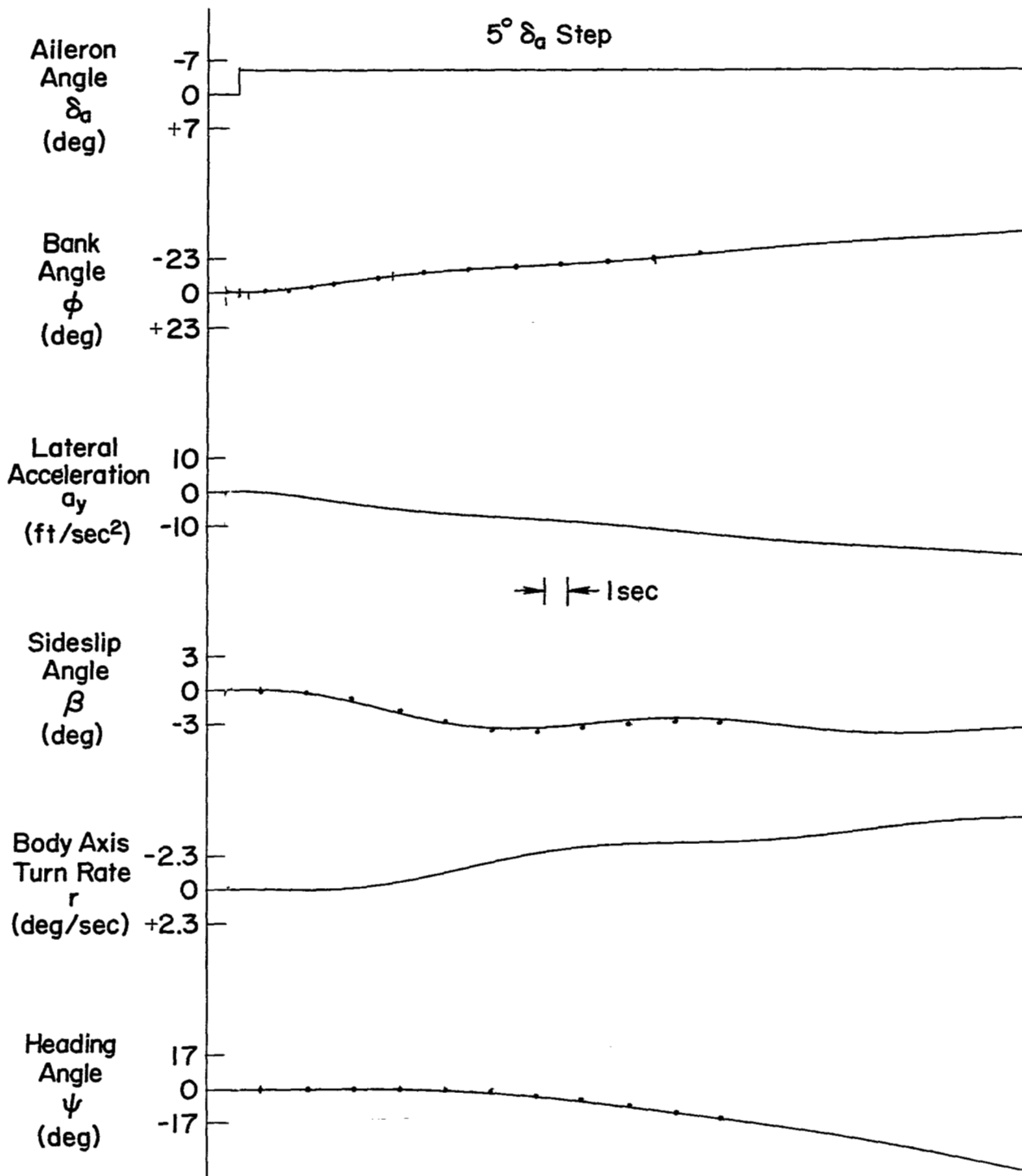
Figure B-2. Open-Loop Transient Response to 5° Aileron Step Input
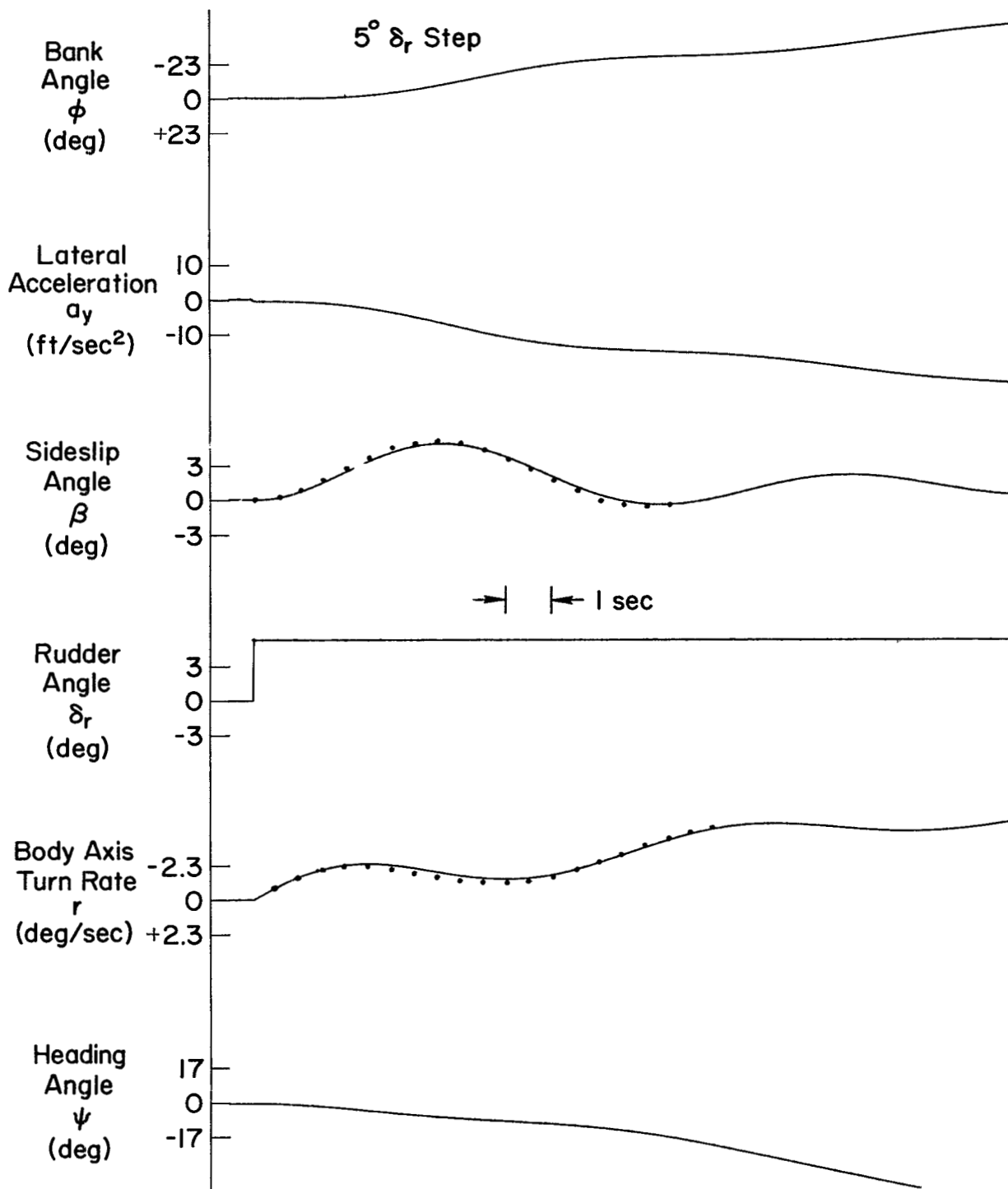
Figure B-3. Open-Loop Transient Response to 5° Rudder Step Input

director are arbitrary and determined by the instrument scaling. The approximate display scalings using pitch and roll angles as references were: 1 rad $FD_p \doteq 6$ rad of displayed θ; 1 rad $FD_r \doteq 0.10$ rad of displayed φ.

Longitudinal

$$-FD_p = 6\left(0.0005h_\epsilon + \frac{0.5s\theta}{s+0.082}\right) \quad , \quad \text{radians } \theta \qquad (B-3)$$

h_e is the altitude deviation from a given glide slope (in ft) and it is computed by multiplying the angular glide slope error, ϵ_{GS}, by the range to glide slope transmitter.

Lateral

$$-FD_r = 0.1\left[\frac{0.62s}{(s+1.06)(s+0.16)} E + 2.7\varphi + 22.9\epsilon_{LOC}\right] \quad , \quad \text{radians } \varphi \quad (B-4)$$

$$E = 8.6\psi + 0.9\varphi + 97.5\epsilon_{LOC} \quad , \quad \text{radians}$$

ϵ_{LOC} is the angular deviation from the localizer beam (in rad). It can be transformed to lateral displacement (γ) by multiplying by the range to the localizer transmitter. Positive deviations are to the right.

It is important to note the influence of variable range on these instruments. Since altitude error is used in the longitudinal director, the dynamics are unaffected by range, but any angular glide slope noise will be attenuated in the flight director as range decreases. In the lateral flight director, noise would not be attenuated and the instrument becomes more sensitive as range decreases.

The open-loop transfer functions calculated for a localizer range of 45,000 ft (approximately 30,000 ft from threshold) are:

$$\frac{FD_p}{\delta_e} = \frac{N_{\delta_e}^{FD_p}}{\Delta_{long}} = \frac{-6 \times 0.453(0.048)(0.065)[0.8 ; 0.4]}{(0)(0.082)[0.087 ; 0.166][0.63 ; 1.23]} \tag{B-5}$$

$$\frac{FD_r}{\delta_a} = \frac{N_{\delta_a}^{FD_r}}{\Delta_{lat}} = \frac{-0.1 \times 3.06(1.32)(0.318)[0.5 ; 0.05][0.086 ; 0.59]}{(0)^2(1.06)(0.16)(0.047)(1.181)[0.107 ; 0.728]} \tag{B-6}$$

These are obtained by substituting the appropriate vehicle transfer functions from Tables B-II and B-III into Eqs. B-3 and B-4, respectively. For a range of 15,000 ft (approximately at the threshold) the lateral flight director transfer function becomes

$$\frac{FD_r}{\delta_a} = \frac{-0.1 \times 3.06(1.32)(0.071)[0.8 ; 0.186][0.07 ; 0.59]}{(0)^2(1.06)(0.16)(0.047)(1.18)[0.107 ; 0.728]} \tag{B-7}$$

Comparing Eqs. B-6 and B-7 shows that as range decreases the low frequency gain increases. This is a desirable feature since lateral errors will be smaller for the same crossover frequency.

The transfer functions include the vehicle dynamics, and a closed-loop transient response to elevator or lateral offset will check the dominant modes of the controlled element. This check can be demonstrated by feeding the flight director output back to the control surface with unity gain as shown below:
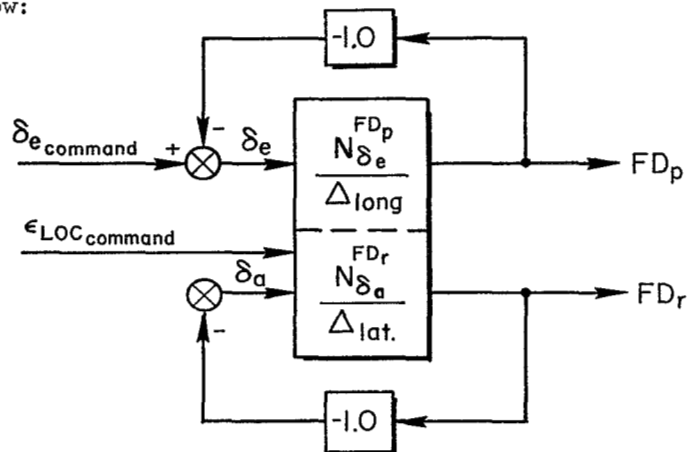
Figure B-4 is the closed-loop longitudinal response to a 5° elevator step. The points overplotted on the analog output represent the theoretical response from the linear transfer function. The dominant mode is the closed-loop phugoid/flight director complex pair, $\omega_p - \omega_{FD}$.

Figure B-5 is the closed-loop lateral response to a step lateral offset of 250 ft. The closed-loop dutch roll is apparent in the aileron response. The common closed-loop roll-spiral coupled pair is dominant in the heading response and the low frequency is dominated by the flight director complex zero pair.

LATERAL AUTOPILOT

A lateral autopilot was used to simulate human pilot control when the test subjects were flying the split-axis (longitudinal only) Configuration B. The result was a describing function "analog pilot" which looked like a low gain autopilot.

The analog pilot output was

$$\delta_a = Y_{p_1}(K_{p_\varphi}\varphi + K_{p_\psi}\psi + K_{p_y}R\epsilon_{LOC}) \tag{B-8}$$

where

$$Y_{p_1} = \frac{(T_{L_\varphi}s + 1)\ (-\tau s/2 + 1)}{(T_{L_\varphi}s + 1)\ (\tau s/2 + 1)} \tag{B-9}$$

The parameter values used were

$$K_{p_\varphi} = 1.5$$

$$K_{p_\psi} = 1.3$$

$$K_{p_y} = .00063\ ,\quad K_{p_{\epsilon_{LOC}}} = K_{p_y} \times RANGE = 28.4$$
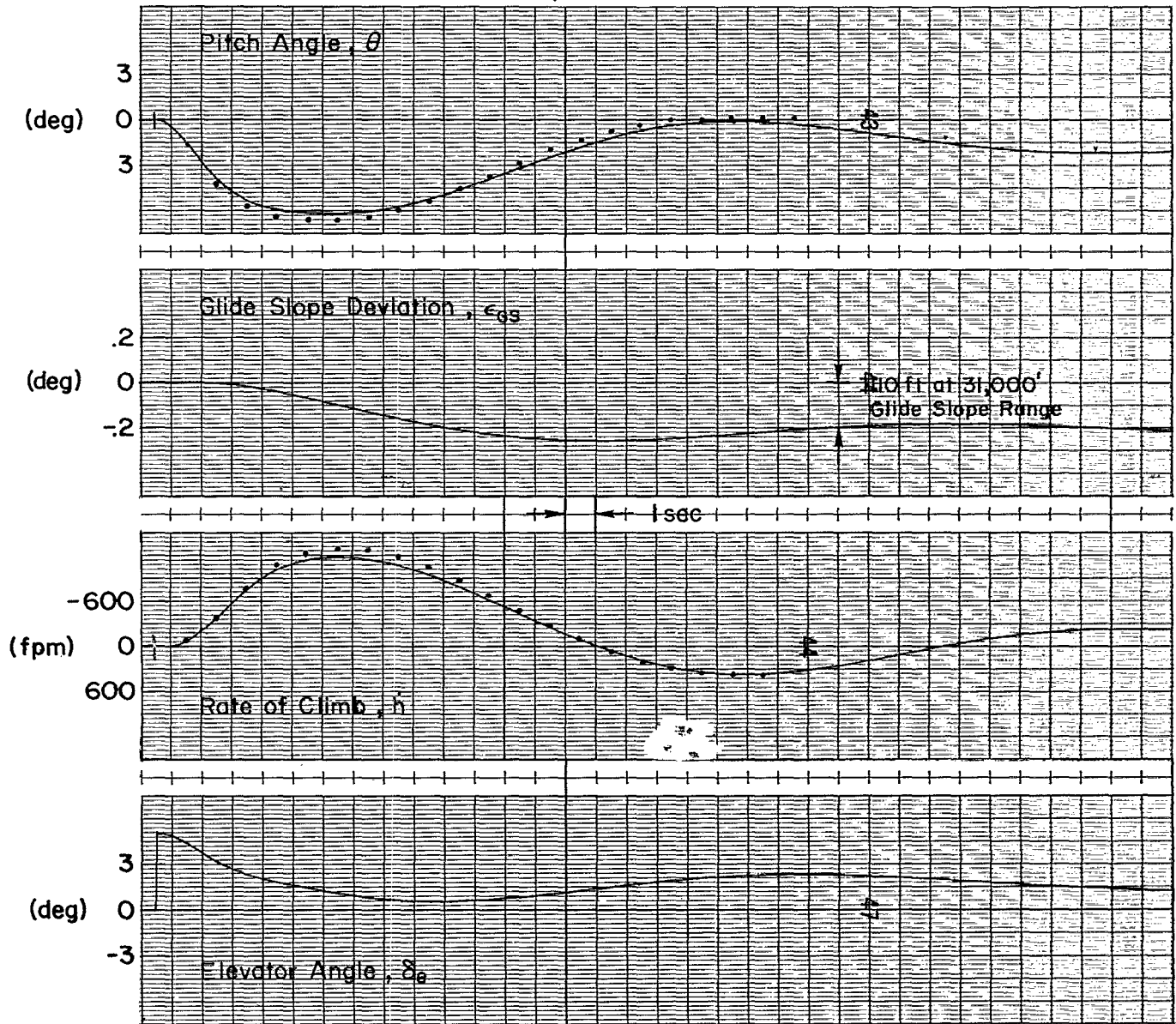
Figure B-4. Check of Closed-Loop Longitudinal
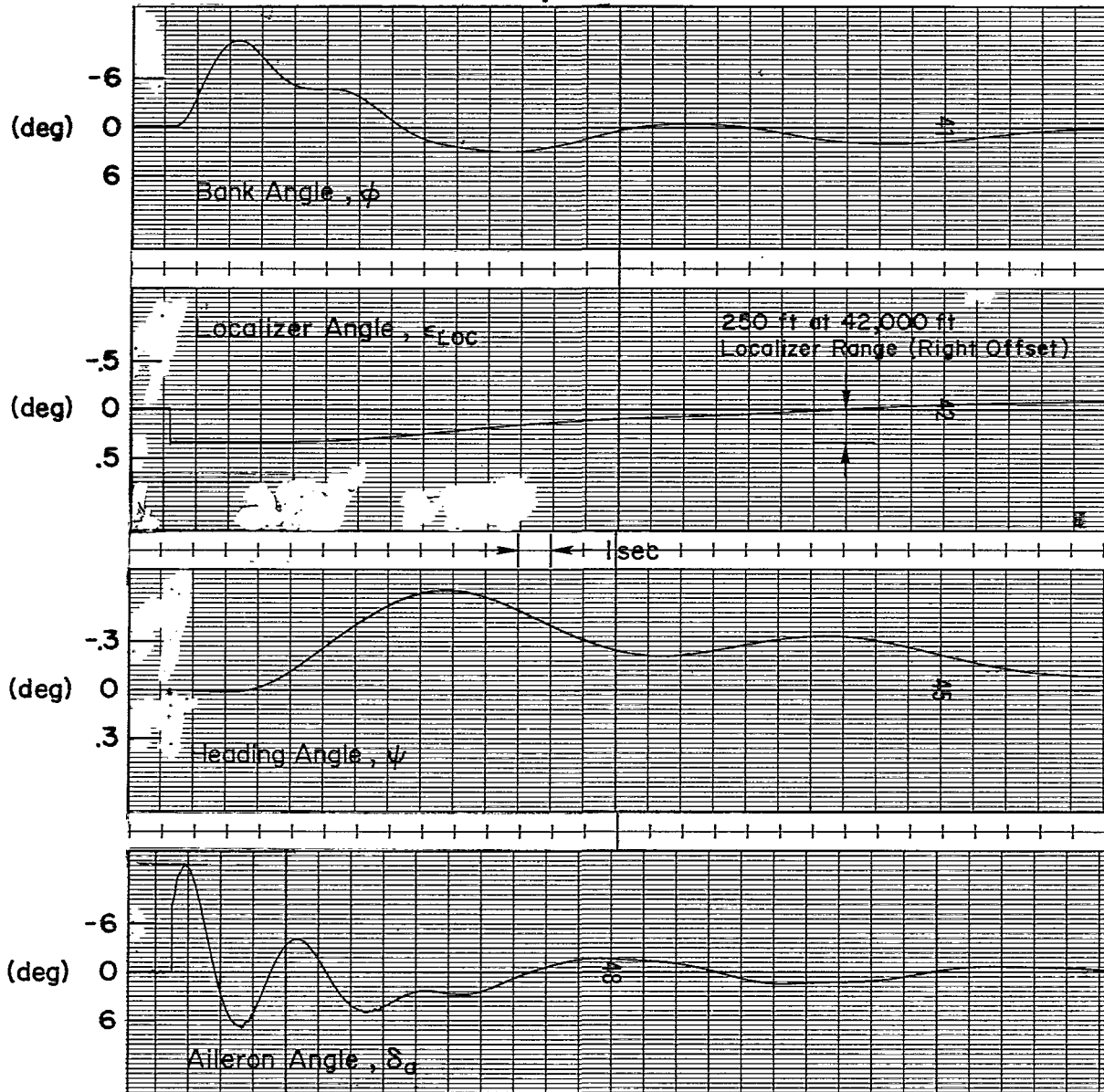Flight Director Response

B-9a

Figure B-5. Check of Closed-Loop Lateral
Flight Director Response

$$T_{L_\varphi} = .67 \text{ sec}$$

$$T_{I_\varphi} = .1 \text{ sec}$$

$$\tau = .59 \text{ sec}$$

$$R = 45,000 \text{ ft}$$

Note that the human pilot's reference to lateral displacement is through the localizer bar, an angular measurement which must be divided by range to obtain linear displacement.

INSTRUMENTATION

The cockpit instrumentation layout is shown in Fig. B-6. The angle of attack and sideslip indicators were not operational. A 1/2 scale detail drawing of the basic six instruments is given in the main text. The scaling and graduations of all the instruments can be obtained from that figure, except for the localizer, glide slope, and flight directors. These were:

Localizer:	±1 dot	$\equiv \pm1^\circ \epsilon_{LOC}$
Glide slope:	±1 dot	$\equiv \pm0.2^\circ \epsilon_{GS}$
Flight director, pitch:	±6 rad θ scale	$\equiv \pm1 FD_p$ units
Flight director, roll:	±0.1 rad φ scale	$\equiv \pm1 FD_r$ units

The flight director was mechanically stopped at about $\pm25^\circ$ pitch and about $\pm5^\circ$ roll.

Frequency response measurements were made for all the cockpit instrumentation. This was done using a photo cell and calculating the phase shift from the zero axis crossings. Amplitude ratios were taken subjectively by the experimenter. Figures B-7 − B-9 present these results. Attempts to fit the phase angle points with second-order systems are shown by the dotted lines.
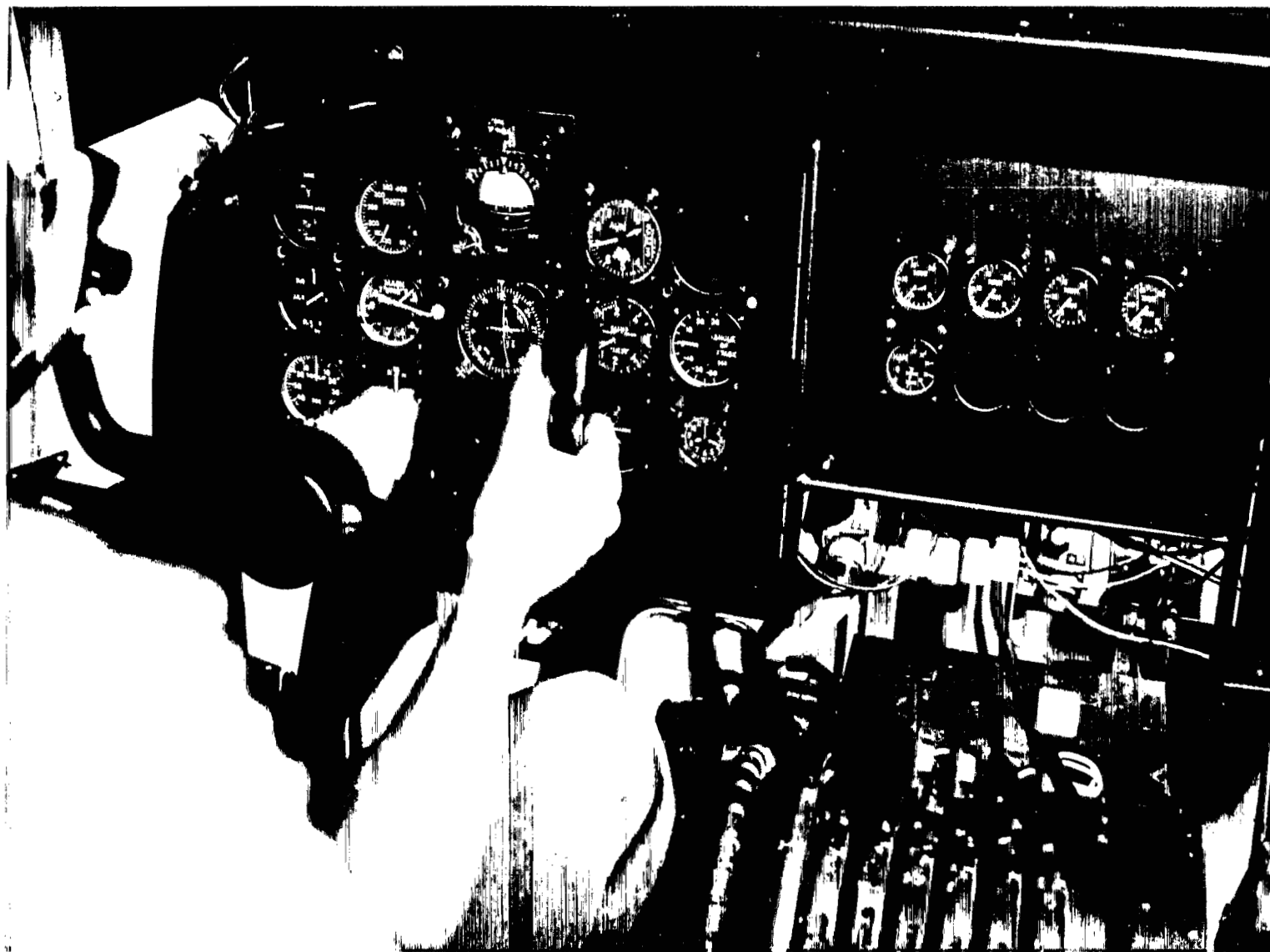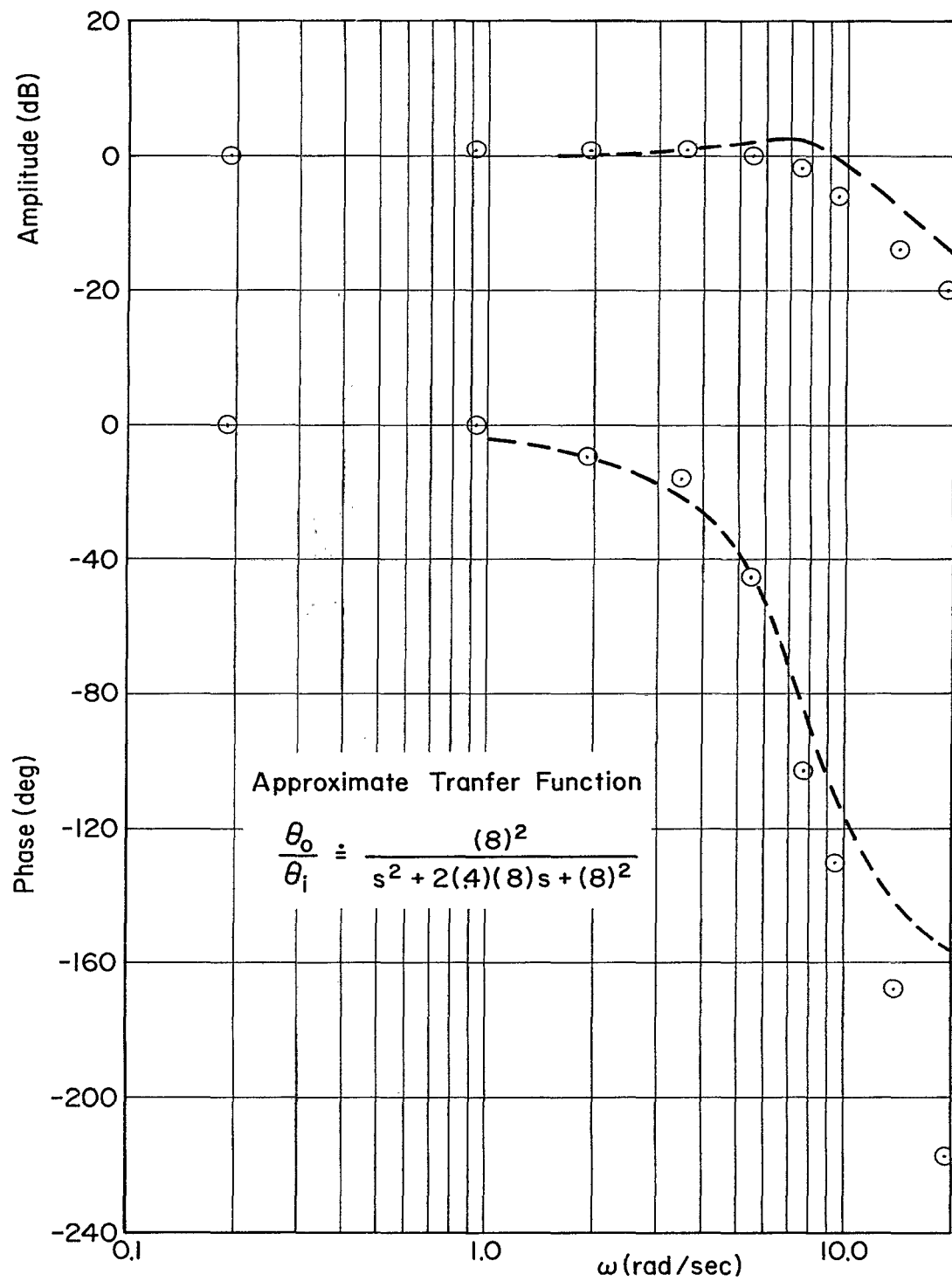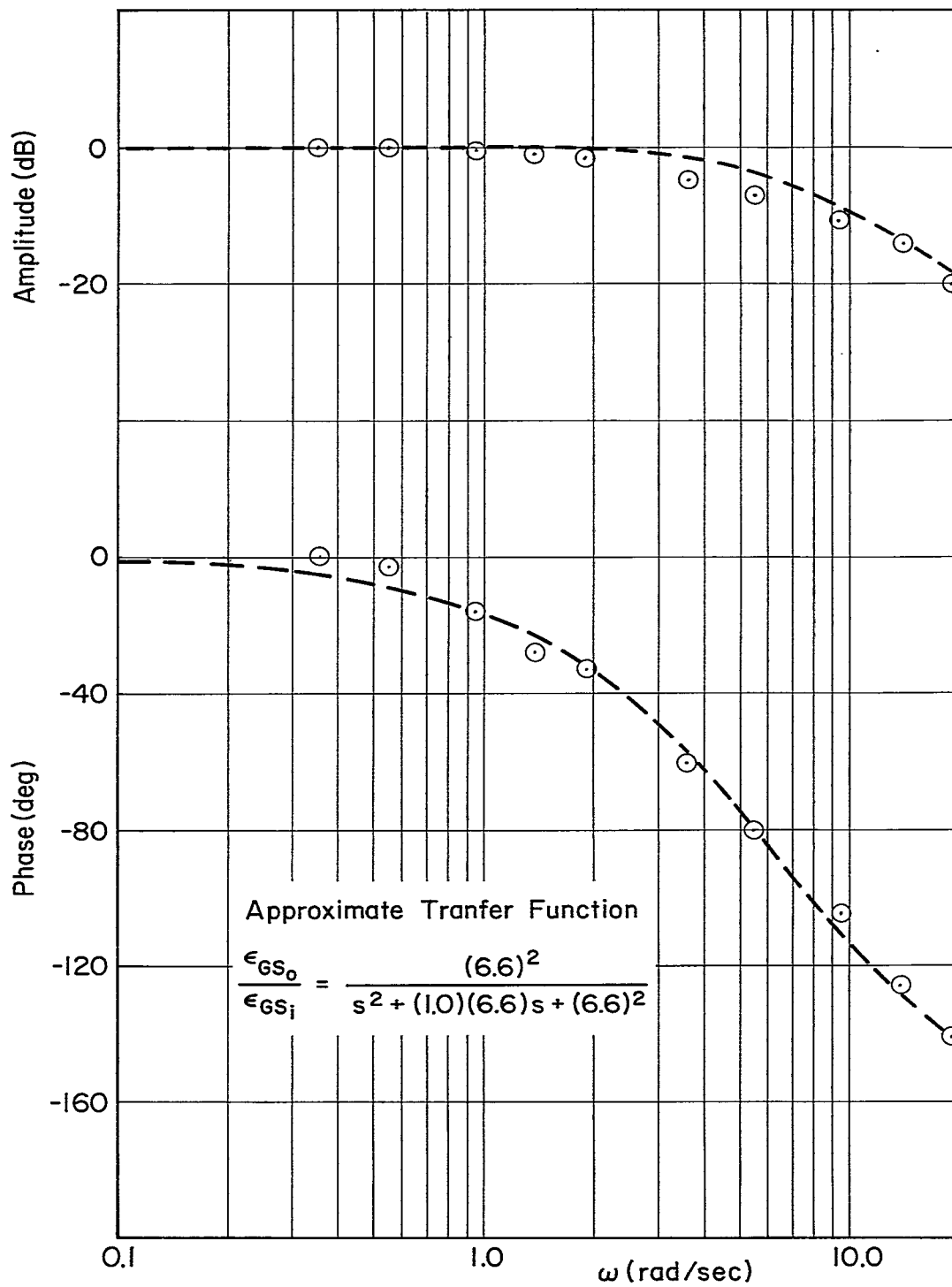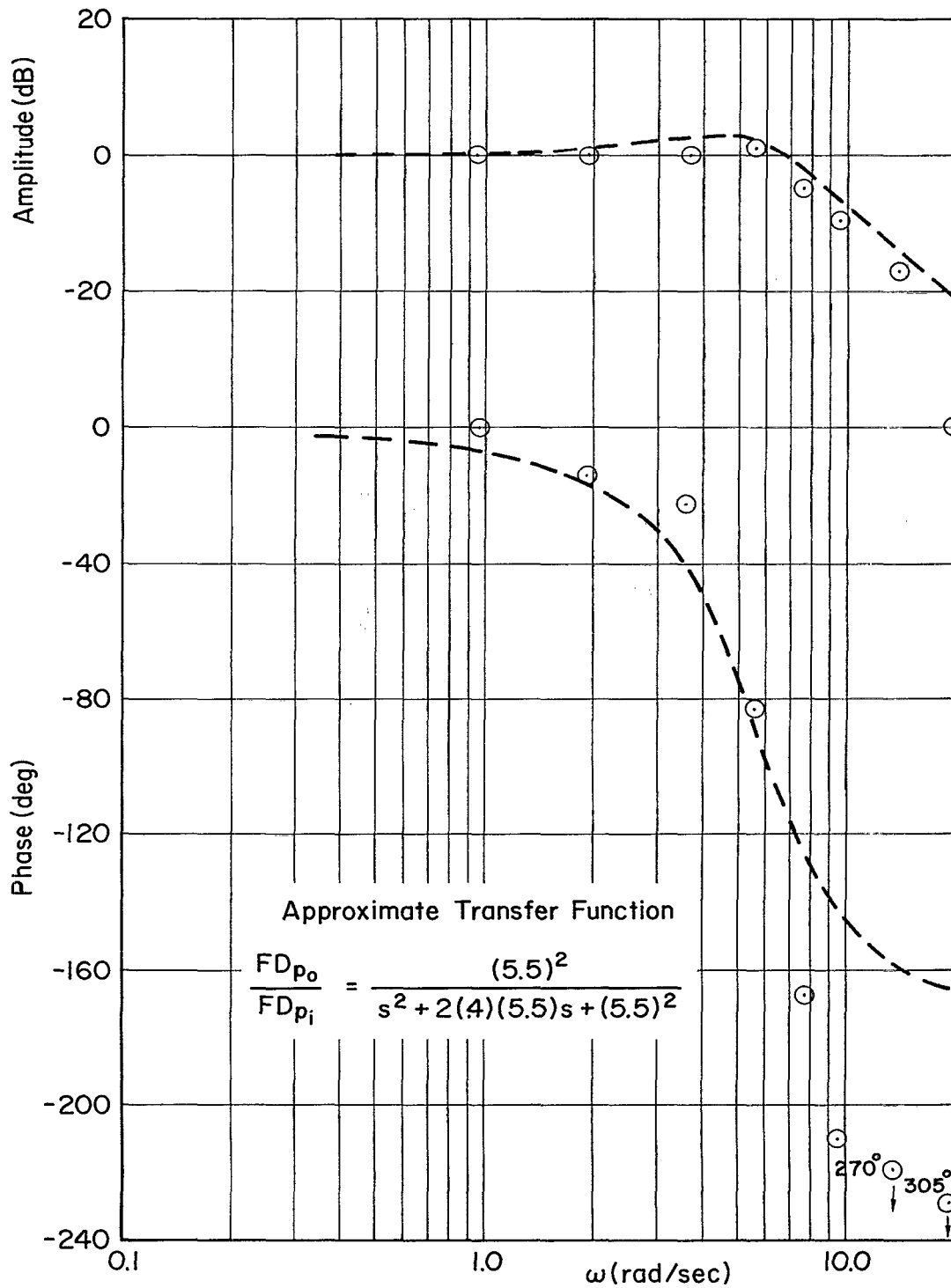
Figure B-6. Cockpit Instrument Layout

Approximate Tranfer Function

$$\frac{\theta_o}{\theta_i} \doteq \frac{(8)^2}{s^2 + 2(4)(8)s + (8)^2}$$

(a)   Pitch Angle Instrument Frequency Response

Figure B-7.   Primary Longitudinal Instruments

B-12a

Approximate Tranfer Function

$$\frac{\epsilon_{GS_o}}{\epsilon_{GS_i}} = \frac{(6.6)^2}{s^2 + (1.0)(6.6)s + (6.6)^2}$$

(b)   Glide Slope Instrument Frequency Response

Figure B-7   (Continued)

B-12b

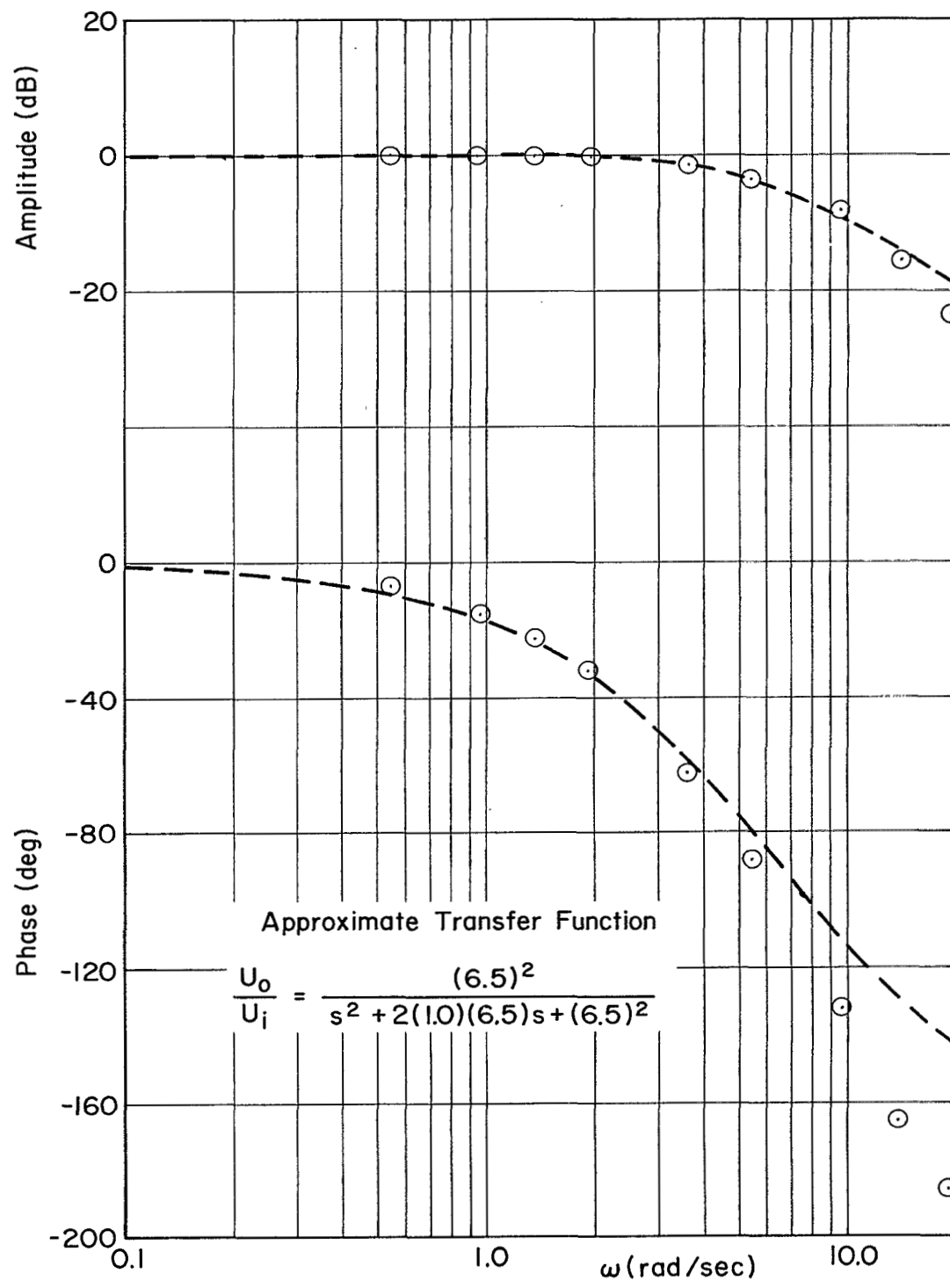(c) Longitudinal Flight Director Instrument Frequency Response

Figure B-7 (Concluded)
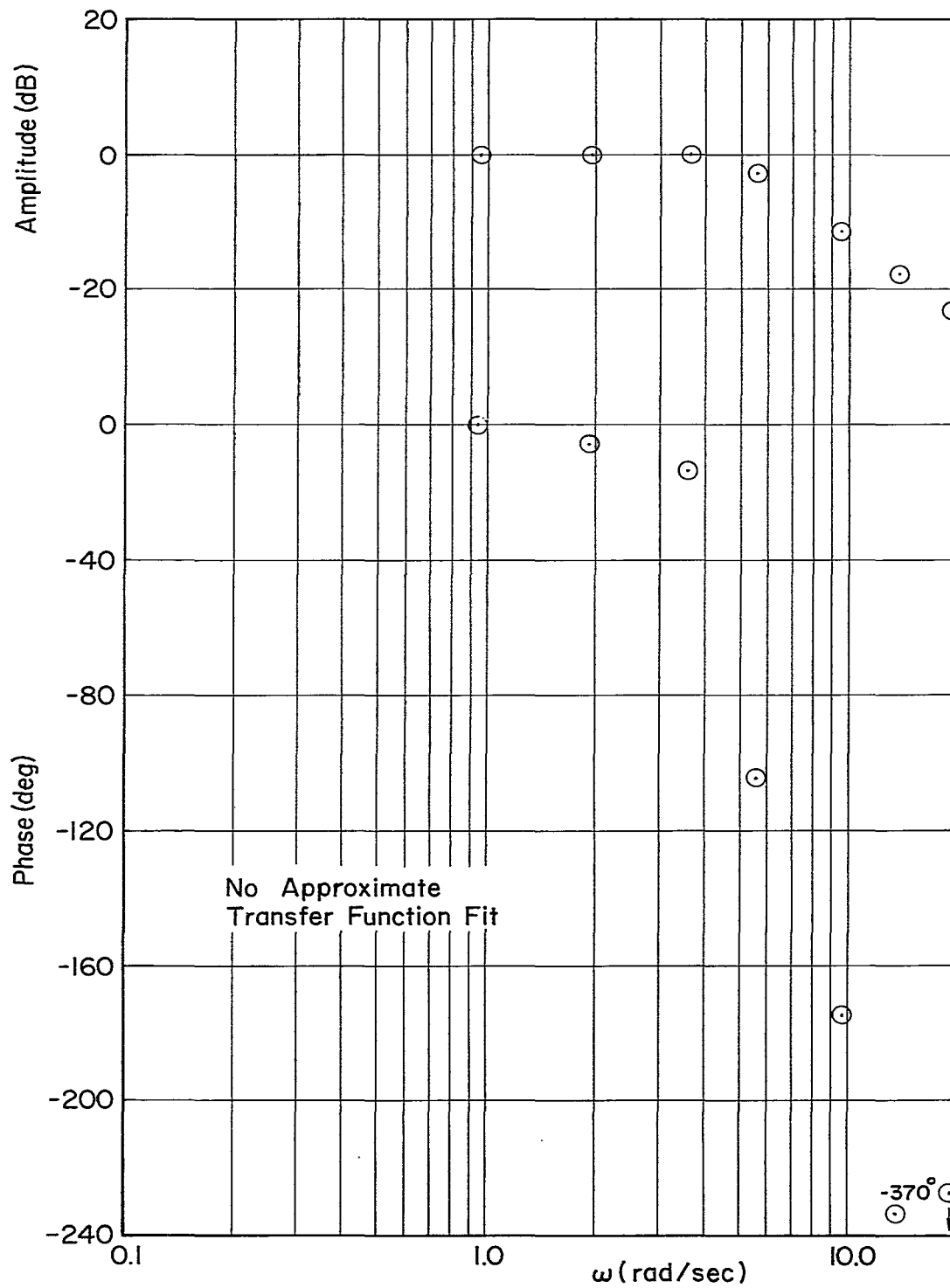
(a) Bank Angle Instrument Frequency Response

Figure B-8. Primary Lateral Instruments

Approximate Transfer Function

$$\frac{\epsilon_{LOC_o}}{\epsilon_{LOC_i}} = \frac{(7)^2}{s^2 + 2(1)(7)s + (7)^2}$$

(b) Localizer Instrument Frequency Response

Figure B-8 (Continued)

B-13b

(c) Lateral Flight Director Instrument Frequency Response

Figure B-8 (Concluded)

B-13c

Approximate Transfer Function

$$\frac{\dot{h}_o}{\dot{h}_i} = \frac{(200)^2}{s^2 + 2(1.0)(200)s + (200)^2}$$
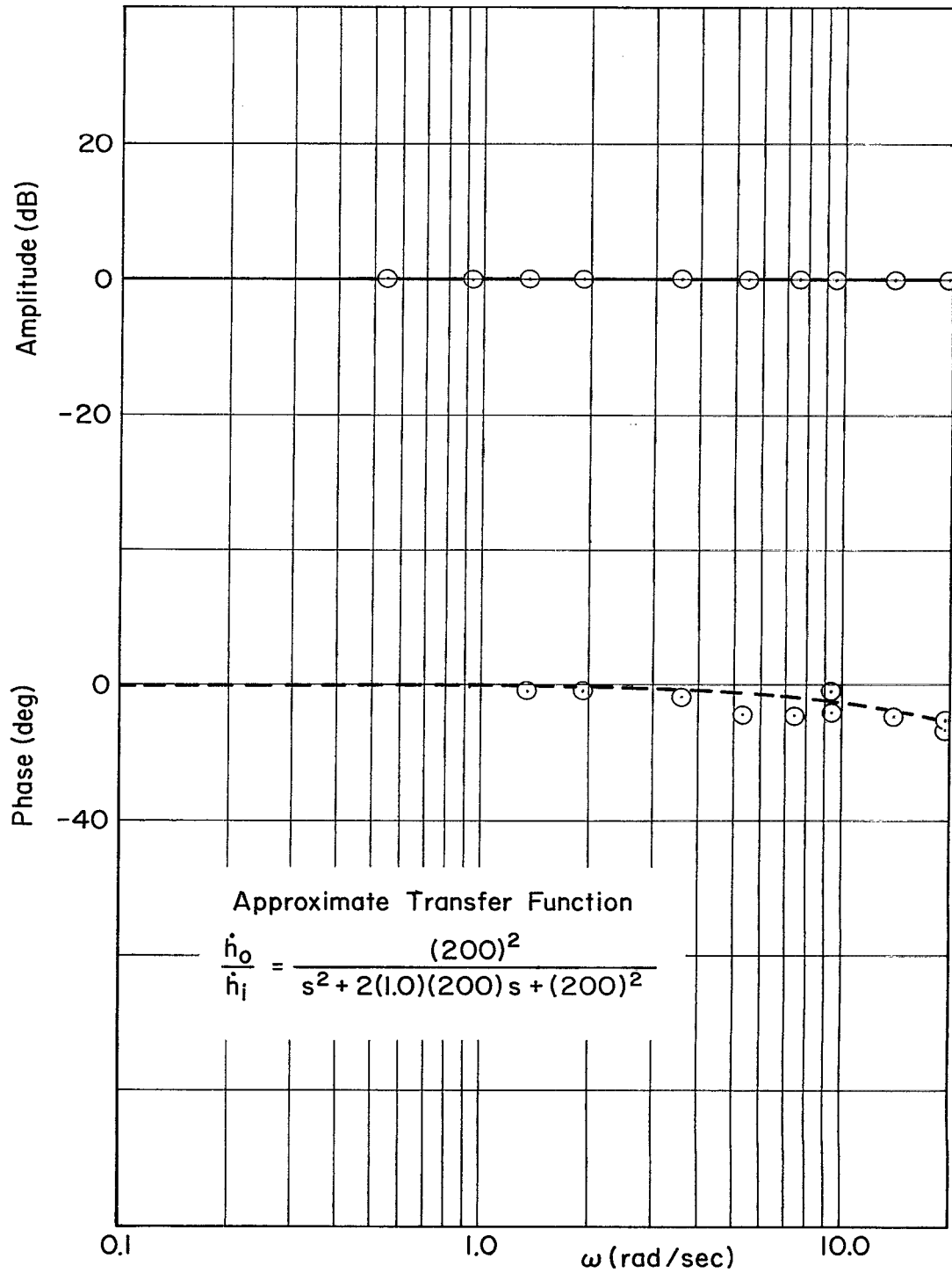
(a)   Rate of Climb Instrument Frequency Response

Figure B-9.   Peripheral Longitudinal Instruments

Approximate Tranfer Function

$$\frac{h_o}{h_i} = \frac{(26)^2}{s^2 + 2(4)(26)s + (26)^2}$$
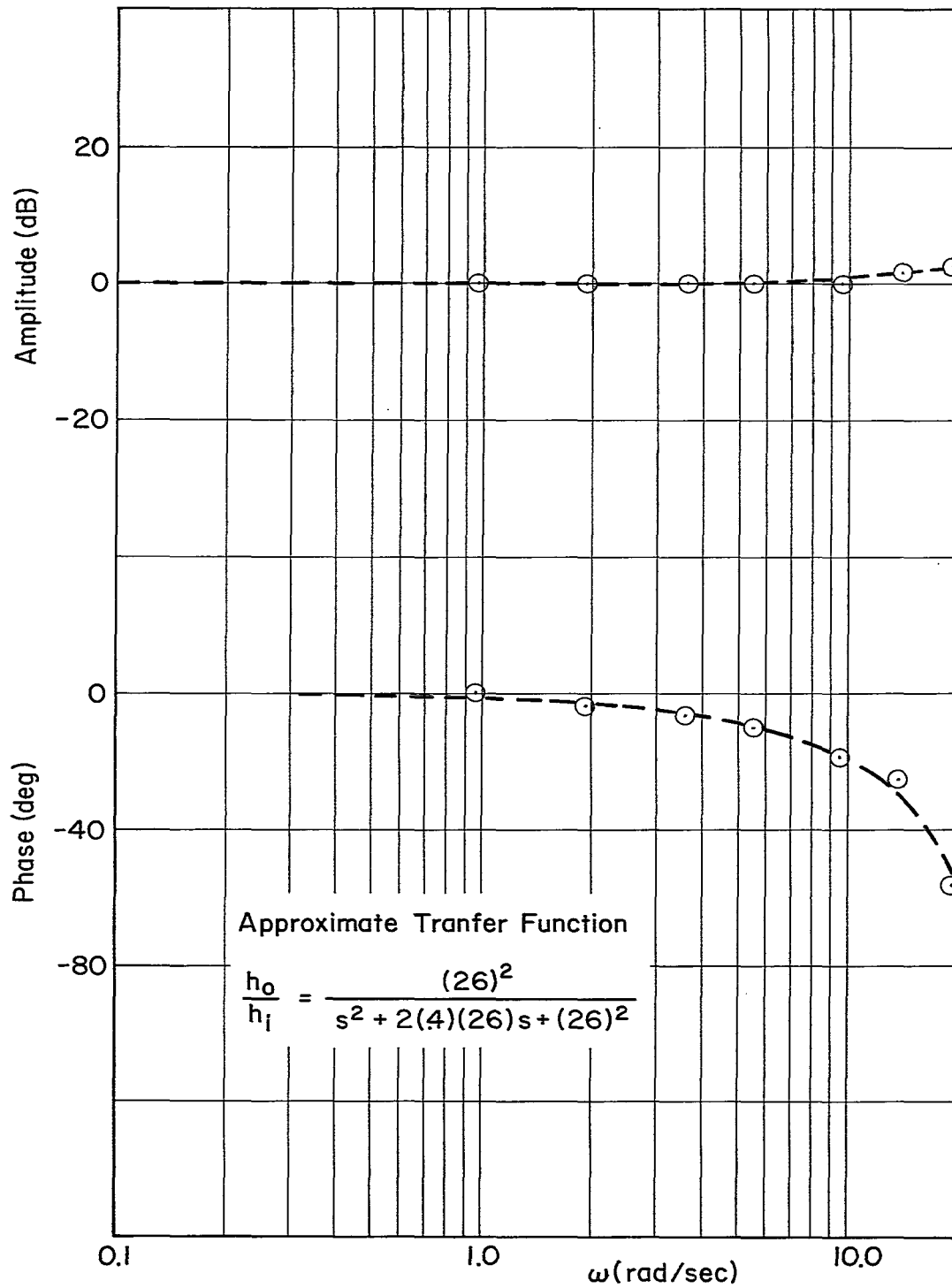
(b)   Altimeter Frequency Response

Figure B-9   (Continued)

Approximate Transfer Function

$$\frac{U_o}{U_i} = \frac{(6.5)^2}{s^2 + 2(1.0)(6.5)s + (6.5)^2}$$

(c) Airspeed Instrument Frequency Response

Figure B-9 (Concluded)

MANIPULATOR PROPERTIES

Static force-displacement data was taken on the simulator elevator and aileron systems. These are presented in Figs. B-10 and B-11, respectively. The large hysteresis in the rudder system precluded any measurements. The rudder was subsequently disconnected (electrically) from the simulation during the test program. Although dynamic responses were not taken, a measure of the system's frequency and damping may be estimated from Fig. B-12 for releases from a given displacement.

The throttle system was mechanized such that approximately 6 in. of throttle movement from the full aft stops represented 100 percent power. Individual throttle settings could be varied, but no moments were computed. A 1 sec time delay was mechanized to represent spool-up time.
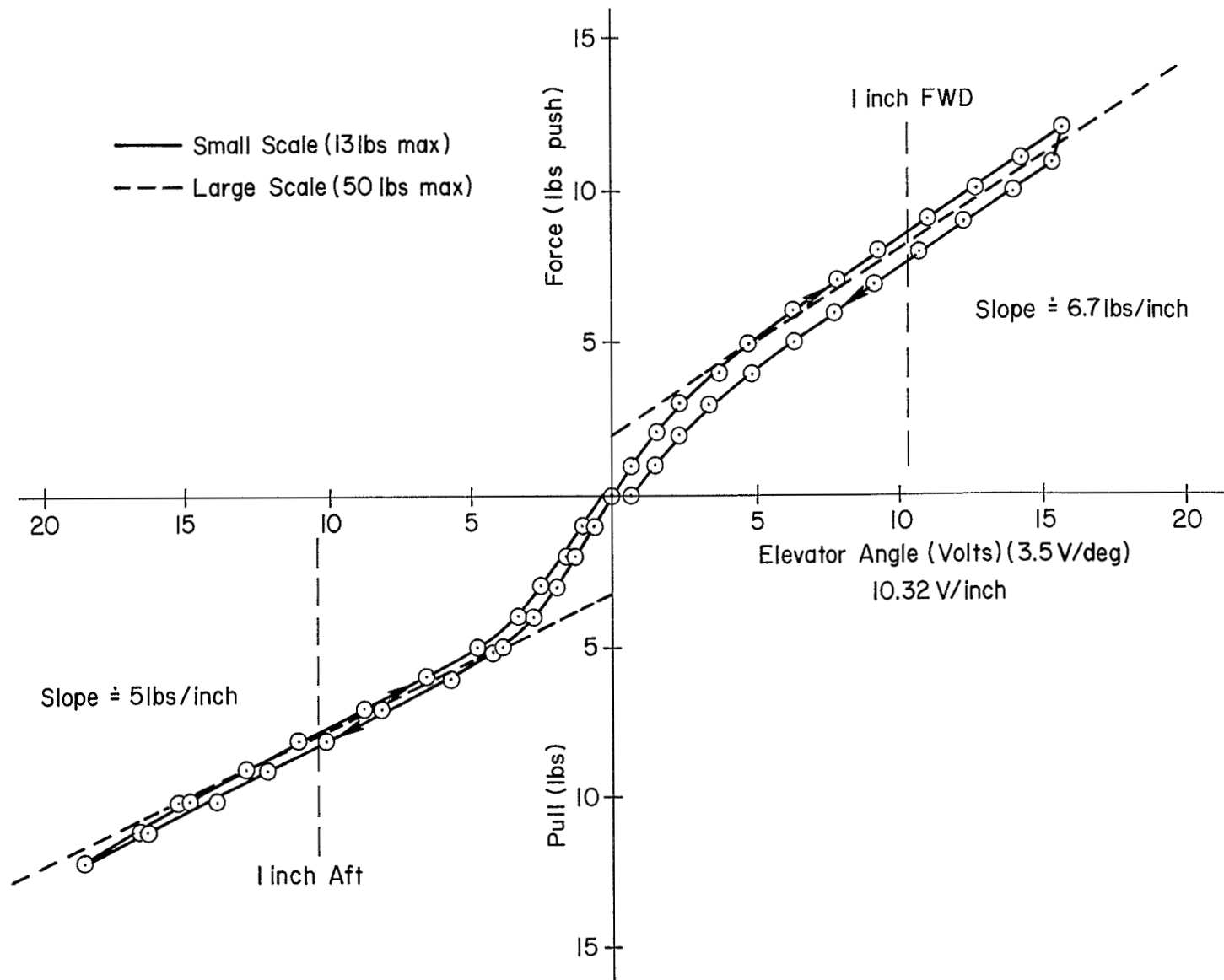
Figure B-10. Elevator Control Force Characteristics
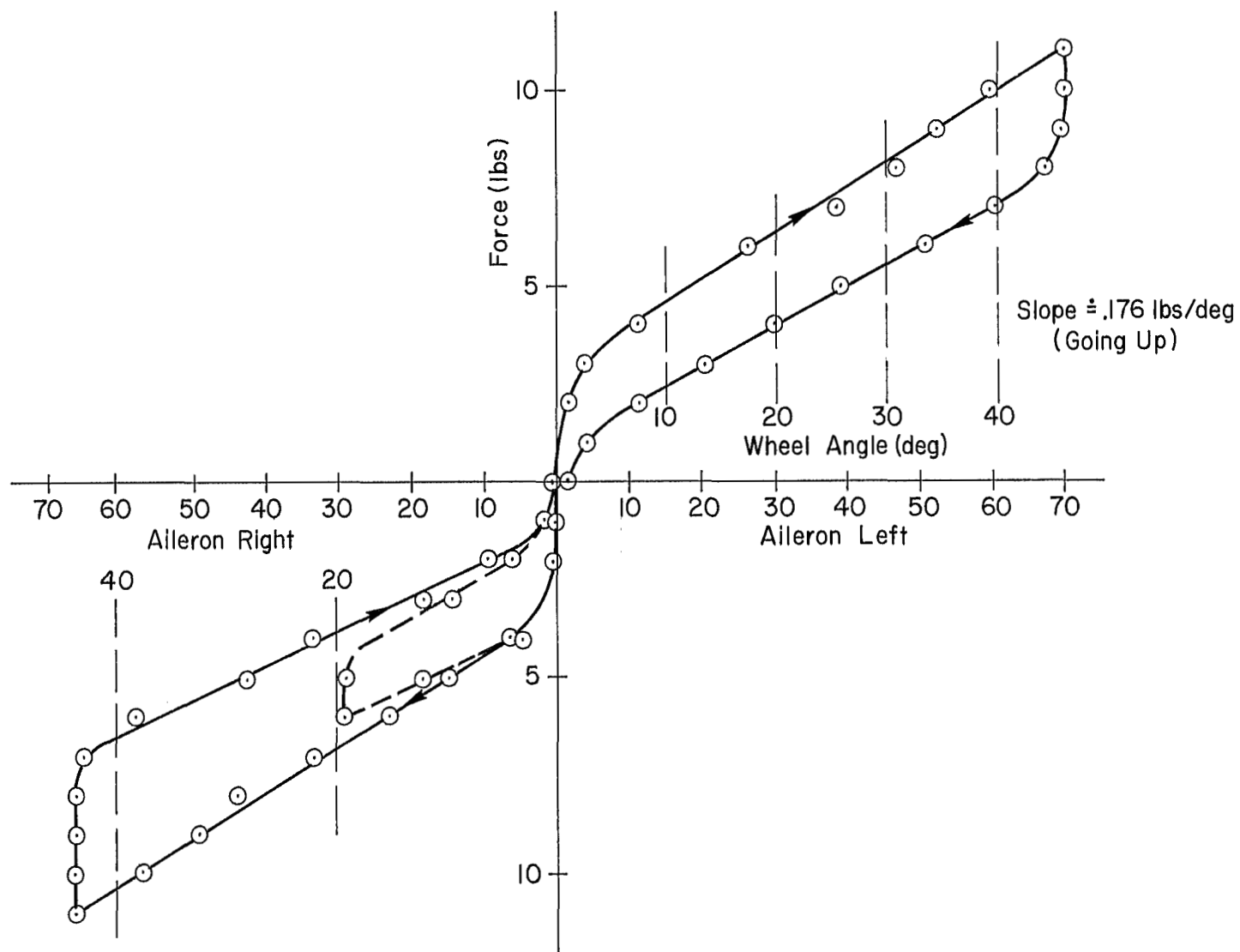
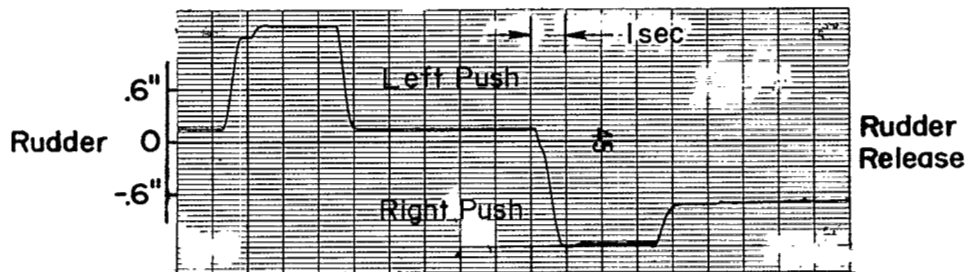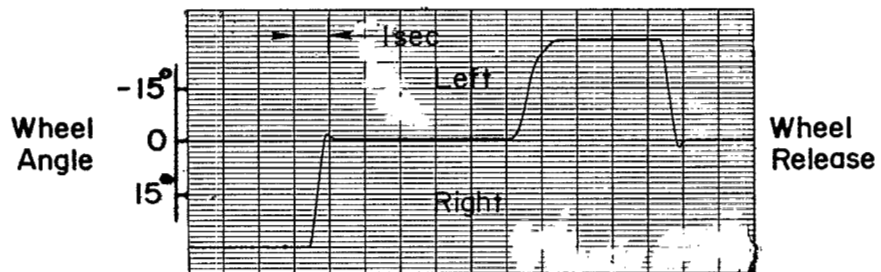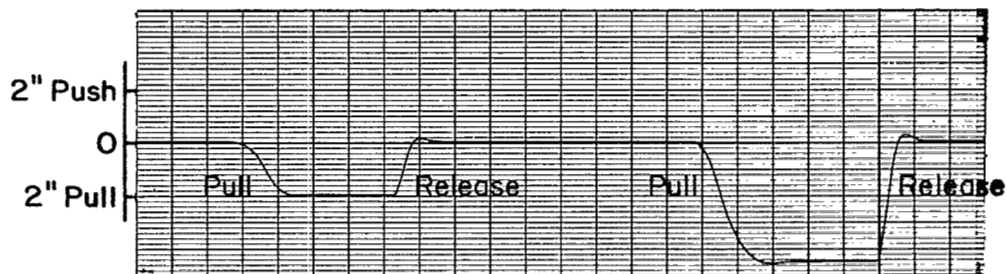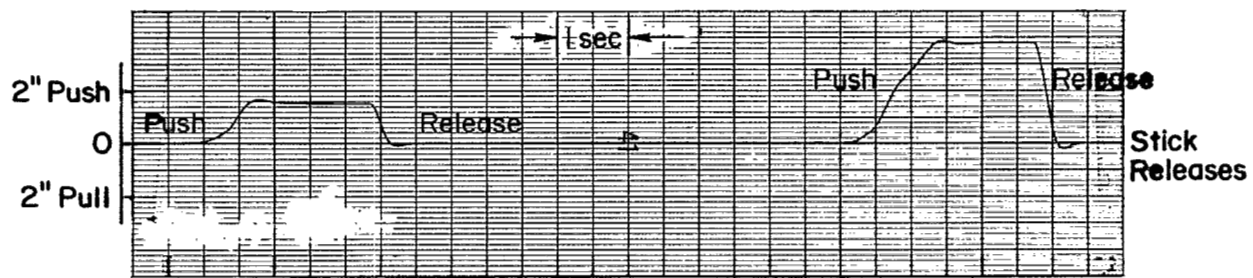Figure B-11. Aileron Control Force Characteristics

Figure B-12. Control Response from a Displacement Release

APPENDIX C

FORCING FUNCTIONS AND TRACERS

The multiloop system studied is shown in block diagram form in Fig. C-1. The dominant feedback loops include pitch attitude, θ, deviation from glide slope, ϵ_{GS}, rate of climb, $\dot{h}$, and airspeed, U. Glide slope command, ϵ_{GS_c}, and pitch attitude command, θ_c, forcing functions were used, generated with interleaved sums of sine waves. Tracer frequencies were added to other signals to detect additional pilot response. These methods allow several display and control variables to be correlated and the dominant closed-loop responses to be measured.

FORCING FUNCTIONS

Command inputs in pitch angle and glide slope deviation provided realism and aided measurements. They were shaped to represent a vertical gust disturbance and glide slope beam noise, respectively.

Gusts actually enter the system through the airframe, not as commands, but a true gust input results in poor measurements. The signal/noise ratio is low at high frequency, and the forcing function shape (an important task variable) is determined by the closed-loop pilot/vehicle properties. This attenuation is shown by Fig. C-2, a plot of the predicted closed-loop θ/w_g response. An equivalent pitch attitude command was used to avoid these measurement problems.

The forcing function bandwidths must be well below the anticipated crossover frequency to avoid regression in pilot crossover frequency, yet still have significant power in the mid-frequency region for good measurements. Large signal amplitudes are desirable, yet the signals should be fairly small for realism in an ILS approach situation.

The power spectrum of the pitch attitude forcing function is shown by the solid line in Fig. C-3.* The circles indicate the sine wave components

---

*This input tape was made on 14 February 1969 and used on subsequent runs. The inputs used prior to this date and during the shakedown runs had slightly higher bandwidths and different shelf amplitudes.
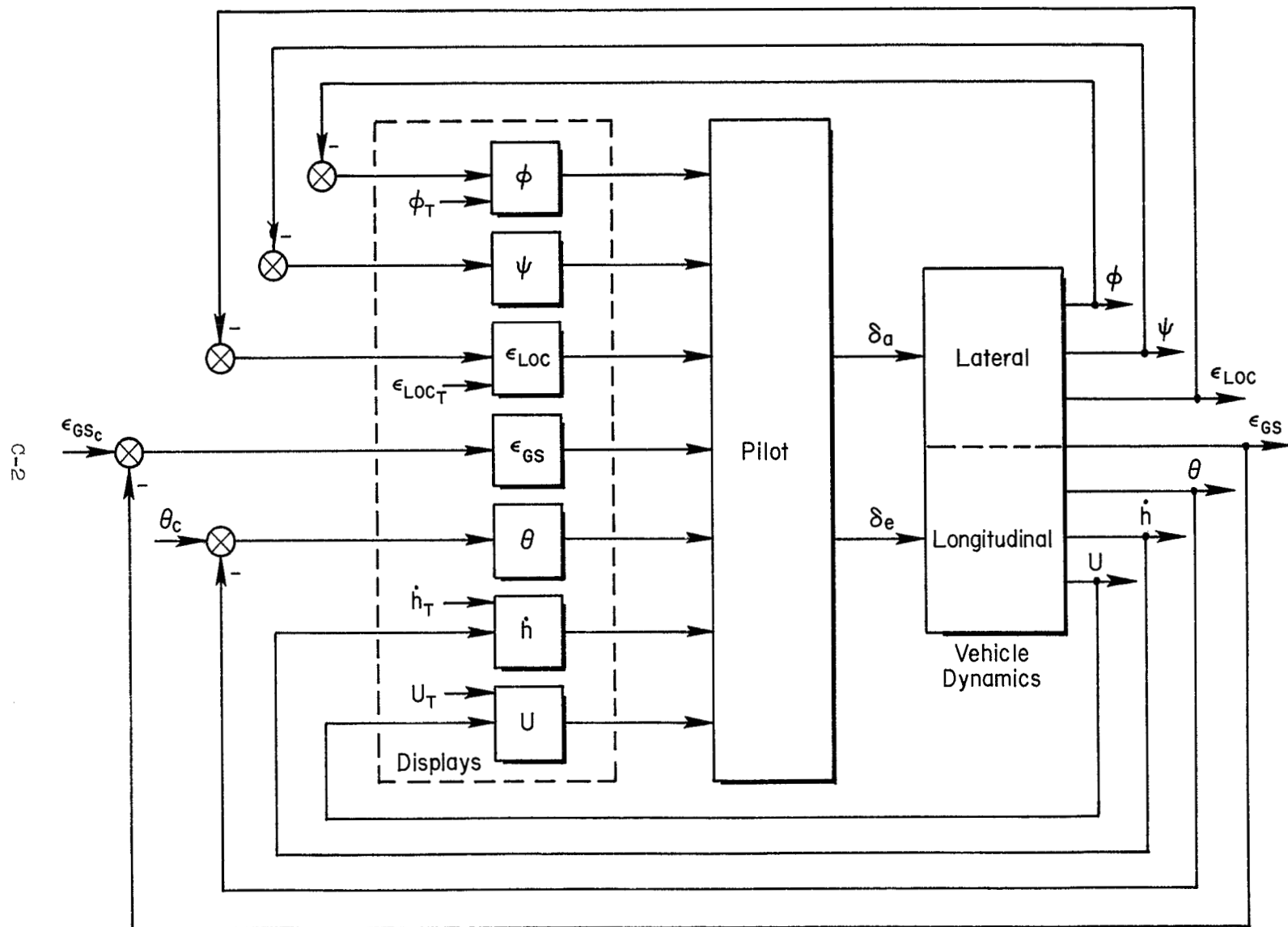
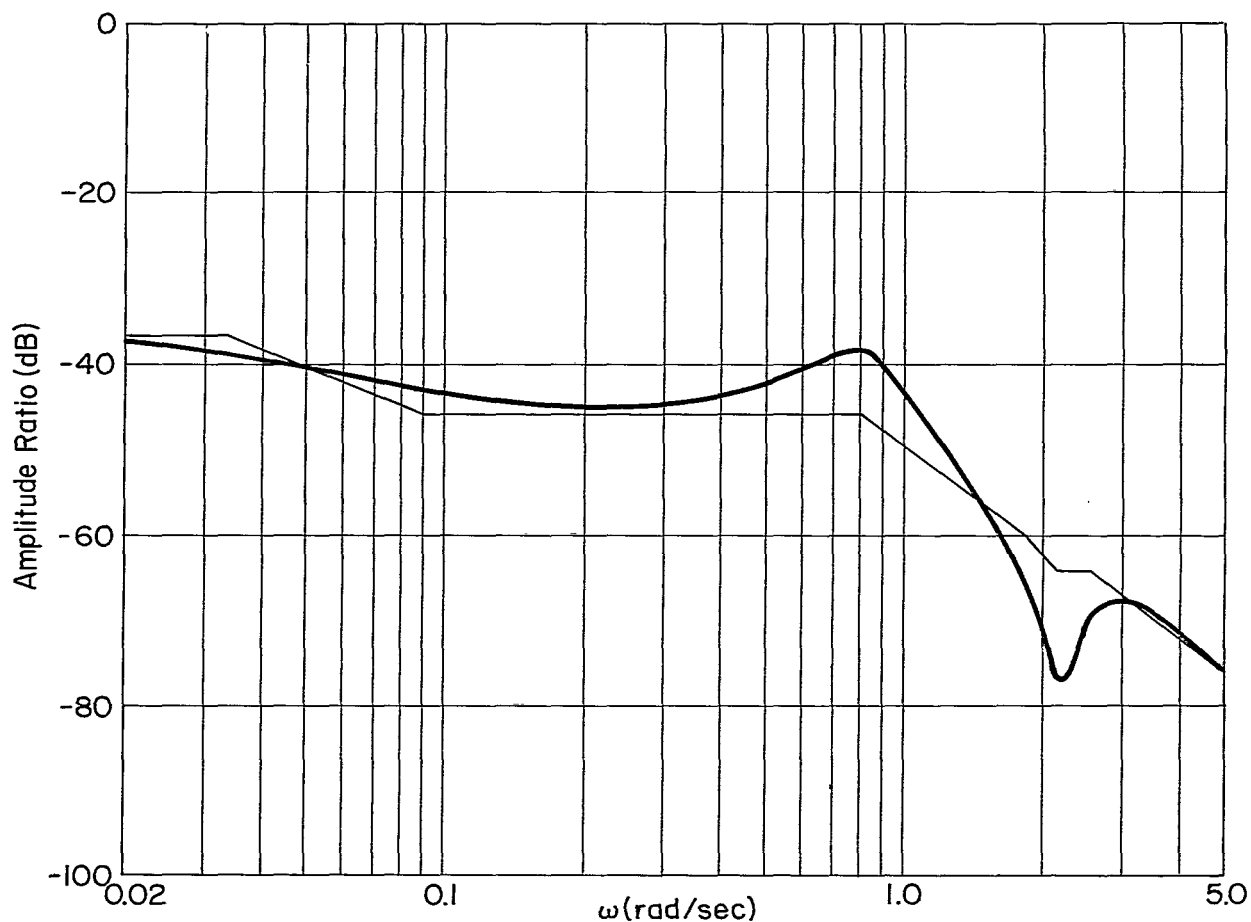Figure C-1. Pilot/Vehicle System with Forcing Functions and Tracers

Figure C-2. Amplitude Ratio of θ/w_g with $\theta \rightarrow \delta_e$
and $\epsilon_{GS} \rightarrow \delta_e$ Loops Closed

used to generate the spectrum. The predicted pilot crossover frequency
was 2 to 2.5 rad/sec. The effective forcing function bandwidth is about
0.8 rad/sec. The high frequency "shelf" provides some measurement power
at and beyond crossover. The input had an rms pitch deviation of about
1.2°, equivalent to a vertical gust with an rms amplitude of about 5 ft/sec.
It was on input recorder channel 1.* This forcing function is roughly

---

*The input recorder head configuration had channels 1, 3, 5, and 7 on
head 1 and channels 2, 4, 6, and 8 on head 2. The heads were displaced
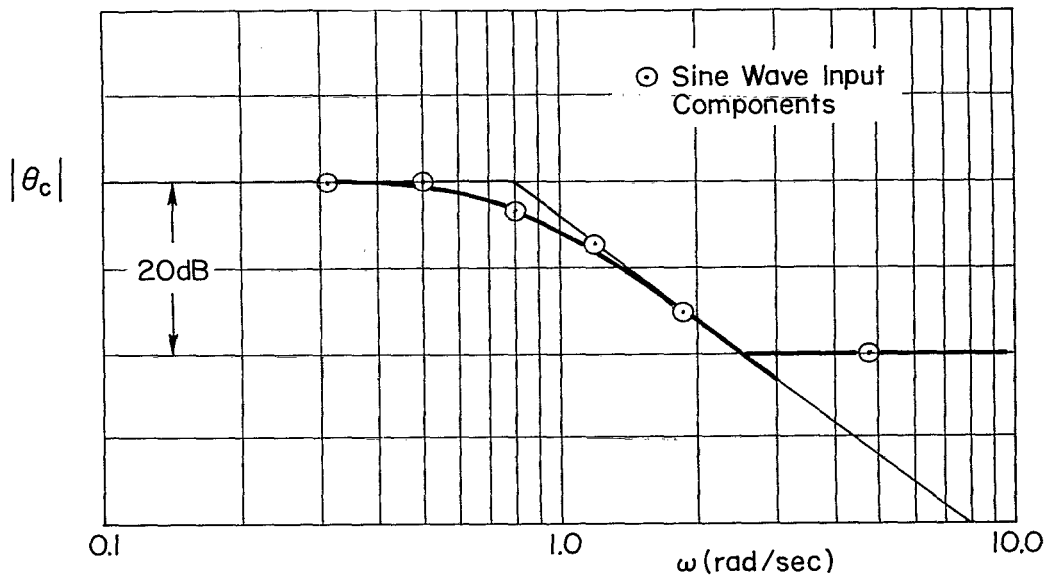from each other by 1 track width.

Figure C-3. Power Spectrum of Pitch Angle Forcing Function

consistent with that used in Ref. 14, which had a bandwidth of 1 rad/sec
and an rms of 8 ft/sec.

The glide slope forcing function is shown in Fig. C-4. The circles
represent the sine wave input components. The pilot crossover frequency
predicted in this loop was approximately 0.5 rad/sec. The effective
forcing function bandwidth is about 0.3 rad/sec with a second-order
rolloff and −20 dB shelf. The relative amplitude was set to have an
rms of 0.04° path angle, or about 0.2 dots of rms needle deflection.
It was on input recorder channel 4. This forcing function is consistent
with beam bend data of Ref. 20.

TRACERS

Tracer frequencies were added to the displayed signals on some of the
remaining instruments. The tracers were single (in one case, two) sinusoids
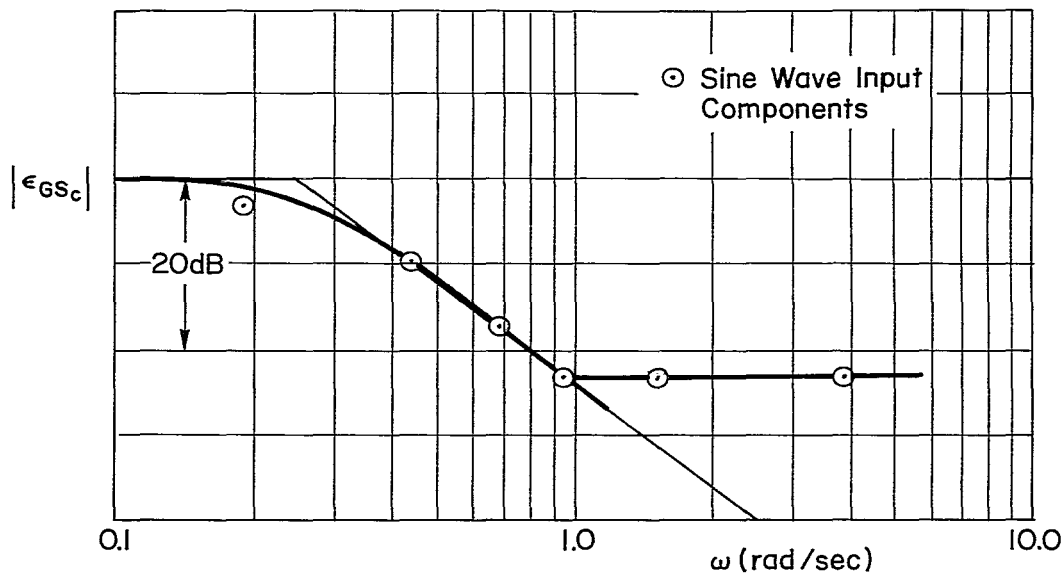with their magnitudes adjusted to be barely perceptible to the pilot. The

Figure C-4. Power Spectrum of Glide Slope Forcing Function

tracer properties are summarized in Table C-I. The selection considerations
could not all be satisfied, primarily because of the limited number of
nonharmonically related, low frequency sinusoids in a 100 sec run length.

INPUT TAPE RECORDER

The input tape recorder (Vetter Model A) was set up with all record
channels "full on." The first 50 ft of tape was recorded with a grounded
input in order to have a null reference for removing biases. The record
and playback speeds were 7.5 ips. About 10 min of recording was made.
With the Vetter playbacks full on, the output level in playback is one-half
the input level when recorded.

TABLE C-I

TRACER PROPERTIES

TRACER	SELECTION CONSIDERATION	FREQUENCY (RAD/SEC)	AMPLITUDE (PEAK)	RECORDER CHANNEL
Localizer deviation, ϵ_{LOC_T}	Low frequency, near the pilot/vehicle lateral deviation crossover frequency	0.251	±.2 dots	3
Roll angle, φ_T	Mid-frequency, near pilot/vehicle crossover frequency in roll	2.32	±1°	2
Rate of climb, $\dot{h}_T$	Mid-frequency, representative of a vertical gust disturbance	5.96 + 9.24	±50 fpm	6
Forward velocity, U_T	Low or mid-frequency, near pilot/vehicle crossover frequency for airspeed control, or similar to a u-gust	2.89	±1 to 2 kts	5

PRESENTATION TO THE PILOT

A 100 sec sample of the forcing functions and tracers is shown in Fig. C-5. They went from the input recorder to a TR-48 analog computer for scaling. From there, the signals went to the instrument bay and then to the panel in the cockpit. The forcing functions and tracers were only present on the instrument display to the pilot, and did not drive the vehicle equations of motion directly.

The longitudinal forcing functions drove the longitudinal flight director (as well as the basic instruments) when that configuration was used. The lateral tracers did not appear on the lateral flight director.
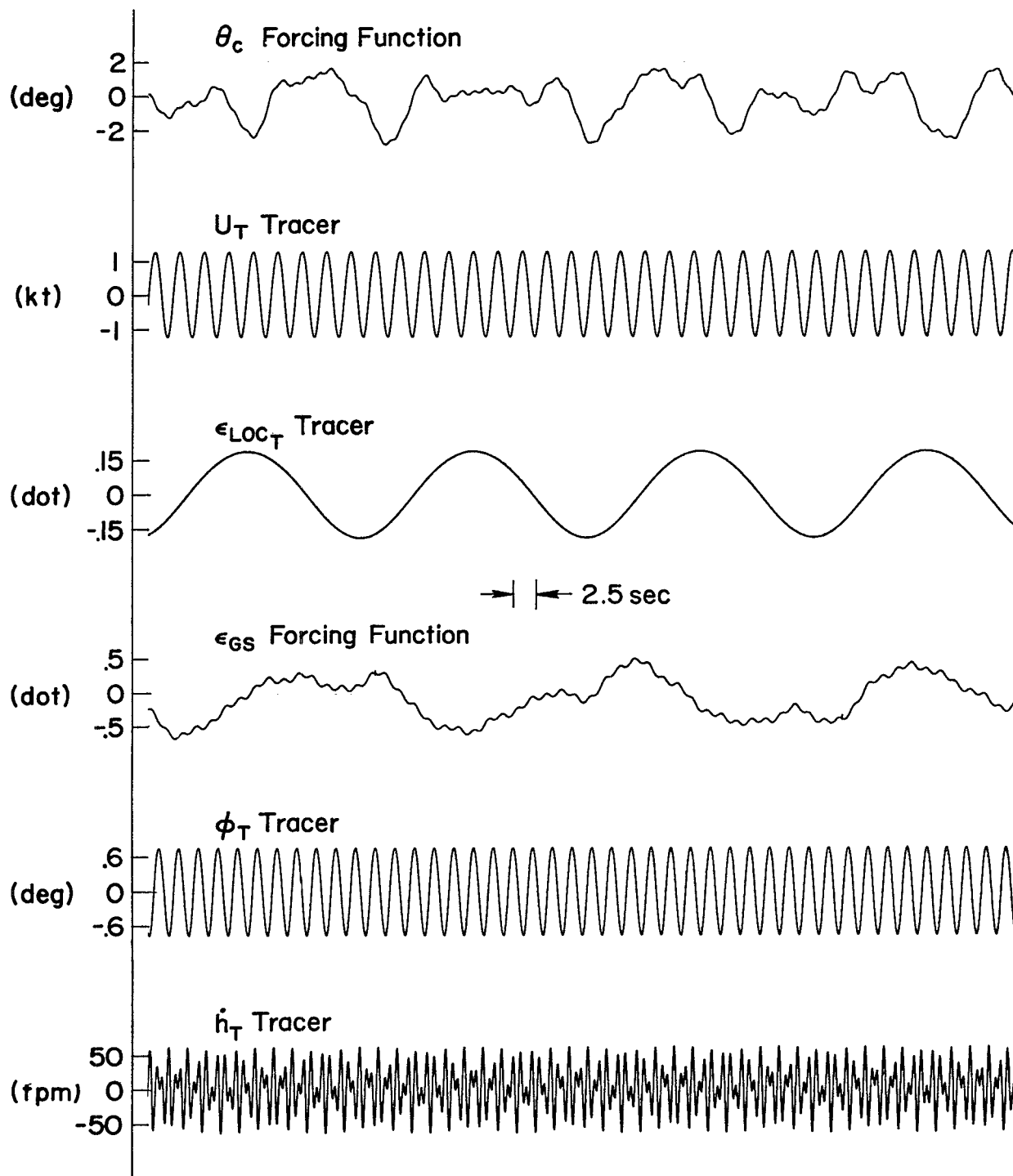
Figure C-5. Sample of Forcing Function and Tracers

APPENDIX D

BACKGROUND OF PILOT SUBJECTS

This appendix summarizes the background and qualifications of the
four key pilots who participated in the test program. Three other subjects
were used but their data have not been analyzed. The tables show their
experience level, training background, and current status including air-
craft and instrument panel configuration.

The subjects are all subsonic jet transport pilots by profession. They
vary in age and experience. Note that Pilot 2 has a general aviation (light
plane), rather than military, background. Pilot 3 is the only subject with
significant and current high performance (military) single-engine jet experi-
ence. He is still active in the Marine Corps Reserve.

CURRENT EQUIPMENT   EXPERIENCE

Aircraft: B-707
Flight Director: Sperry
Panel Configuration:

HORIZON

IAS   RADAR ALT.   PALT

FD

HDG

RMI   IVSI   CLOCK

PDI*
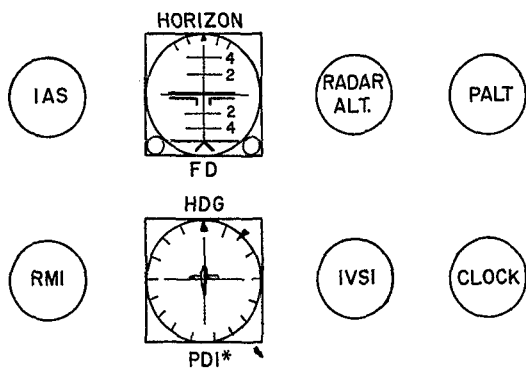
*Glide slope and localizer

Pilot No. 1   Age: 50

Position: Training Captain (PAA)

Total Hours: 14,500

Commercial Flight Experience:

     1,600 hrs jet (707, 720)
     10,800 hrs recip. (DC-3, DC-4, Convair 340, 240)

Military Flight Experience:

     1,300 hrs recip. (B-25, C-121, Bristol)
     300 hrs fighter (P-51)

Private Flight Experience: None

Number of ILS Approaches: 500

Hours Last 6 Months: 230

Number of Category II Landings: 55
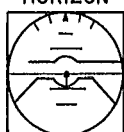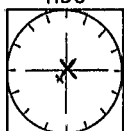
Last Category II Landing Within: 1 week

Aircraft: B-720B
Flight Director: Collins FD-108
Panel Configuration:

HORIZON

IAS   PALT   RADAR ALT.

FD

MACH   ADF   VS

HSI/GSD
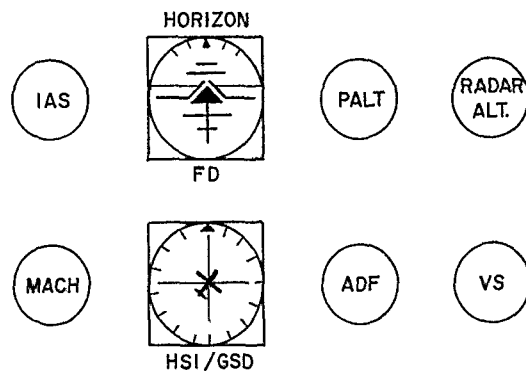
Pilot No. 2   Age: 26

Position: Copilot (Western)

Total Hours: 3,400

Commercial Flight Experience:

     1,200 hrs jet (707)
     145 hrs simulator

Military Flight Experience: None

Private Flight Experience:

     2,500 hrs (Cessna 120, 310)

Hours Last 6 Months: 200

Number of ILS Approaches: 100 (est.)

Last Category II Landing Within: None

Aircraft: B-707 and A-4
Flight Director: Bendix
Panel Configuration:

HORIZON

(IAS)   [FD]   (PALT)   ( )

(RMI)   [HDG / FPI*]   (VS)   ( )

*Glide slope and localizer

Pilot No. 3   Age: 29

Position: Copilot (TWA)

Total Hours: 4,050

Commercial Flight Experience:

     2,000 hrs jet (B-707)

Military Flight Experience:

     1,750 hrs (A-4, etc.)

Private Flight Experience:

     300 hrs

Hours Last 6 Months: 450

Number of Category II Landings: None

Last Category II Landing Within:

Aircraft: CV-990-A
Flight Director:
Panel Configuration:

(IAS)   GSD [ATT/FD]   (PALT)   (IVSI)

(T and B)   [HSI]   (ADF)   (CLOCK)

(MACH)

Pilot No. 4   Age: Approximately 50

Position: Captain (Northrop Test Pilot)

Total Hours: 11,500

Commercial Flight Experience:

     3,100 jet (CV-990)
     7,000 recip.

Military Flight Experience:

     800 recip. (B-36)
     25 fighter (P-51)

Private Flight Experience: None

Hours Last 6 Months: 200

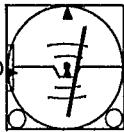Number of Category II Landings: Unknown

Last Category II Landing Within: 1 Month

APPENDIX E

DETAILED EPR RESULTS

This appendix presents detailed scanning traffic results, discussed
in Section III. Table E-I presents the individual results for the 31 runs
analyzed in detail. Table E-II are the one-way link transition matrices
for the average of each of the subject/configuration cells. Each matrix
cell gives the fraction of the total number of transitions which went from
the row (instrument) to the column (instrument).

Dwell time histograms for the 10 subject/configuration cells on each
of the 5 instruments are presented in Figs. E-1 through E-5. There were
no dwells on instrument 4.

TABLE E-I

INDIVIDUAL RUN EPR DATA

RUN # 6902	CONFIG.	PILOT	INSTRUMENT NO. 1						NO. 2						NO. 3						NO. 5						NO. 6						ALL INSTRUMENTS		
			N_1	$\bar{T}_{d_1}$	σ_{T_d}	$\bar{T}_{s_1}$	η_1	ν_1	N_2	$\bar{T}_{d_2}$	σ_{T_d}	$\bar{T}_{s_2}$	η_2	ν_2	N_3	$\bar{T}_{d_3}$	σ_{T_d}	$\bar{T}_{s_3}$	η_3	ν_3	N_5	$\bar{T}_{d_5}$	σ_{T_d}	$\bar{T}_{s_5}$	η_5	ν_5	N_6	$\bar{T}_{d_6}$	σ_{T_d}	$\bar{T}_{s_6}$	η_6	ν_6	T_R	N	$\bar{T}_s$
17-18	B	1	6	.71	.20	.059	.042	.055	40	.61	.24	.393	.24	.367	8	.40	.06	.079	.031	.073	47	1.43	1.07	.462	.662	.431	4	.43	.18	.039	.017	.037	101.66	109	1.072
19-5	B	1	12	.50	.12	.122	.061	.077	49	.71	.32	.499	.352	.316	15	.38	.15	.153	.057	.097	64	.72	.28	.652	.472	.413	6	.37	.13	.061	.023	.039	98.11	155	1.580
19-17	B	2	2	.64	.05	.020	.013	.015	61	.82	.36	.607	.498	.462	2	.57	.04	.020	.011	.015	57	.78	.25	.567	.443	.432	1	.55	.00	.010	.005	.008	100.53	132	1.313
17-15	C	1	5	.82	.17	.050	.041	.040	47	.85	.35	.469	.398	.379	9	.50	.16	.090	.045	.073	53	.92	.65	.529	.486	.427	4	.40	.06	.040	.016	.032	100.16	124	1.238
19-4	C	1	3	.45	.17	.030	.014	.022	55	.69	.35	.551	.380	.404	8	.39	.11	.080	.031	.059	58	.91	.49	.581	.532	.426	4	.32	.09	.040	.013	.029	99.77	136	1.363
19-10	C	1	4	.50	.22	.039	.019	.036	45	.62	.24	.442	.272	.402	7	.47	.29	.069	.032	.063	47	1.40	1.03	.461	.645	.420	4	.38	.06	.039	.015	.036	101.9	112	1.099
19-11	C	1	8	.77	.30	.080	.062	.065	49	.71	.31	.493	.352	.395	9	.34	.04	.090	.031	.073	50	1.05	.56	.503	.530	.403	2	.45	.03	.020	.009	.016	99.47	124	1.247
19-13	C	1	5	.74	.32	.049	.037	.048	42	.87	.30	.416	.363	.404	7	.42	.13	.069	.029	.067	47	1.21	.70	.465	.561	.452	2	.37	.03	.020	.007	.019	101.05	104	1.029
19-16	C	2	← NO LOOKS →						51	1.06	.40	.513	.542	.455	← NO LOOKS →						49	.89	.37	.492	.438	.438	← NO LOOKS →						99.5	112	1.126
19-21	C	2	1	.63	.00	.010	.006	.009	49	.98	.36	.500	.492	.441	← NO LOOKS →						47	.96	.30	.480	.463	.423	← NO LOOKS →						97.97	111	1.133
19-23	C	2	← NO LOOKS →						55	.85	.25	.549	.469	.451	2	.39	.28	.020	.008	.016	50	.95	.32	.499	.476	.410	1	.63	.00	.010	.006	.008	100.19	122	1.218
19-25	C	2	← NO LOOKS →						51	.95	.33	.510	.484	.447	1	.52	.00	.010	.005	.009	48	.96	.52	.480	.463	.421	1	.30	.00	.010	.003	.009	99.94	114	1.141
19-19	C	2	← NO LOOKS →						48	.92	.25	.481	.441	.471	2	.38	.01	.020	.008	.020	48	1.12	.46	.481	.540	.471	← NO LOOKS →						99.85	102	1.022
17-16	D	1	6	.73	.41	.058	.042	.048	55	.93	.36	.536	.496	.440	3	.38	.19	.029	.011	.024	53	.84	.42	.517	.432	.424	← NO LOOKS →						102.59	125	1.218
26-5	D	1	12	.59	.13	.121	.071	.083	64	.78	.30	.644	.499	.444	6	.47	.19	.060	.028	.042	53	.71	.29	.533	.376	.368	2	.47	.21	.020	.009	.014	99.45	144	1.448
26-9	D	1	10	.60	.19	.099	.059	.074	60	.82	.51	.596	.490	.441	6	.42	.06	.060	.025	.044	51	.79	.29	.506	.399	.375	2	.44	.16	.020	.009	.015	100.7	136	1.351
27-3	D	1	7	1.06	.59	.070	.074	.059	47	.82	.42	.468	.384	.398	6	.54	.43	.060	.032	.051	50	.98	.58	.498	.486	.424	1	.19	.00	.010	.002	.008	100.37	118	1.176
27-6	D	1	8	.60	.25	.080	.048	.061	56	.70	.25	.560	.389	.427	6	.43	.07	.060	.026	.046	58	.91	.47	.580	.526	.443	← NO LOOKS →						100.04	131	1.309
28-5	D	3	1	.88	.00	.010	.009	.008	43	.92	.37	.430	.395	.364	5	.39	.07	.050	.020	.042	52	.99	.57	.520	.513	.441	16	.37	.09	.16	.059	.136	99.96	118	1.180
28-8	D	3	2	.88	.56	.020	.017	.017	42	1.09	.52	.417	.455	.350	4	.51	.21	.040	.020	.033	44	.86	.44	.436	.374	.367	27	.49	.14	.268	.131	.225	100.84	120	1.190
13-20	E	1	12	.45	.08	.121	.055	.148	38	2.12	2.17	.384	.814	.469	12	.35	.07	.121	.042	.148	13	.49	.10	.131	.064	.160	5	.44	.15	.051	.022	.062	98.91	81	.819
17-19	E	1	8	.49	.07	.080	.039	.091	38	2.14	2.10	.378	.808	.432	9	.37	.06	.090	.033	.102	15	.45	.05	.149	.067	.170	3	.40	.04	.030	.012	.034	100.44	88	.876
19-8	E	1	12	.57	.09	.120	.069	.120	43	1.59	1.40	.429	.682	.430	14	.48	.08	.140	.067	.140	21	.70	.25	.210	.147	.210	3	.45	.13	.030	.014	.030	100.18	100	.998
19-12	E	1	12	.66	.20	.120	.079	.099	52	1.26	1.08	.580	.654	.430	16	.38	.12	.160	.061	.132	27	.58	.19	.270	.155	.223	5	.46	.12	.050	.023	.041	100.09	121	1.209
19-18	E	2	6	.51	.13	.058	.029	.109	24	3.70	3.91	.231	.857	.436	7	.51	.13	.067	.034	.127	11	.48	.13	.106	.051	.200	2	.48	.00	.019	.009	.036	103.75	55	.530
19-22	E	2	4	.55	.10	.040	.022	.067	28	2.98	3.64	.282	.842	.467	5	.50	.02	.050	.025	.083	12	.53	.08	.121	.064	.200	3	.58	.20	.030	.017	.030	99.19	60	.605
19-24	E	2	3	.58	.13	.030	.017	.043	32	2.57	2.76	.315	.809	.457	6	.50	.15	.059	.030	.086	18	.52	.15	.177	.092	.257	9	.47	.07	.089	.041	.129	101.6	70	.689
26-7	F	1	20	.55	.15	.200	.109	.172	51	1.42	1.07	.509	.721	.440	14	.36	.09	.140	.050	.121	22	.44	.09	.220	.097	.190	3	.32	.11	.030	.010	.026	100.21	116	1.158
26-8	F	1	20	.54	.09	.201	.109	.169	56	1.28	1.09	.563	.722	.475	11	.34	.05	.111	.038	.093	21	.47	.14	.211	.098	.178	6	.40	.10	.060	.024	.051	99.46	118	1.186
27-5	F	1	13	.60	.22	.131	.078	.143	40	1.92	1.88	.404	.755	.440	9	.34	.05	.091	.031	.099	16	.47	.19	.161	.075	.176	1	.17	.00	.010	.002	.011	99.12	91	.918
28-7	F	3	6	.59	.10	.059	.035	.079	37	2.19	1.80	.366	.800	.487	4	.34	.05	.040	.013	.053	27	.54	.25	.267	.145	.355	1	.49	.00	.010	.005	.013	101.1	76	.752

TABLE E-II

TABLE E-II
ONE-WAY LINK TRANSITION MATRICES

| CONFIGURATION | ONE-WAY LINK MATRICES* | | | | | | | | | | | | |

Configuration B

PILOT 1							PILOT 2						
	1	2	3	4	5	6		1	2	3	4	5	6
1		0.012	0.004	0.008	0.043	0.004	1		0.016				
2	0.031		0.024		0.278	0.016	2	0.016	0.016	0.008		0.451	
3	0.004	0.020			0.059	0.008	3		0.008			0.008	
4		0.012			0.008		4						
5	0.035	0.306	0.059	0.012	0.008	0.012	5		0.451	0.008	.		0.008
6			0.004		0.035		6					0.008	

Configuration C

PILOT 1							PILOT 2						
	1	2	3	4	5	6		1	2	3	4	5	6
1		0.017	0.003	0.003	0.019		1		0.002				
2	0.019	0.005	0.028	0.002	0.351	0.007	2	0.002	0.016	0.010	0.002	0.472	0.002
3	0.002	0.019			0.042	0.007	3		0.006			0.004	
4		0.002			0.003		4		0.002				
5	0.021	0.366	0.036		0.005	0.014	5		0.474			0.002	0.002
6	0.002	0.002	0.002		0.023		6		0.002			0.002	

Configuration D

PILOT 1							PILOT 3						
	1	2	3	4	5	6		1	2	3	4	5	6
1		0.034	0.005	0.002	0.027	0.002	1		0.004				0.009
2	0.048	0.002	0.027	0.002	0.369	0.002	2			0.026		0.268	0.068
3	0.003	0.022			0.016	0.002	3		0.026			0.013	
4	0.003						4						
5	0.014	0.390	0.010		0.002	0.003	5	0.004	0.277	0.013		0.004	0.106
6		0.002	0.002		0.005		6	0.009	0.051			0.123	

Configuration E

PILOT 1							PILOT 2						
	1	2	3	4	5	6		1	2	3	4	5	6
1		0.102	0.008	0.006	0.006		1		0.076				
2	0.108	0.014	0.119	0.008	0.199	0.025	2	0.076	0.029	0.088	0.012	0.211	0.070
3	0.006	0.127				0.008	3		0.094			0.006	0.006
4	0.003	0.011					4		0.006			0.006	
5	0.006	0.182	0.008			0.011	5		0.228	0.006			0.006
6		0.036	0.003		0.006		6		0.058	0.006		0.018	

Configuration F

PILOT 1							PILOT 3						
	1	2	3	4	5	6		1	2	3	4	5	6
1		0.165			0.010		1		0.081				
2	0.165	0.010	0.109		0.175	0.020	2	0.081		0.041		0.351	0.014
3		0.102			0.007	0.003	3		0.054				
4							4						
5	0.007	0.175	0.003			0.010	5		0.351	0.014			
6		0.030			0.003		6		0.014				

*Format:

To Instrument

```
        1 2 3 4 5 6
      1
From  2
Inst- 3   Transition
rument    Matrix
      4
      5
      6
```

Note: Transition from i to i indicates an
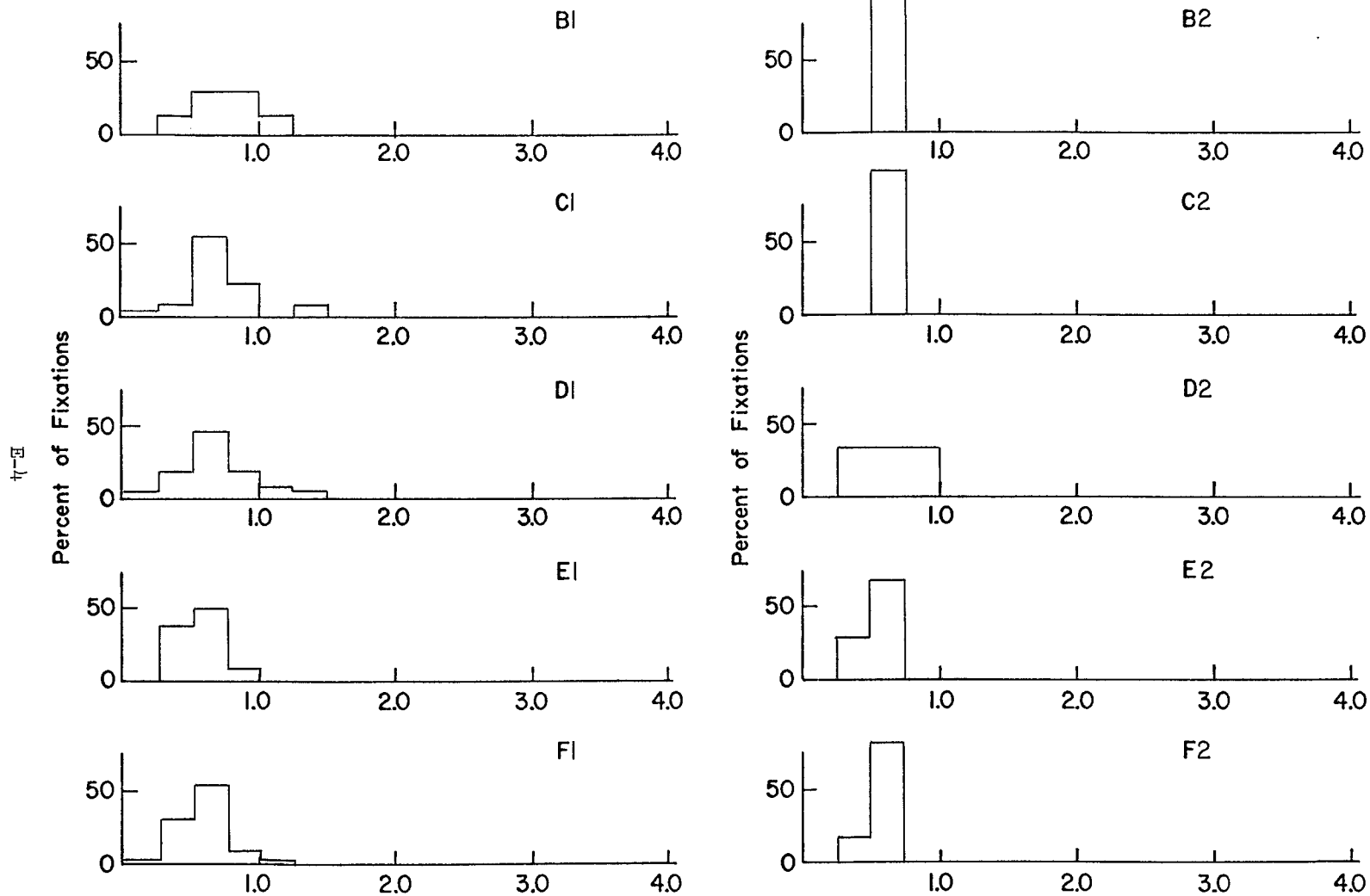interruption due to a blink.

E-3

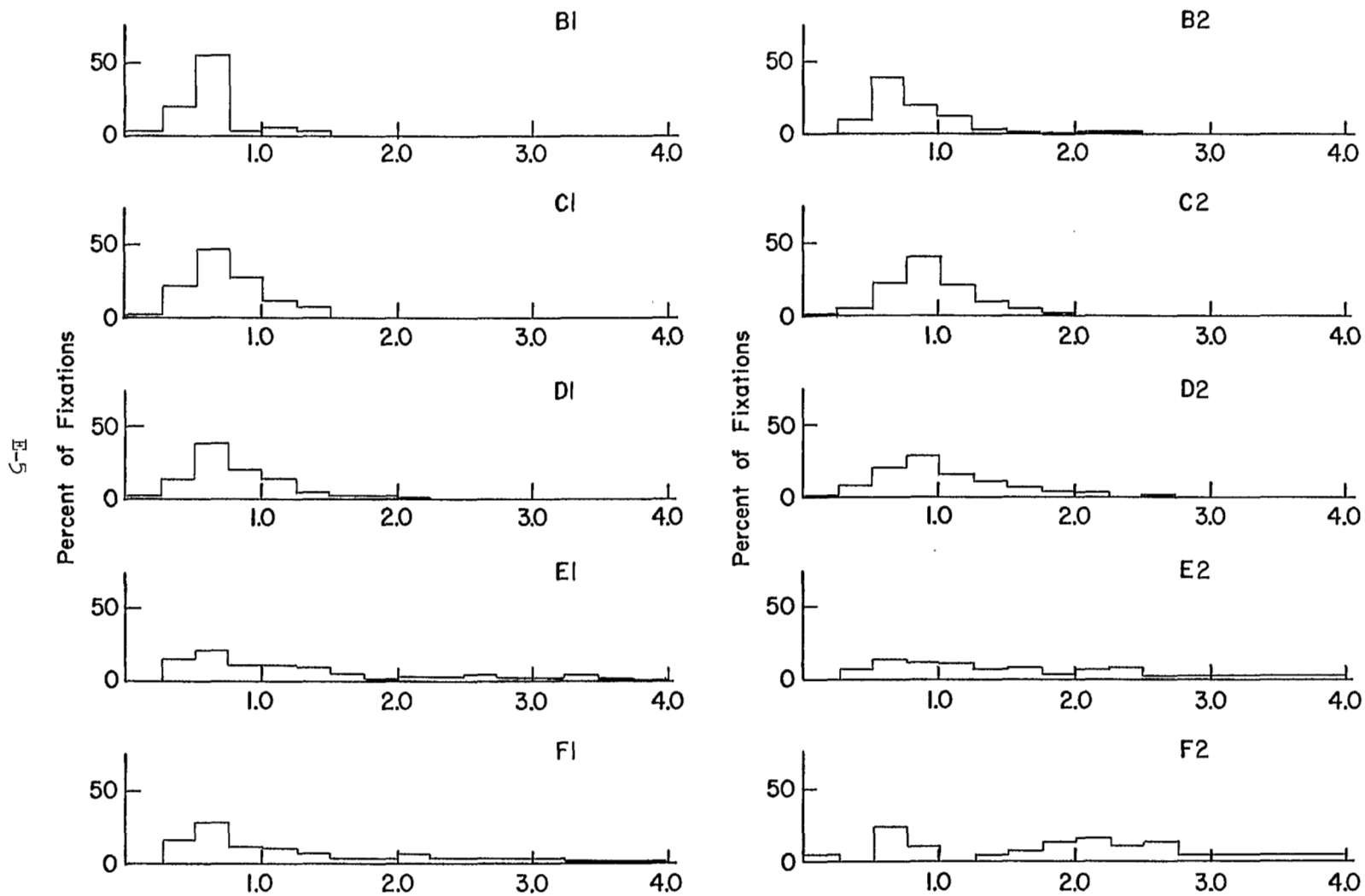Figure E-1. Dwell Time Histograms for Instrument 1, IAS

Figure E-2. Dwell Time Histograms for Instrument 2, ATT/FD
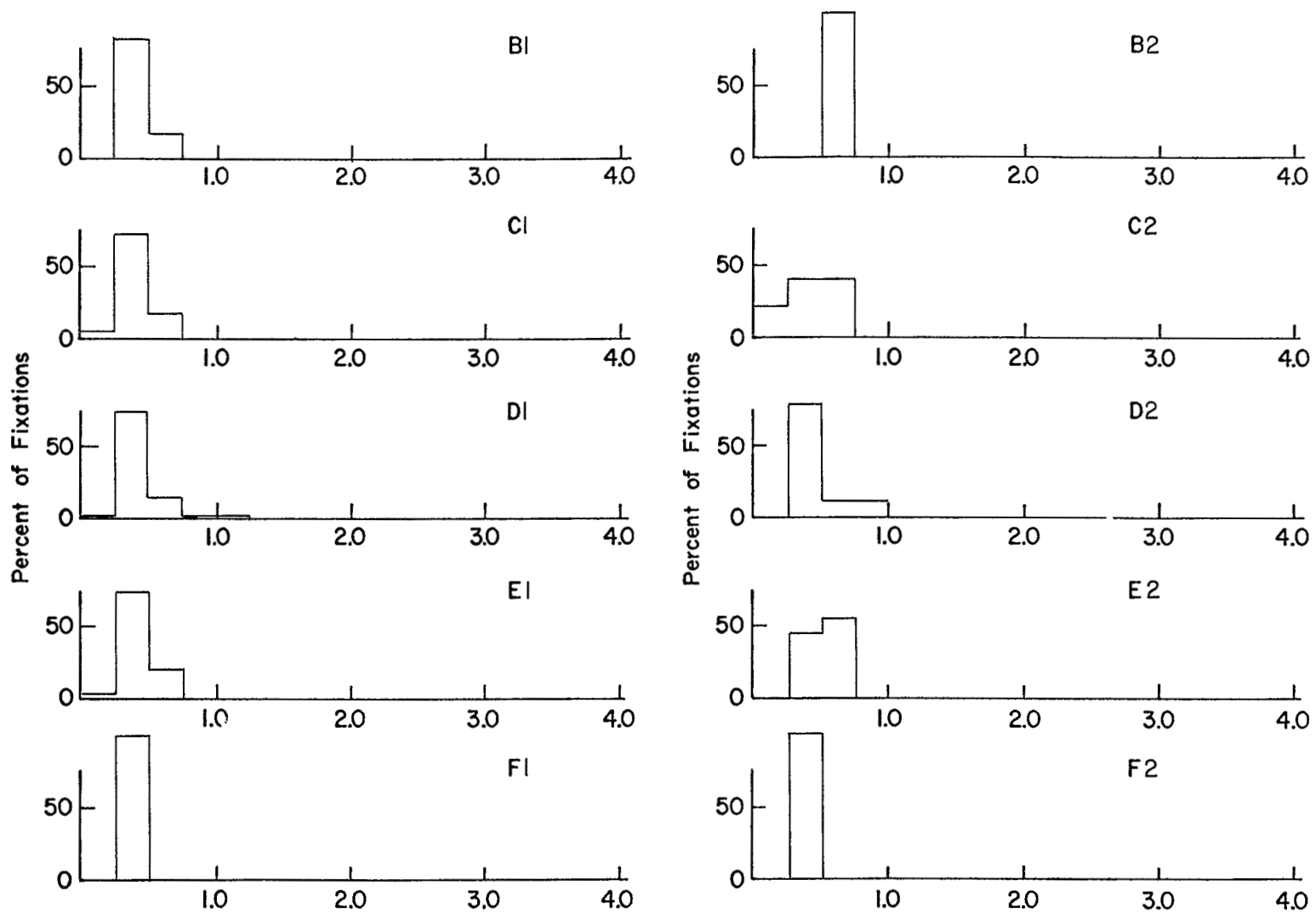
Figure E-3.   Dwell Time Histograms for Instrument 3, PALT
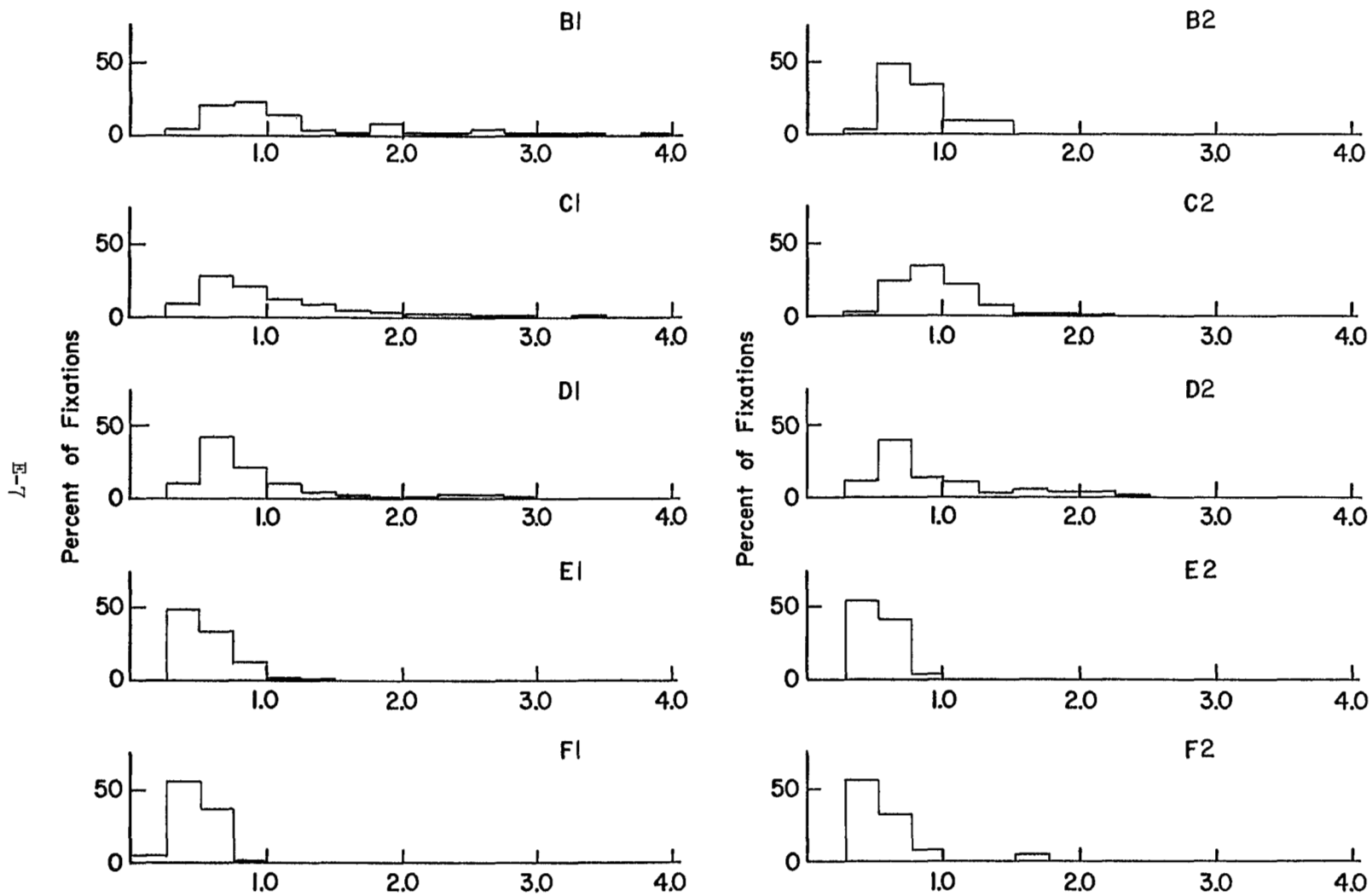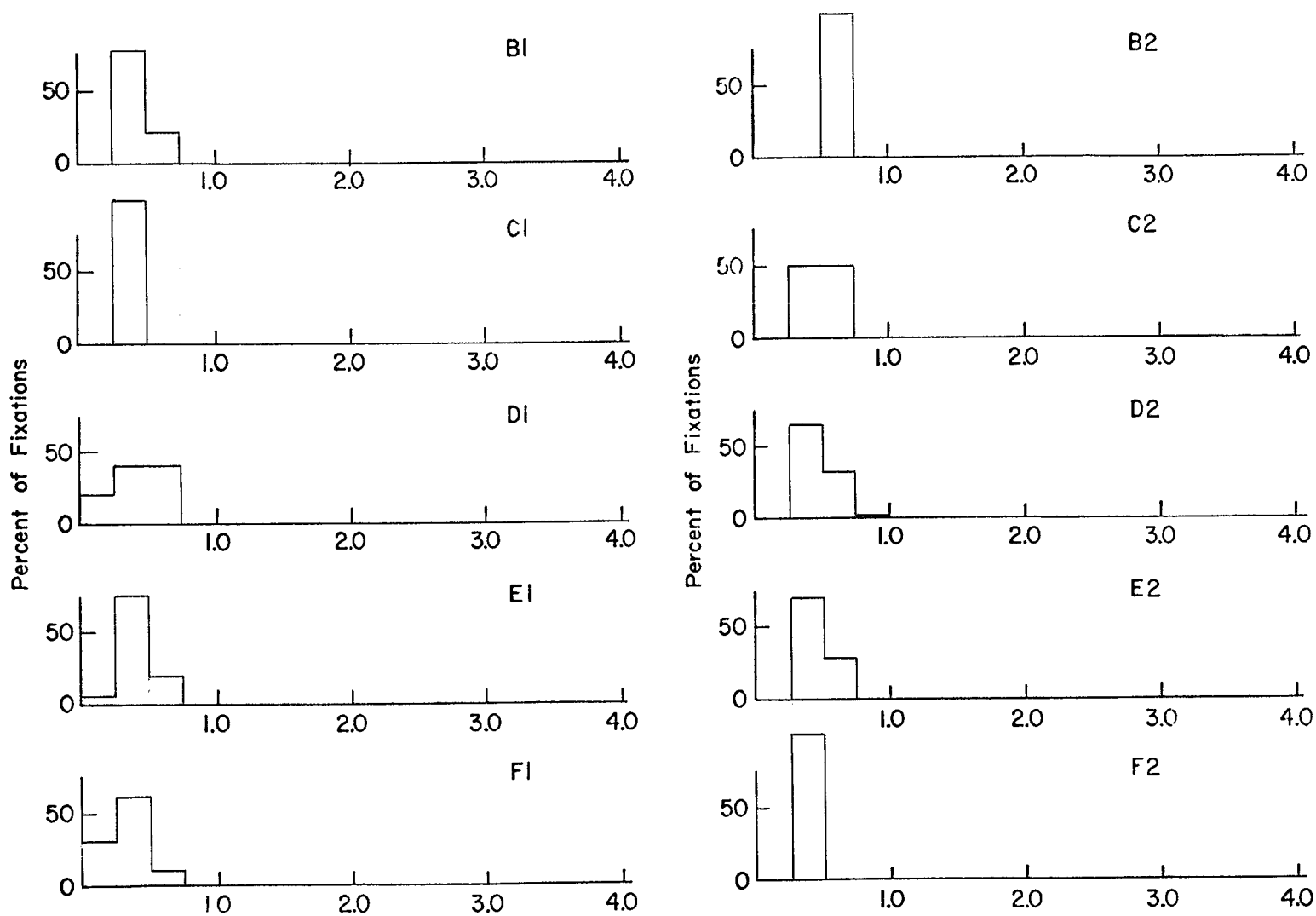
Figure E-4. Dwell Time Histograms for Instrument 5, HSI/GSD

Figure E-5. Dwell Time Histograms for Instrument 6, IVSI